FLEXIBLE NANOSCALE COMPOSITES WITH CO-CONTINUOUS MORPHOLOGY

PREPARED BY CONTROLLED CAVITATION OF THERMOPLASTIC MATERIALS

AND IN SITU POLYMERIZATION OF CONDUCTIVE NETWORKS

FLEXIBLE NANOSCALE COMPOSITES WITH CO-CONTINUOUS MORPHOLOGY

PREPARED BY CONTROLLED CAVITATION OF THERMOPLASTIC MATERIALS

AND IN SITU POLYMERIZATION OF CONDUCTIVE NETWORKS

By Anton B. Kornberg

A Thesis Submitted to the School of Graduate Studies

in Fulfilment of the Requirements for

the Degree Doctor of Philosophy

DOCTOR OF PHILOSOPHY (2022)   McMaster University

Department of Chemical Engineering   Hamilton, Ontario

TITLE: Flexible Nanoscale Composites with Co-Continuous Morphology Prepared by Controlled Cavitation of Thermoplastic Materials and In Situ Polymerization of Conductive Networks

AUTHOR: Anton B. Kornberg

                M.A.Sc. (McMaster University, Canada)

SUPERVISORS: Dr. Shiping Zhu

                Dr. Michael R. Thompson

NUMBER OF PAGES: XVII, 151

LAY ABSTRACT

We have been using flexible conductors for various technological needs: in stretchable displays, wearable sensors, pacemakers, neuroprosthetic implants, and robotics actuators, for example. This thesis project aims to employ a combination of chemical and physical methods to create such conductors that exhibit both flexibility and high electrical conductivity, two properties that are usually difficult to conjoin in a single material, especially in a commodity resin. In the presence of certain liquid media and stretching forces, channels passing through an otherwise non-functional polymer can be created, and by polymerizing in this open space, a conductive network can be formed. The internal structure of a thermoplastic or elastomer has a noticeable effect on the channels formed, which was used in this project to control the final properties of newly created high-value materials, such as conductivity and mechanical behavior.

ABSTRACT

For the purpose of creating inexpensive micro- and nano-scaled network structures of ion- or electron-conductive nature without significant deterioration to the inherent mechanical nature of a commodity thermoplastic or elastomer, a novel investigation was undertaken to use controlled cavitation in the matrix of a commodity polymer. To thoroughly examine the capabilities of this approach with cavitation, the initial morphology of the matrix was varied based on the distribution and structure of its crystalline phase. This action of significant cavitation intensification created a void space within which a secondary polymer network of unique functionality could be introduced. The preliminary experiments showed that the approach under exploration was able to incorporate a continuous ion-conductive network into a polyethylene matrix, with remarkably minor losses in its mechanical properties despite the soft gel-like nature of the new polymer phase. Control over the resulting matrix morphology was gained by varying experimental conditions, such as applied pressure and degree of matrix elongation. The frequency of interface defects, on which transverse crazes were initiated, was increased by expanding the crystal-amorphous boundary area. The reactive polymerization solution, while penetrating the matrix, lowered the energy of the inner surface of the emerging crazes, thereby influencing the channels by which it penetrated. Upon polymerization and soaking with an electrolyte, a continuous conductive acrylic hydrogel now formed an internal network in the polyethylene specimen. The resulting material displayed ion conductivity approaching that of the pure acrylic hydrogel while its modulus declined by only 12%.

The continued experiments examined the creation of a continuous nanoscaled network in an olefinic matrix to impart it with higher value-added functionality, in that case, potentially

combined ion and electron conductivity. Such structures were fabricated based on the same procedure in a high-pressure reactor by stretching polyethylene films while immersing them in an emulsified medium of aniline in chloroform, which resulted in the formation of crazes filled with doped polyaniline. The important element to these experiments was the pre-compounded addition of synthesized polyaniline fibers as a nucleating agent in the polyethylene matrix, which reduced the size of its crystallites and subsequently enhanced the material conductivity by acting as nodes to the emerging polyaniline network synthesized withing the deformation-induced crazing. Excessively high craze frequency was not desirable since it resulted in a decrease in the craze diameter, making it difficult for the polyaniline emulsion droplets to penetrate the matrix.

The final part of the work was focused on alternative matrix materials, such as polyolefin elastomers (POE), which could increase the flexibility of a resulting conductive materials. The experiments aimed at studying the effect of initial domain structure on cavitation behavior with three different POEs and, accordingly, characterize their resulting conductivity. Successful materials were demonstrated, though only after overcoming their excessive elastic recovering which would otherwise collapse the craze voids before the secondary polymer phase could permanently established itself as a conductive network.

The results presented in this study demonstrate the capability of controlled crazing through morphological tuning to create inexpensive materials for battery and flexible electronics manufacturing, where conductive polymer composites are widely adopted.

ACKNOWLEDGMENTS

I am deeply indebted to my supervisors, Dr. Shiping Zhu and Dr. Michael Thompson. They supported my ideas and motivated me in moving forward and completing this thesis, teaching me and providing countless guidance in my research and future career. Thank you for all your support and trust throughout these years. I would also like to thank my supervisory committee members, Dr. Li Xi and Dr. Stephen Veldhuis. They are both very knowledgeable scientists passionate about chemical and mechanical engineering research. I am thankful for their time, patience, thought-provoking questions, and valuable suggestions, which broadened and deepened the understanding of my own research.

I want to extend my gratitude to Tim Stephens, a technician in our department, for his emotional support, incomparable kindness and patience, exciting and valuable discussions about everything in the world, and for sharing his knowledge and experience. My utmost appreciation to you for being a fantastic friend. I am thankful to Lijun Liu, a former PolyMac Zhu research group member. We shared the office and the lab every day. Because of you, I didn't feel alone. From you, I learned a lot about your culture. Thank you for being an amazing neighbor and loyal friend. I would like to thank all my colleagues at the McMaster Manufacturing Research Institute. In addition, I want to thank all the professors of the Department of Chemical Engineering at McMaster University who supported my educational development.

Last but not least, my deepest gratitude goes to my family: my dear wife, Tatiana Kornberg, and my precious and beloved kids, Sasha and Liza Kornberg. You have always been there for me to rely on and get support, courage, and hope.

TABLE OF CONTENT

LIST OF FIGURES

LIST OF TABLES

DECLARATION OF ACADEMIC ACHIEVEMENT

Following the guidelines for preparing a doctoral thesis established by the McMaster University School of Graduate Studies, this research has been organized based on a "sandwich" style, consisting of two published journal articles and one manuscript, written and ready for submission. The research described in this thesis was conducted, interpreted, and written by Anton Kornberg, author of this thesis. The work has been completed under the supervision of Dr. Shiping Zhu and Dr. Michael Thompson; they revised the articles drafts and final version of the thesis. Outlines of authors' contributions are provided at each chapter's opening statements.

LIST OF PUBLICATIONS

- Kornberg, A.B., Thompson, M.R., Zhu, S., Developing continuous submicron-scale conductive interpenetrating hydrogel network in polyethylene matrices through controlled crazing and polymerization, *ACS, Industrial & Engineering Chemistry Research*, **2020**, 59(14), 6609-6616, DOI: 10.1021/acs.iecr.9b07010.

- Kornberg, A.B., Thompson, M.R., Zhu, S., Flexible conductive substrate incorporating submicron co-continuous polyaniline phase within polyethylene by controlled crazing, *ACS, Applied Polymer Materials*, **2021**, 3(4), 1880-1889, DOI: 10.1021/acsapm.0c01416.

- Kornberg, A.B., Thompson, M.R., Zhu, S., Flexible nanoscale co-continuous structures prepared by controlled crazing of ethylene-octene elastomers and in situ polymerization of conductive networks, *Wiley, The Canadian Journal of Chemical Engineering*, **2022**, DOI: 10.1002/cjce.24796.

1   INTRODUCTION

Polymer composites are being used for an ever-growing number of diverse applications in the microelectronics and biomedical industries due to their remarkable ability to be engineered chemically and structurally at different scale levels, simultaneously combining frequently contradicting properties such as electrical conductivity and elasticity. Such a combination is essential for elements of batteries or wearable electronics[4,5] the devices embedded in moving mechanisms[6] and biological tissues,[7–9] which need to be stretchable and mechanically robust.[10,11]

Previously, the realization of flexible conductive composites has focused on blending a single or hybrid conductive filler into an insulative thermoplastic matrix to achieve suitable electrical percolation. A newly conceived alternative in this thesis relies on the synthesis of ion- and electron-conductive materials in continuous channels formed within the matrix via

controlled cavitation. While applied at the submicron and nanoscale levels, this approach has a greater opportunity of preserving the bulk properties of a matrix and yet adding new properties to the material overall. Due to the co-continuous morphology, a high level of electrical percolation is achieved at a low content of this newly added conductive secondary phase, and the approach of polymerization *in situ* provides a much more flexible and efficient way to design the conductive network. This thesis explores this new fabrication method.

Neglecting a molecular structure, the cavitation of the deformed materials can be generally expressed via the Griffith equation $\sigma_G = \sqrt{E\gamma_{1-2}/r}$,[12] which determines whether a crack will occur under a certain tensional stress σ, depending on the modulus and surface energy of the material, as well as a size of the primary defect, on which the crack is initiated. The parameter σ_G in the formula is the threshold stress by Griffith, which determines whether a crack is initiated from the primary defect of the size r (if the applied tensile stress σ exceeds σ_G), or not (if the applied tensile stress σ does not exceed σ_G). As seen from the equation, the stress σ is directly proportional to the material modulus E and its surface energy γ_{1-2}, and reversely proportional to the size r.

The size r is normally critical to the material's reliability; small defects remain stable and do not lead to crack initiation. However, if the internal surface of a defect is wet by a liquid, the solid-air interfacial energy in the Griffith equation is replaced by the solid-liquid interfacial energy (determined from the Young equation),[13] resulting in a proportional decrease of the threshold stress. Such situations may cause catastrophic product failures if the resulting threshold stress exceeds the stress to which the product is subjected ($\sigma > \sigma_G$). This phenomenon, called the Environmental Stress Cracking (ESC), is considered highly undesired. It occurs while a

structural material absorbs the surrounding liquids through the existing yet stable defects, and experiences crack propagation under mechanical stress.

Over time, the phenomenon has been better understood so as to advantage of them, for example, facilitating machining of hard-to-cut materials by applying suitable cutting fluids. The idea of using the mechanism of controlled cavitation of materials in the presence of liquids and under mechanical stress to create mutually percolating, or so-called co-continuous structures, was originally derived from the earlier works of two investigators, Joffe[14,15] and Rebinder.[16] Joffe observed that the brittle crystalline materials become ductile while immersed in water. Rebinder found that certain liquids, while applied to the surface, could affect the microhardness of many materials, making them compliant. Such phenomena, as it later turned out to be of a surface nature, became known as the Joffe-Rebinder effects.[17]

In the case of the thesis research, crack initiation was also a beneficial process. In macromolecules, cracks are stabilized by the backbone chains being drawn from the undeformed surrounding volume and grouped into perpendicular strands called fibrils. Such cracks are denoted as crazes. The structure of crazes prevents severe material damage but results in cavitation. The fibrils function as reinforcing beams, attempting to preserve original mechanical properties and transmitting applied mechanical stress within the sample, thereby distributing load uniformly among defects and causing craze initiation throughout the entire polymer volume. These fibrils do not interfere with liquid movement, which penetrates farther through the growing craze due to capillary pressure and continuing to wet the craze tip.

The liquid medium in the presented approach is a key factor with an almost unrestricted capability of adjustment. It can be subsequently removed from the material volume or replaced by other liquids of a different nature and composition. Non-volatile particles carried by the liquid

can be deposited in the pores' volume, adding functionality to the materials. Alternatively, the liquid can be involved in polymerization, thereby giving us broad opportunities for incorporating a secondary phase of desired functionality, like electrical conductivity, on the nanoscale. Assuming also that the matrix materials can be selected from inexpensive commodity polymers, copolymers, and blends, based on their chemical composition and length of alternating sequences, the approach can be considered quite versatile and affordable for obtaining composites with flexibly adjustable properties.

1.1 RESEARCH OBJECTIVES

The objectives of this thesis can be formulated as follows:

- Examine the effect of the chemical composition and initial morphology of the deformed matrix materials on their mechanical and cavitation behavior during tensile deformation in the different surrounding environments and under different experimental conditions.

- Investigate the efficiency of the initiation of crazes on the emerging cavities, their propagation through the matrix volume, and the degree of electrical percolation of the secondary conductive networks polymerized *in situ* in the crazed space, using direct assessment methods, such as measurement of conductivity.

- Evaluate the effect of cyclic mechanical deformation of the obtained materials on their conductivity.

- Based on the results of the previous steps, evaluate the potential of various matrix polymers for creating nanoscale co-continuous conductive composites. Select a few commodity materials to fabricate such composites by applying the experimental condition determined within the previous steps.

1.2 THESIS ORGANIZATION

This thesis is compiled in a "sandwich" style and includes a literature review on the topic under exploration (Chapter 2) and three published research articles in peer-reviewed journals (Chapters 3-5). The format was brought to a unified style for all articles, with all the figures and tables re-numbered for ease of navigation.

Chapter 1 is the introduction to the thesis topic and defines its main objectives.

Chapter 2 gives a literature review covering conductive polymer composites research. The approach of this thesis is comparatively evaluated against the other methods of fabricating electrically percolating structures reported in the literature, with an emphasis on the significance and potential advantages of the approach, as well as the identification of its current functional limitations.

Chapter 3 is devoted to the creation of an ion-conductive continuous structure derived from acrylic monomer. The monomer acted both as a surface-active liquid medium that contributed to the polyethylene matrix cavitation via crazing and a precursor for the conductive hydrogel that was polymerized within the matrix cavities. The craze frequency was controlled by the addition of a crystallizing nucleating agent to the matrix polymer before its casting, resulting in an increase in its crystal-amorphous interface area, within which the crazes were initiated. Variation of experimental conditions, such as the degree of elongation and applied pressure, produced different morphologies and, therefore, conductivity for the obtained materials. This chapter is a reproduction of the results presented at the 68th Canadian Chemical Engineering Conference (CCEC) 2018 (Toronto, Canada), McMaster University Chemical

Engineering Conference (MUCEC) 2019 (Hamilton, Canada), and published in ACS Industrial & Engineering Chemistry Research, **2020**, 59, 14, 6609–6616 (doi: 10.1021/acs.iecr.9b07010).

Chapter 4 reports on the creation of a continuous network in a polyethylene matrix with imparted electron conductivity derived from doped polyaniline. The experimental conditions, such as elongation, stretching rate, and applied pressure, were mainly adopted from the previous research. The previous acrylic monomer was replaced with an emulsified aniline. The project's major difference was using the pre-synthesized polyaniline fibers, which first acted as nucleating particles in the polyethylene matrix and subsequently merged with the polymerized *in-situ* polyaniline, thereby contributing to the formation of a highly conductive secondary phase. The use of an emulsion as a medium significantly expanded the method's applicability since it potentially enables the transport of various polymerization precursors into the crazed space of the matrix that cannot be delivered as a bulk medium. This chapter is a reproduction of the results presented at the 70th Canadian Chemical Engineering Conference (CCEC) 2020 (Ottawa, Canada) and published in ACS Applied Polymer Materials, **2021**, 3, 4, 1880-1889 (doi: 10.1021/acsapm.0c01416).

Chapter 5 aimed to replace polyethylene with materials from the polyolefin elastomer (POE) family. The study considers the initial morphology of the matrix elastomers, specifically the size and frequency of the crystalline domains distributed in the matrix volume, as a factor that determines the materials' cavitation behavior and, accordingly, the quality of the conductive network polymerized *in situ*. This chapter is reproduced from a newly prepared manuscript for the peer-reviewed journal Polymer.

Chapter 6 is the conclusion of the thesis that summarizes the authors' contributions and outlines the idea for future research.

1.3   REFERENCES

(1)   Chortos, A.; Bao, Z. Skin-Inspired Electronic Devices. *Materials Today* **2014**, *17* (7), 321–331. https://doi.org/https://doi.org/10.1016/j.mattod.2014.05.006.

(2)   Graz, I.; Krause, M.; Bauer-Gogonea, S.; Bauer, S.; Lacour, S. P.; Ploss, B.; Zirkl, M.; Stadlober, B.; Wagner, S. Flexible Active-Matrix Cells with Selectively Poled Bifunctional Polymer-Ceramic Nanocomposite for Pressure and Temperature Sensing Skin. *J Appl Phys* **2009**, *106* (3), 034503. https://doi.org/10.1063/1.3191677.

(3)   Reich, S.; Burgard, M.; Langner, M.; Jiang, S.; Wang, X.; Agarwal, S.; Ding, B.; Yu, J.; Greiner, A. Polymer Nanofibre Composite Nonwovens with Metal-like Electrical Conductivity. *npj Flexible Electronics* **2018**, *2* (1), 5. https://doi.org/10.1038/s41528-017-0018-5.

(4)   Simon, D. T.; Kurup, S.; Larsson, K. C.; Hori, R.; Tybrandt, K.; Goiny, M.; Jager, E. W. H.; Berggren, M.; Canlon, B.; Richter-Dahlfors, A. Organic Electronics for Precise Delivery of Neurotransmitters to Modulate Mammalian Sensory Function. *Nat Mater* **2009**, *8* (9), 742–746. https://doi.org/10.1038/nmat2494.

(5)   Simon, D. T.; Larsson, K. C.; Nilsson, D.; Burström, G.; Galter, D.; Berggren, M.; Richter-Dahlfors, A. An Organic Electronic Biomimetic Neuron Enables Auto-Regulated Neuromodulation. *Biosens Bioelectron* **2015**, *71*, 359–364. https://doi.org/10.1016/J.BIOS.2015.04.058.

(6)   Jonsson, A.; Song, Z.; Nilsson, D.; Meyerson, B. A.; Simon, D. T.; Linderoth, B.; Berggren, M. Therapy Using Implanted Organic Bioelectronics. *Sci Adv* **2015**, *1* (4), e1500039. https://doi.org/10.1126/sciadv.1500039.

(7)   Savagatrup, S.; Printz, A. D.; O'Connor, T. F.; Zaretski, A. V; Lipomi, D. J. Molecularly Stretchable Electronics. *Chemistry of Materials* **2014**, *26* (10), 3028–3041. https://doi.org/10.1021/cm501021v.

(8)   Hammock, M. L.; Chortos, A.; Tee, B. C.-K.; Tok, J. B.-H.; Bao, Z. 25th Anniversary Article: The Evolution of Electronic Skin (E-Skin): A Brief History, Design Considerations, and Recent Progress. *Advanced Materials* **2013**, *25* (42), 5997–6038. https://doi.org/https://doi.org/10.1002/adma.201302240.

(9)   Griffith, A. A.; Gilman, J. J. The Phenomena of Rupture and Flow in Solids. *Transactions of the ASM* **1968**, *61*, 855–906.

(10)   Owens, D. K.; Wendt, R. C. Estimation of the Surface Free Energy of Polymers. *J Appl Polym Sci* **1969**, *13* (8), 1741–1747. https://doi.org/10.1002/app.1969.070130815.

(11)   Joffe, A. F.; Kirpitschewa, M. W.; Lewitzky, M. A. Deformation Und Festigkeit Der Kristalle. *Zeitschrift für Physik* **1924**, *22* (1), 286–302. https://doi.org/10.1007/BF01328133.

(12)   Joffe, A. F.; Loeb, L. B. *The Physics of Crystals*; McGraw-Hill, 1928.

(13)   Rebinder, P. A. Effect of Surface Energy Changes on Cohesion, Hardness, and Other Properties of Crystals. In *Proceedings of the 6th Physics Conference*; 1928; p 29.

(14)   Ciftan, M.; Saibel, E. Rebinder Effect and Wear. *Wear* **1979**, *56* (1), 69–80. https://doi.org/10.1016/0043-1648(79)90007-3.

2   LITERATURE REVIEW

Polymer circuits are often desirable for providing a combination of conductivity and flexibility. However, intrinsically conductive materials are usually brittle and rigid; large deformations will damage their structure, making the desired properties fundamentally complex to combine into a single material. As such, pure materials are rarely used individually and are usually incorporated into a flexible substrate to form numerous conductive pathways, which enables the material's electrical properties without sacrificing its mechanical properties. These conductive network materials offer flexibility but are often expensive since they need high concentrations of the expensive conductive polymer for a continuous pathway and often use costly polymers for the flexible matrix as well (though commodity polymers are attracting new attention).

The electrical performance of these conductive network materials is highly dependent on the secondary phase morphology, particularly whether the phase emerges as a continuous network within the matrix polymer. When the degree of interconnection of individual conductive domains reaches a specific critical value, the originally insulative material becomes a conductor, with an increase in conductivity by several orders of magnitude. This phenomenon is commonly referred to as overcoming the percolation threshold. Additional growth in the frequency of domain intersections promotes the establishment of additional electrical pathways, resulting in a gradual increase in conductivity until a saturation plateau is reached.

There are two essential strategies to produce electrically conductive composites with a polymer matrix: filling the matrix with conductive particles or synthesizing a conductive phase directly within the matrix. These will be discussed as follows.

2.1   FILLING THE MATRIX WITH CONDUCTIVE PARTICLES

The incorporation of conductive particles is a conventional approach to impart electrical properties into insulative matrices. Due to their ease of processing, lower price, tunable mechanical characteristics, and capacity to survive high flexural stress with negligible impact on electrical performance, these materials have found wide applications for antistatic films, electromagnetic shielding, and touch sensors.[18–20]

Melt compounding is the conventional well-studied method for producing various polymer hybrids with conductive particles. Unfortunately, since the particles form a randomly organized network, the method implies a high content of filler is required to achieve high conductivity, affecting the materials' mechanical properties.[21] With spherical particles (e.g., metallic particles, carbon particles, and conductive polymer particles) uniformly distributed in

the matrix, the percolation threshold is overcome at a content of approximately 15-20 vol%; this is close in magnitude to 16 vol%, which is the value predicted by classical percolation theory.[22,23] Materials fabricated using this technology typically demonstrate relatively low conductivity values in the order of 1×10^{-5} S·cm⁻¹.[24,25] Some non-spherical particles, such as carbon nanotubes (CNTs), have an improved interconnecting capability ensured by the higher particle surface area. [26,27] However, materials dispersed in a matrix on this basis of use are also prone to exhibiting a high "practical" percolation threshold due to the tendency of such particles to clump together during processing.

Numerous works show the positive effect of collaborative associations between fillers of different shapes on overall composite conductivity. In the study by Motlagh et al., the authors investigated the simultaneous effect of carbon fibers and carbon black at various ratios.[28] It was found that the two fillers synergistically contributed to the development of a conductive network within the matrix, which enabled lowering the viscosity of the melt and not overloading the processing equipment while maintaining the required level of conductivity. A 5 vol% of conductive fibers admixed with conductive particles, making a total conductive material content of 5 vol% based on the volume of the matrix, was required for electrical conductivity at the level of 1×10^{-3} S·cm⁻¹. The conductivity rapidly increased by incorporating more conductive fibers, 20 vol%, thereby achieving the values in the order of 10 S·cm⁻¹. In the study by Thompson et al.,[29] the authors described the effect of foaming on the electrical conductivity of carbon-filled polyolefin matrices by incorporating both chopped carbon fibers and carbon black. The electrical conductivity increased by an order of magnitude on average, reaching 1×10^{-1} S·cm⁻¹. This conductivity occurred due to the expansion of the gas domains in the filled polymer matrix,

13

which displaced the carbon particles into the inter-domain space, thereby forming dense conducting agglomerates. The agglomerates, in turn, became interconnected with the carbon fibers, resulting in the development of a percolating carbon network.

In the studies by Grunlan et al.,[30,31] and later by Al-Saleh et al.[32] and Pang et al.,[33,34] the authors investigated the concept of a segregated conductive network, originally proposed by Turner et al.,[35,36] which implies that the conductive particles were located at the interface between the individual polymer beads instead of being randomly distributed within the matrix. The approach made it possible to reduce the demand for the conductive material, decreasing the percolation threshold to much lower content values. These structures can be fabricated, for example, by compressing polymer granules, which were preliminarily covered with the conducting particle powder in various ways. Depending on the kind of matrix polymer and technique for depositing the particles onto the granules, such composites can exhibit different conductivity levels and filler volume fractions. As shown in the research by Linares et al., the composites based on polyamide 6,6 and conductive nanofibers, which were prepared by dry grinding, exhibited a conductivity of 1×10^{-4} S·cm^{-1} with a filler volume fraction of 13 vol%.[37] In the research by Zhang et al., the achieved conductivity was 1×10^{-4} S·cm^{-1} with a filler volume fraction of 5 vol% by using polyamide-11 as a matrix material, PANI fibers as a filler, and dry mixing with a subsequent orientation as a technique for the blend preparation. When the fraction of PANI fibers reached 18%, the conductivity increased to 1×10^{-1} S·cm^{-1}.[38] This approach is limited by the melt viscosity of the polymer matrix since the granules should maintain their shape to a degree during compression in order to prevent distorting the conductive coating.

Deposition of latex beads is an alternative method to fabricating such structures. The conductive particles are retained on the bead surface while freeze-drying the emulsion, which allows for a uniform distribution of the particles on the bead surface and eliminates limitations related to the melt viscosity. In the research by Jurewicz et al., the authors obtained composite materials with a conductivity of 1×10^{-4} S·cm⁻¹ for a filler volume fraction of 13 wt.% by incorporating single-walled nanotubes (SWNTs) into complex latex matrices.[39] In the research by Ghislandi et al., the authors used an anionic aqueous emulsion of maleic anhydride-modified polypropylene and multi-walled carbon nanotubes (MWCNTs) as a filler, which allowed them to achieve a conductivity of 1.5×10^{-2} S·cm⁻¹ with a low filler volume fraction of 1 wt%.[40]

Another method is based on the extrusion of two immiscible polymers with a conductive powder, which becomes entrapped at the interface forming a thin conductive layer between the two polymer phases. The method is inexpensive but requires complex adjustments in batch production. In the research by Gubbels et al., the authors processed two "not entirely" miscible polymers, polyethylene, and polystyrene, with the addition of 1 wt.% of conductive particles, which enabled reaching conductivity values in the order of 1.5×10^{-3} S·cm⁻¹.[41] The same approach was applied in the research by Chen et al.[42] The authors demonstrated the effect of carbon nanotube distribution at the interface of an incompatible polycarbonate/acrylonitrile-butadiene-styrene (PC/ABS) blend while it was processed with the addition of maleic anhydride grafted ABS (ABS-g-MA). This method reached a conductivity of 1×10^{-4} S·cm⁻¹ for a filler volume fraction of 2 wt.%.

With unique morphological and mechanical properties, cellulose nanocrystals have revolutionized material science.[43,44] Short cellulose nanocrystals are referred to as CNC, whereas

nanofibrillated cellulose with a diameter of 2-40 nm and a length of more than 1 μm and more,[45] is referred to as NFC.[46] Widely adopted terms rice-like and spaghetti-like for CNC and NFC, respectively, have been given by Cranston.[47] By dispersion in an aniline mixture, nanocellulose fibers can be coated with a thin layer of polyaniline (PANI-NFC) upon polymerization,[48] thereby becoming electrically conductive as well as exceptionally strong and lightweight. According to the research by Guo et al., Young's modulus of pure PANI-NFC can be more than 100 GPa.[49] The composite materials compounded with PANI-NFC can be used, for example, as a basis for wearable sensors or, in the case of aircraft fuselages, used to dissipate a charge caused by lightning strikes while in flight. The relatively small PANI-NFC content required for conductivity is due to its fibers' shape (long and narrow), which ensures a high probability of contact even at relatively low material loading. Thus, in the research by Merlini et al., the polyurethane matrix reinforced with PANI-NFC showed electrical conductivity at a level of 1.5×10^{-1} S·cm^{-1}, with a total fiber content of 31 wt.% based on the mass of the composite material.[50] Due to its natural flexibility, PANI-NFC can be used by itself, without being embedded into the olefinic matrix, demonstrating electrical conductivity up to 6.5×10^{-1} S·cm^{-1}, with a total PANI content of 65 wt.% based on the mass of PANI-NFC.[51] The advantages of PANI-NFC are cost of production and the wide availability of raw materials.

The above approaches have evolved from the blending of conductive particles into a melt to yield modest conductivity levels with relatively low content of conductive materials, but there are some significant limitations. The conductive phase structure is predetermined by the structure of the particles, which limits bulk modification of the phase domain material, for example, chemical crosslinking. The options for chemical compatibility between the phases are

also limited. Depending on the conductive particles' nature, processing such composites can be difficult due to possible mechanical or thermal degradation and, therefore, changes in the functional properties of all components. These limitations are overcome by an alternative approach to producing conductive composites, with the synthesis of a secondary phase directly in the matrix as described below.

2.2   SYNTHESIS OF A CONDUCTIVE PHASE IN A MATRIX

Synthesis of a conductive percolating network within insulative matrices can provide a significant advantage compared to the approach given above, yielding a large reduction in the number of junctions between individual conductive domains, which results in lowering the contact resistance of the system. Among other advantages, one can highlight the exceptional flexibility in chemical choices for the conductive phase and better mechanical properties of the final material by allowing a higher fraction of a matrix polymer in the composite.

2.2.1   *Motivation: tailoring material properties and functionality*

In situ synthesis lends itself well to fabricating materials with ion conductivity for its secondary phase, in which ionic groups must be evenly distributed for the effective transport of counterions when in the presence of an electrolyte. A potential difference in the electrolyte produces an electric field, resulting in ion migration in the direction of the field. The counterions are embedded in the conductive network and remain immobile. This charge transport mechanism imposes certain requirements on the conductive phase, such as continuity and chemical cross-linking, to ensure insolubility and effective retention of the electrolyte. The conductive phase

can also be engineered as either non-selective or selective, which depends on the presence of certain counterions in the network and is ultimately determined by the method of fabrication.[52] Such flexibility can be achieved by *in situ* polymerization of the secondary phase within a matrix.

Electron-conductive conjugated polymers offer a different mode of conductivity for the secondary phase. These polymers are a different class of materials, among which polyaniline (PANI) is the most well-studied. The charge transport in PANI occurs predominantly through the bulk of the conductive material, along the molecular chains, or between the neighbor chains, as shown in Fig. 2-1. However, the synthesis of an ideally continuous PANI network is challenging. Normally, such a network is formed by a multitude of interconnected individual fibers, in which size and spatial distribution ultimately determine the number of interfiber junctions and hence affect bulk conductivity of the system.
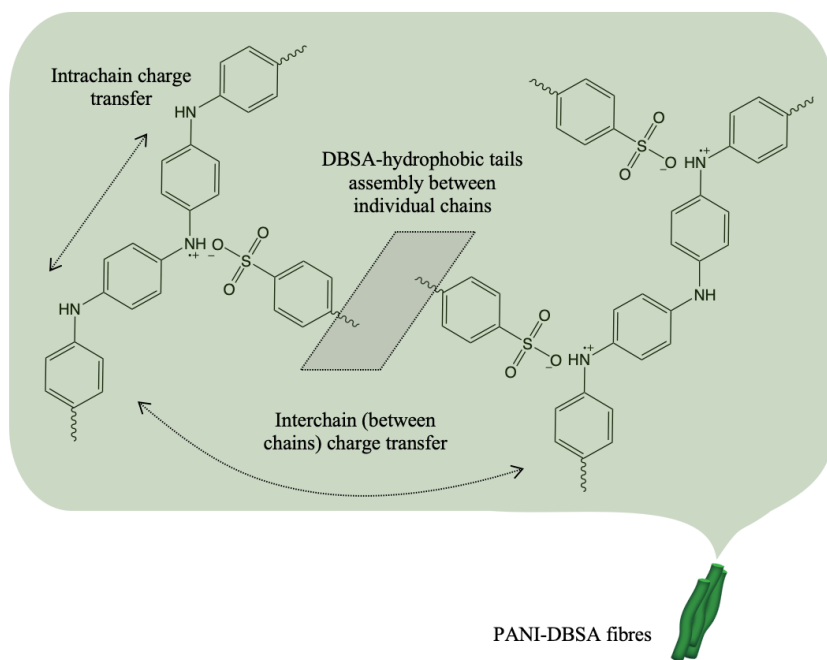
Figure 2-1. Schematic illustration of PANI-DBSA emeraldine salt form organization.

The most widely used method of polyaniline preparation is chemical oxidative polymerization (radical cationic), carried out in an acidic medium in the presence of ammonium persulfate (APS), with the intermediate formation of an anilinium-dopant complex. The reaction conditions determine the polyaniline morphology within the non-conductive matrix, which may be a fiber if prepared as an emulsion. In such a case, fiber length, packing density, and internal fiber structure are essential to gaining bulk conductivity. The polymerization of PANI occurs inside thin and long micelles, resulting in the formation of the fibers, ranging in length from 1 to 10 μm depending on the amount and nature of a surfactant, emulsion medium, oxidative agent, intensity of agitation, reaction viscosity, and other factors.[53]
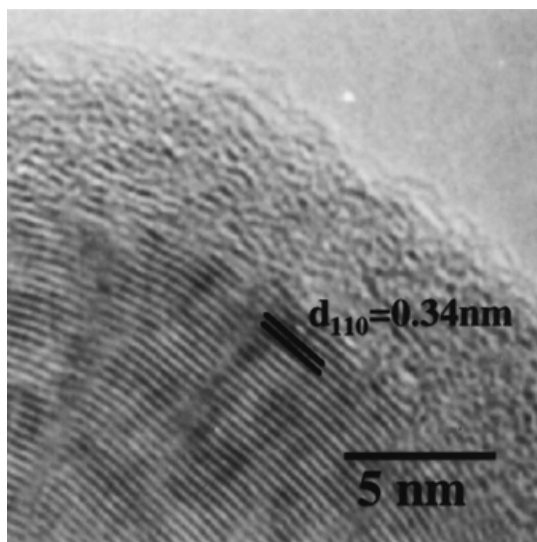
Figure 2-2. HR-TEM image of a PANI fiber cross-section exhibiting concentric the highly conductive crystalline area and the poorly conductive amorphous periphery on edge. Reproduced from ref [1]. Copyright 1999 American Chemical Society.

An individual PANI fiber is highly conductive due to the crystal core (Fig. 2-2), which was demonstrated in the research by Sapurina et al. The authors found that the core demonstrates the highest electrical performance, whereas the amorphous periphery is weakly conductive.[54] *In situ* polymerization of PANI results in forming a substance consisting of densely adjacent fibers. This is due to the high initial affinity of emulsion micelles, the outer layers of which are formed by hydrophobic tails of 4-Dodecylbenzenesulfonic acid (DBSA) molecules. The thickness and degree of amorphousness of the outer fiber layers in such a substance are lower, resulting in the diffuse scattering mechanism of charge transport (so-called resistor-type connection), which reduces contact resistance between fibers, thereby providing higher conductivity.[54] Contact resistance is one of the essentially retarding parameters of the conductive phase of a composite. It should always be considered an integral part of the overall resistance of a material, determined by a combination of the intrinsic polymer domains' conductivity and the conductivity through the interdomain contact area. *In situ* polymerization of a conductive phase is an effective way to increase the contribution of the first characteristic and mitigate the influence of the second characteristic.

2.2.2   *Current progress in the area of in situ synthesis within a matrix*

Over the past decade, many research groups designed composites with a high level of percolation by incorporating secondary polymers into insulative matrices via *in situ* synthesis. There are numerous aspects to consider when developing such materials. As indicated above, the conductive secondary phase should have a dense, continuous morphology to increase the contact area between the individual fibers, which minimizes the phase's total contact resistance.

Also, the total cross-section of the phase must be sufficient to ensure the proper density of charge carriers that pass through the material. At the same time, the matrix material must ensure sufficient mechanical strength and elasticity of the composite, which is achieved due to its volume integrity. In other words, the cross-section of a conductive network, at any location throughout the matrix volume, should be composed of numerous fine channels rather than a few wider channels of the equivalent total area since it will better preserve the original properties of the matrix material. This beneficial combination of electrical and mechanical properties is achieved by having a small total volume and a high degree of branching for the secondary phase; the morphology of voids in the matrix, particular if there are highly branched micro and nanochannels, dictates whether the subsequently introduced secondary phase will percolate throughout the matrix volume.

Numerous methods are known to create the proper internal morphology within a polymer matrix by the subsequent post-polymerization of a conductive network, including soft lithography,[55] self-assembly,[56] patterning by nanomachining,[57] Pickering emulsion templates processing,[58] and wetting of ordered porous templates processing.[59] Among the earlier studies, a microstructure-controlled secondary phase within a polymer matrix was created by photochemical deposition of several thousand hemispherical individual droplets with a diameter of 2.8 μm and at a distance of 3.6 μm between their centers.[60] This enabled the fabrication of the fiber chemical sensors to detect oxygen and changes in pH with subsecond response times by polymerizing a chemically sensitive phase based on fluorescein within the obtained matrix.

Hydrogels, usually a basis for conductive secondary phase fabrication, can also be used as a high-quality matrix material. Particular interest in hydrogel matrices derives from the feature that they can be covalently grafted or electrostatically adhered by hydrogen bonding to a

secondary phase due to the high density of functional groups. In research by Tang et al., the authors obtained conductive composites based on a PANI network and potassium polyacrylate matrix.[61] The technique used in the experiment was traditional for these types of conductive composites preparation: a synthesized acrylic hydrogel of the given morphology was saturated with an aqueous aniline emulsion, followed by immersing the swollen system in an ammonium persulfate solution and subsequent polymerization to polyaniline. The resulting composites demonstrated electrical conductivity of 1×10^{-3} S·cm^{-1} for a polyaniline fraction of 1 wt.%. It is noteworthy that the authors tested the swollen composites, which gave the conductivity of both phases: polyaniline-electron and hydrogel-ion.

Similarly, in the research by Rivero et al., the authors obtained conductive pressure and microwave-sensitive composites based on a hybrid polyaniline-polypyrrole network and a poly(N-isopropylacrylamide) hydrogel matrix.[62] The incorporation of a PANI network, in addition to imparting conductivity to the matrix, also improved the hydrogel's mechanical properties, significantly increasing its swelling capacity. The resistance of the samples gradually decreased from 22 kΩ to 17 kΩ with increasing compression stress from 0 to 400 Pa.

In the research by Kim et al., the authors obtained conductive composites by electropolymerization of pyrrole within an acrylic matrix that was attached to an electrode.[63] Cyclic voltammograms of the composites showed redox responses similar to those observed for conventional electrophoretically deposited polypyrrole films but with more positive oxidation waves and more negative reduction waves, which can be explained by increased resistance compared to conventional films. The content of polypyrrole in the composites did not exceed 5 wt.%.

Simultaneous polymerization of both matrix and conductive phases is a promising approach to fabricating conductive materials with co-continuous morphology. In 2005, Barbetta et al. reported developing highly permeable microscale composites by polymerizing mutually continuous phases from a so-called high internal phase emulsion (HIPE).[64] The HIPEs are basically formed by a combination of two immiscible recipes for post-polymerization that form a thermodynamically unstable mixture, normally stabilized with a bipolar surfactant (Span 80 or similar),[65] but can also be of a Pickering type.[66] The mechanical and electrical properties, as well as chemical sensitivity, are determined by the polymerization precursors of each fraction. For example, the one forms a mechanically durable scaffold, whereas the second one yields a conductive network. Depending on the emulsion characteristics, the diameter of the secondary phase channels can vary from 1 to 100 μm, resulting in an interfacial area of up to 700 $m^2 \cdot g^{-1}$.[64] The composites obtained by the HIPEs method can yield a conductivity of 1×10^{-2} S·cm^{-1} for a secondary phase material fraction of 1 wt.%.[67] Extrusion is effectively used for the homogenization of HIPEs. In the research by Zhou et al., the authors applied a miniature twin-screw extruder with a customized circulation slot, which elevate the performance of prepared HIPE material.[68]

Composite systems formed by the interlacing of electrically conductive and matrix polymer chains are commonly referred to as interpenetrating polymer networks (IPNs). The main advantage of such composites compared to those considered earlier is that their electrical conductivity is ideally the same through the entire volume of the sample and in all directions. In the research by Min, a poly(vinyl alcohol) matrix was treated with concentrated pyrrole vapour followed by polymerization to polypyrrole. The electrical conductivity of the obtained

composites was at the level 5×10^{-3} S·cm^{-1} for a polypyrrole fraction of 6.5 wt.%. The author investigated a cross-section of the obtained composite and confirmed the presence of an interpenetrating polymer network.

In the research by Li et al.,[69] the authors produced a composite with nanoscaled structures for the secondary phase by templating polystyrene with porous silica obtained by anodic electrochemical etching of crystalline silicon wafers. After removing the template by chemical dissolution, polystyrene replicated the nanostructured morphology of the silica matrix. It was used as a scaffold for tissue engineering by polymerizing ion-conductive materials in the scaffolds' porous space. Due to the exceptional density of produced conductive channels, and depending on the choice of secondary phase material, these composites can yield a high conductivity, up to 1.1 S·cm^{-1} with the use of poly(3,4-ethylenedioxythiophene) (PEDOT).[70]

One of the most common and cost-effective methods used to produce matrices on the nanoscale is electrospinning. With this method, three-dimensional fiber networks are created from polymer solutions or melts, reaching diameters down to a few nanometers and surface-volume ratios that are 1000 times greater than microfibers.[71,72] Electrospinning can be carried out by various techniques, including those that allow the production of multiphase fibers in a one-step operation. For example, a coaxial capillary system with two channels produces uniform nanofibers from two polymer sources. By this method, two otherwise poorly compatible polymers form a well-blended homogeneous material.[73] Another setup utilized several syringes with only one outlet valve, producing multi-component nanofibers consisting of semiconducting polymer and durable mesoporous matrix.[74] Electrospinning can also be combined with simultaneous polymerization of a secondary phase. For example, in the research by Xie et al.,[75]

the authors obtained the nanostructured electron-conductive composite by a combination of electrospinning of poly(ε-caprolactone) (PCL) and poly(L-lactide) (PLA) and aqueous *in situ* polymerization of polypyrrole (PPy). Likewise, in the research by Kyung Hwa Hong et al.,[76] the authors reported obtaining conductive composites prepared by a combination of electrospinning of nylon-6 nanofibers and *in situ* polymerized polyaniline conductive layer on the fibers' surface. The material conductivity reached 1.8 S·cm⁻¹ by this method, with a secondary phase material fraction of 1 wt.%.

2.3   MECHANICALLY AND ENVIRONMENTALLY INDUCED CONTROLLED CRAZING AS A METHOD OF MATRIX CAVITATION

An alternative approach to dispersing the conductive phase within a matrix is to purposely deform the matrix, thereby creating a void space and filling that space with a conductive material. This is the foundational principle of this thesis. From a practical standpoint, we have developed electron and ion conductive composites based on different olefinic matrices by simultaneously applying their mechanical and environmental cavitation.

Since the creation of the void space is preferentially done mechanically with semicrystalline polymers, their deformation response to applied stress will be based on both crystalline and amorphous phases present. The variety of polymer crystal structures, as well as the complexity of the internal mechanical and interfacial processes caused by their deformation, have been the subject of numerous studies and reviews.[77–82] According to the literature, the processes that accompany crystalline polymers' deformation are very diverse and include expansion, slip, lamellas bending and reorientation, fragmentation, micro-fibrillation, local melting, martensitic transformations, crystallization under stress, cavitation, etc. However, to

preserve the matrix's physical and mechanical properties, the deformation in its crystalline areas should be suppressed as much as possible. From a practical point of view, the most interesting is Galeski and Pawlak's research,[79,83–91] which covers the phenomenon of cavitation during deformation in polymers at the early stages of yielding in great detail. The authors studied the cavitation mechanism that starts in the amorphous polymer areas, with the subsequent gradual involvement of the crystalline fraction if the polymer continues to undergo stress. But the stress required for amorphous phase deformation is 2% to 10% of the stress needed to deform the crystalline phase, as found by Peterson and Lindenmeyer,[92] and later confirmed by Bartczak et al.[93–95] This observed nature prevents significant deformation of the crystalline fraction under normal conditions. By varying the size and number of crystals present, the polymer's mechanical response can also be changed over a wide range. Nucleating agents mixed in the polymer and immersion of the sample in a surface-active liquid media control and helps preserve the crystalline phase integrity during this deformation process, and are discussed in this chapter.

Crazing, as a special case of deformation occurring within the amorphous phase of a semicrystalline polymer, has been well studied to date. Crazes are localized zones of deformation that resemble cracks oriented perpendicular to the tension axis. Unlike a crack, however, a craze is a relatively rigid system and can transmit stresses due to the presence of fibrils that connect its internal surfaces. According to Kramer, the fibrils typically have a diameter of 5 to 50 nm, with the interfibrillar distance varying from 20 to 60 nm, and the volume fraction of the fibrils can reach up to 50% of the volume associated with the craze.[96] Additionally, so-called secondary fibrils emerge perpendicular to the primary fibrils and connect them, increasing craze rigidity.

From the beginning of sample plastic deformation, crazing proceeds in several stages, which cannot be clearly isolated from each other since they occur simultaneously, and the

experimental results reflect their combined effect. The first stage is craze initiation and sometimes called craze nucleation. It was well-described in the research by Bucknall[97] that the initiation of crazes is associated with defects or inhomogeneities in the bulk or surface of a polymer part. The highest frequency of crazes is achieved at the boundaries between the crystalline and amorphous phases, where voids are formed in large numbers during the crystallization of a polymer, as shown in Kornberg's preliminary experiments (Fig. 2-3).
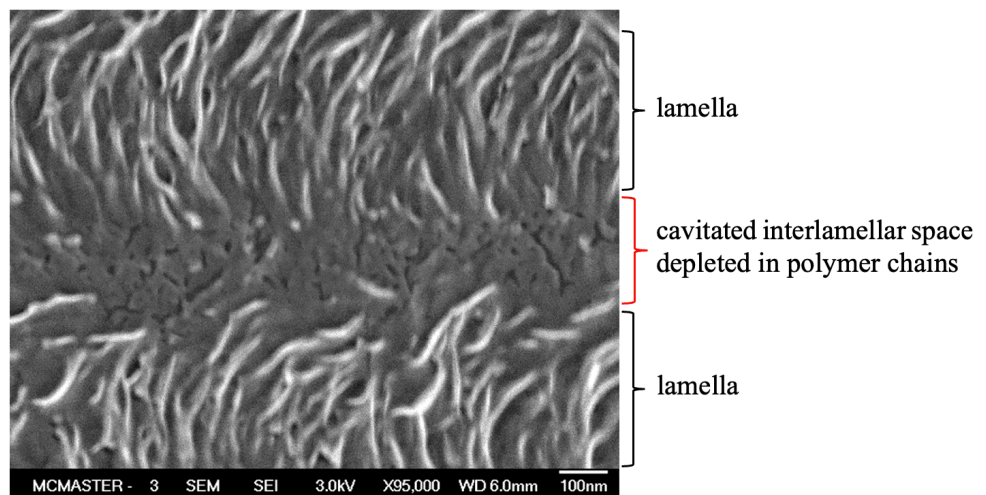
Figure 2-3. Cavitation of interlamellar space due to depletion of polymer chains.

The formation of such defects is previously described in detail in the research by Piorkowska et al.[98] During cooling down, polymer chains with higher content of defects are expelled from growing crystals. Also, the growing crystals form intercrystalline isolated pockets, thereby preventing further inflow of the melt. Since the melt continues to be spent on crystal growth, its exhaustion results in the formation of voids.

By expanding the crystal-amorphous interfacial area, thereby increasing the number of voids, it is possible to obtain a highly dense and branched cavitated morphology. This, in turn, can be achieved by reducing the size of crystals by adding nucleating particles into a polymer melt or solution during sample preparation. A nucleating agent is a substance of organic or inorganic nature with a melting point higher than that of the matrix polymer. It is also chemically inert towards the matrix polymer and does not dissolve in it. Nucleating with particles results in athermal nucleation, i.e., nucleation at approximately the same time within the whole polymer volume. Once the nuclei are formed (primary nucleation), they will propagate in radial directions (secondary nucleation), forming spherulites. The spherulites grow until they impinge on neighboring spherulites. Due to this mechanism, the introduction of nucleating particles results in the formation of a larger number of spherulites of approximately comparable size, yielding large interspherulitic areas with a highly developed crystal-amorphous interface.

The implications are that a polymer samples' initial structure is critical since it ensures the primary crazes' frequency and uniformity of distribution over the sample. Polyethylene, polypropylene, and other olefinic materials can be effectively cavitated by this crazing mechanism. Their crystallinity ensures a highly developed crystal-amorphous interface on which primary voids are concentrated.

In recent years, the development of mechanophores, molecules that are specifically engineered to switch their chemical composition in response to applied stress, can potentially open up new possibilities for determining the craze nucleation points. In particular, in the research by Li et al., mechanophores that change color or emit light were used to map the build-up of stress in specific locations in the polymer volume under deformation.[99] Fluorophores switched with mechanical stress can be considered the most sensitive among other

mechanophores. Due to the intrinsically good signal-to-noise ratio of fluorescence measurements, the fluorophores develop their full potential at relatively low concentrations. It enables to use of only a small amount of fluorophore-linked polymer embedded into the investigated matrix polymer while the mechanical properties of the resulting composite remain reasonably unchanged.[100]

After initiation, the next stage is the growth of crazes in the direction perpendicular to the sample drawing axis.[101–104] This stage lasts until individual crazes or their ensemble grows through the entire cross-section of the sample. In this thesis, a polymer' capacity to form continuous submicron channels will be used for an introduced secondary phase to penetrate throughout a sample's volume to add conductivity to the original matrix material. Due to these channels' morphological stability, which is ensured by the presence of perpendicularly oriented fibrils,[105] such two-phase materials can substantially retain much of the mechanical properties associated with the matrix polymer.

The presence of a liquid medium distinguishes the crazing method under exploration from conventional dry drawing. Such a medium into which the sample is immersed during deformation works both as a surface-active agent influencing deformation and can act as a precursor for polymerization. As reported by Bucknall,[97] the primary voids' diameter is one of the decisive factors in craze initiation and subsequent propagation. Therefore, the deformation of the sample must be carried out under such conditions so that the liquid reaches the local deformation zone at the craze's tip. The critical parameters taken into account in this research are the tensile strain rate (0.03 mm·min⁻¹ or lower), the sample's thickness (110±10 μm), and the high affinity of a liquid medium with a polymer matrix.

The third stage is the widening of existing crazes along the drawing axis, with a subsequent further drawing of the fibrils. Bucknall[97] points out that at this stage, through the mechanism of fibrillation, a newly formed craze can increase in thickness by a factor of more than 100. If the sample elongates only due to the mechanism of craze widening, this will eventually lead to the depletion of chains and the fibrils' scission. In the presence of a liquid, however, the craze tip's surface energy is decreased, which facilitates its opening. It is useful to note that polymer contact with any liquid promotes the new surface formation, which can be observed via Environmental Stress Cracking (ESC), and is described in the research by Bernier and Kambour.[106] The phenomenon is observed even at reducing temperatures when samples are drawn in an atmosphere of high boiling gases such as carbon dioxide, provided that the glass transition temperature of the polymer remains below ambient. As a result, the gas liquefies and is deposited on the internal cavities of the sample. Nevertheless, the greater the compatibility of the penetrating liquid with the matrix polymer, the less energy is required for craze growth. With a sufficient decrease in this energy threshold, fibrillation can be largely suppressed while simultaneously increasing the frequency of newly formed crazes, due to which the elongation of the sample predominantly occurs. The inner diameter of the resulting channels remains small, which contributes to higher capillary pressure and, therefore, maintains effective penetration of the liquid to the matrix. Elevating the system pressure can increase the efficiency of delivering a liquid medium into the disclosing space after the capillary pressure is dropped due to the crazes' widening.

The possibility of functionalization of a liquid medium and its immobilization within a matrix, if the medium at the same time is a mixture of polymerization precursors, could be a vital advantage of the method. This enables to form a continuous secondary phase of a given nature,

to impart the matrix with value-added functionality, in particular, to impart to it ion or electron conductivity. In our early experiments, the polyethylene films gained additional hardness and wear resistance via polymerization of styrene in which the samples were preliminarily deformed. In subsequent studies, olefinic matrices were given ion and electron conductivity due to the use of media that consisted of polyacrylic hydrogel and polyaniline precursors, respectively.

2.4   SUMMARY

In this chapter, the concept of creating conductive polymer composites was reviewed from the perspective of morphological requirements to the conductive phase, the comparison of two different approaches to creating such a phase, compounding vs. *in situ* polymerization, and the newly developed method of polymerization of the secondary phase within a matrix. This new method is preliminarily reliant upon cavitation, mechanically and environmentally, with the use of surface-active liquid media, resulting in the formation of a highly-branched conductive network.

2.5   REFERENCES

(1)   Villmow, T.; Pegel, S.; John, A.; Rentenberger, R.; Pötschke, P. Liquid Sensing: Smart Polymer/CNT Composites. *Materials Today* **2011**, *14* (7–8), 340–345. https://doi.org/10.1016/S1369-7021(11)70164-X.

(2)   Ma, P. C.; Siddiqui, N. A.; Marom, G.; Kim, J. K. Dispersion and Functionalization of Carbon Nanotubes for Polymer-Based Nanocomposites: A Review. *Composites Part A: Applied Science and Manufacturing*. Elsevier Ltd October 1, 2010, pp 1345–1367. https://doi.org/10.1016/j.compositesa.2010.07.003.

(3)   Antunes, R. A.; De Oliveira, M. C. L.; Ett, G.; Ett, V. Carbon Materials in Composite Bipolar Plates for Polymer Electrolyte Membrane Fuel Cells: A Review of the Main Challenges to Improve Electrical Performance. *Journal of Power Sources*. Elsevier March 15, 2011, pp 2945–2961. https://doi.org/10.1016/j.jpowsour.2010.12.041.

(4)   Grady, B. P. Recent Developments Concerning the Dispersion of Carbon Nanotubes in Polymers. *Macromolecular Rapid Communications* **2010**, *31* (3), 247–257. https://doi.org/10.1002/marc.200900514.

(5)   Scher, H.; Zallen, R. Critical Density in Percolation Processes. *The Journal of Chemical Physics*. 1970, pp 3759–3761. https://doi.org/10.1063/1.1674565.

(6)   Tang, H.; Chen, X.; Luo, Y. Electrical and Dynamic Mechanical Behavior of Carbon Black Filled Polymer Composites. *European Polymer Journal* **1996**, *32* (8), 963–966. https://doi.org/10.1016/0014-3057(96)00026-2.

(7)   Huang, J.-C. Carbon Black Filled Conducting Polymers and Polymer Blends. *Advances in Polymer Technology* **2002**, *21* (4), 299–313. https://doi.org/10.1002/adv.10025.

(8)   Weber, M.; Kamal, M. R. Microstructure and Volume Resistivity of Composites of Isotactic Polypropylene Reinforced with Electrically Conductive Fibers. *Polymer Composites* **1997**, *18* (6), 726–740. https://doi.org/10.1002/pc.10325.

(9)   Bauhofer, W.; Kovacs, J. Z. A Review and Analysis of Electrical Percolation in Carbon Nanotube Polymer Composites. *Composites Science and Technology* **2009**, *69* (10), 1486–1498. https://doi.org/10.1016/j.compscitech.2008.06.018.

(10)   Kotov, N. A. Carbon Sheet Solutions. *Nature* **2006**, *442* (7100), 254–255.

(11)   Motlagh, G. H.; Hrymak, A. N.; Thompson, M. R. Properties of a Carbon Filled Cyclic Olefin Copolymer. *Journal of Polymer Science Part B: Polymer Physics* **2007**, *45* (14), 1808–1820. https://doi.org/10.1002/polb.21177.

(12)   Thompson, M. R.; Motlagh, G. H.; Oxby, K. J.; Hrymak, A. N. Multiple Percolation in a Carbon-Filled Polymer Composites via Foaming. *Journal of Applied Polymer Science* **2010**, *115* (2), 646–654. https://doi.org/10.1002/app.30177.

(13)   Grunlan, J. C.; Gerberich, W. W.; Francis, L. F. Electrical and Mechanical Behavior of Carbon Black-Filled Poly(Vinyl Acetate) Latex-Based Composites. *Polymer Engineering and Science* **2001**, *41* (11), 1947–1962. https://doi.org/10.1002/pen.10891.

(14)   Grunlan, J. C.; Gerberich, W. W.; Francis, L. F. Lowering the Percolation Threshold of Conductive Composites Using Particulate Polymer Microstructure. *Journal of Applied Polymer Science* **2001**, *80* (4), 692–705. https://doi.org/10.1002/1097-4628(20010425)80:4<692::AID-APP1146>3.0.CO;2-W.

(15)   Al-Saleh, M. H.; Sundararaj, U. An Innovative Method to Reduce Percolation Threshold of Carbon Black Filled Immiscible Polymer Blends. *Composites Part A: Applied Science and Manufacturing* **2008**, *39* (2), 284–293. https://doi.org/10.1016/j.compositesa.2007.10.010.

(16)   Pang, H.; Chen, C.; Bao, Y.; Chen, J.; Ji, X.; Lei, J.; Li, Z. M. Electrically Conductive Carbon Nanotube/Ultrahigh Molecular Weight Polyethylene Composites with Segregated and Double Percolated Structure. *Materials Letters* **2012**, *79*, 96–99. https://doi.org/10.1016/j.matlet.2012.03.111.

(17)   Pang, H.; Xu, L.; Yan, D.-X.; Li, Z.-M. Conductive Polymer Composites with Segregated Structures. *Progress in Polymer Science* **2014**, *39* (11), 1908–1933. https://doi.org/https://doi.org/10.1016/j.progpolymsci.2014.07.007.

(18)   Kusy, R. P.; Turner, D. T. Electrical Conductivity of a Polyurethane Elastomer Containing Segregated Particles of Nickel. *Journal of Applied Polymer Science*. 1973, pp 1631–1633. https://doi.org/10.1002/app.1973.070170528.

(19)   Malliaris, A.; Turner, D. T. Influence of Particle Size on the Electrical Resistivity of Compacted Mixtures of Polymeric and Metallic Powders. *Journal of Applied Physics* **1971**, *42* (2), 614–618. https://doi.org/10.1063/1.1660071.

(20)   Linares, A.; Canalda, J. C.; Cagiao, M. E.; Ezquerra, T. A. Conducting Nanocomposites Based on Polyamide 6,6 and Carbon Nanofibers Prepared by Cryogenic Grinding. *Composites Science and Technology* **2011**, *71* (10), 1348–1352. https://doi.org/10.1016/j.compscitech.2011.05.008.

(21)   Zhang, Q.; Jin, H.; Wang, X.; Jing, X. Morphology of Conductive Blend Fibers of Polyaniline and Polyamide-11. *Synthetic Metals* **2001**, *123* (3), 481–485. https://doi.org/10.1016/S0379-6779(01)00354-X.

(22)   Jurewicz, I.; Worajittiphon, P.; King, A. A. K.; Sellin, P. J.; Keddie, J. L.; Dalton, A. B. Locking Carbon Nanotubes in Confined Lattice Geometries - A Route to Low Percolation in Conducting Composites. *Journal of Physical Chemistry B* **2011**, *115* (20), 6395–6400. https://doi.org/10.1021/jp111998p.

(23)   Ghislandi, M.; Tkalya, E.; Marinho, B.; Koning, C. E.; De With, G. Electrical Conductivities of Carbon Powder Nanofillers and Their Latex-Based Polymer Composites. *Composites Part A: Applied Science and Manufacturing* **2013**, *53*, 145–151. https://doi.org/10.1016/j.compositesa.2013.06.008.

(24)   Gubbels, F.; Jérôme, R.; Teyssié, P.; Vanlathem, E.; Deltour, R.; Calderone, A.; Parenté, V.; Brédas, J. L. Selective Localization of Carbon Black in Immiscible Polymer Blends: A Useful Tool To Design Electrical Conductive Composites. *Macromolecules*. American Chemical Society March 1, 1994, pp 1972–1974. https://doi.org/10.1021/ma00085a049.

(25)   Chen, J.; Shi, Y. Y.; Yang, J. H.; Zhang, N.; Huang, T.; Chen, C.; Wang, Y.; Zhou, Z. W. A Simple Strategy to Achieve Very Low Percolation Threshold via the Selective Distribution of Carbon Nanotubes at the Interface of Polymer Blends. *Journal of Materials Chemistry* **2012**, *22* (42), 22398–22404. https://doi.org/10.1039/c2jm34295b.

(26)   Rivkin, A.; Abitbol, T.; Nevo, Y.; Verker, R.; Lapidot, S.; Kornberg, A. B.; Veldhuis, S. C.; Zilberman, G.; Reches, M.; Cranston, E. D.; Shoseyov, O. Bionanocomposite Films from Resilin-CBD Bound to Cellulose Nanocrystals. *Industrial Biotechnology* **2015**, *11* (1), 44–58. https://doi.org/10.1089/ind.2014.0026.

(27)   Abitbol, T.; Prevo, B. G.; Galli, C.; Choudhary, S.; Corwin, J.; Villalpando-Páez, F.; Nguyen, L.; Kornberg, A. B.; Villalobos, M.; Veldhuis, S. C.; Cranston, E. D.

Comparison of Nanocrystalline Cellulose and Fumed Silica in Latex Coatings. *Green Materials* **2014**, *2* (4), 206–221. https://doi.org/10.1680/gmat.14.00017.

(28)   Turbak, A. F.; Snyder, F. W.; Sandberg, K. R. Microfibrillated Cellulose, a New Cellulose Product: Properties, Uses, and Commercial Potential. In *J Appl Polym Sci Appl Polym Symp*; 1983; Vol. 37, pp 815–827.

(29)   Moon, R. J.; Martini, A.; Nairn, J.; Simonsen, J.; Youngblood, J. Cellulose Nanomaterials Review: Structure, Properties and Nanocomposites. *Chemical Society Reviews* **2011**, *40* (7), 3941–3994. https://doi.org/10.1039/c0cs00108b.

(30)   Marway, H.; Cranston, E. Investigation of Nanocellulose Mechanical Properties and Interactions in Salt and Surfactant Solutions Measured by Atomic Force Microscopy, 2017.

(31)   Casado, U. M.; Aranguren, M. I.; Marcovich, N. E. Preparation and Characterization of Conductive Nanostructured Particles Based on Polyaniline and Cellulose Nanofibers. *Ultrasonics Sonochemistry* **2014**, *21* (5), 1641–1648. https://doi.org/10.1016/j.ultsonch.2014.03.012.

(32)   Guo, R.; Zhang, L.; Lu, Y.; Zhang, X.; Yang, D. Research Progress of Nanocellulose for Electrochemical Energy Storage: A Review. *Journal of Energy Chemistry*. Elsevier B.V. December 1, 2020, pp 342–361. https://doi.org/10.1016/j.jechem.2020.04.029.

(33)   Merlini, C.; Barra, G. M. O.; Schmitz, D. P.; Ramôa, S. D. A. S.; Silveira, A.; Araujo, T. M.; Pegoretti, A. Polyaniline-Coated Coconut Fibers: Structure, Properties and Their Use as Conductive Additives in Matrix of Polyurethane Derived from Castor Oil. *Polymer Testing* **2014**, *38*, 18–25. https://doi.org/10.1016/j.polymertesting.2014.06.005.

(34)   Luong, N. D.; Korhonen, J. T.; Soininen, A. J.; Ruokolainen, J.; Johansson, L. S.; Seppälä, J. Processable Polyaniline Suspensions through in Situ Polymerization onto Nanocellulose. *European Polymer Journal* **2013**, *49* (2), 335–344. https://doi.org/10.1016/j.eurpolymj.2012.10.026.

(35)   Kontturi, K.; Murtomäki, L.; Manzanares, J. A. *Ionic Transport Processes: In Electrochemistry and Membrane Science*; OUP Oxford, 2008.

(36)   Kornberg, A. B.; Thompson, M. R.; Zhu, S. Flexible Conductive Substrate Incorporating a Submicrometer Co-Continuous Polyaniline Phase within Polyethylene by Controlled

Crazing.   *ACS   Applied   Polymer   Materials*   **2021**.
https://doi.org/10.1021/acsapm.0c01416.

(37)   Mazerolles, L.; Folch, S.; Colomban, P. Study of Polyanilines by High-Resolution
        Electron   Microscopy.   *Macromolecules*   **1999**, *32* (25),   8504–8508.
        https://doi.org/10.1021/ma991290a.

(38)   Sapurina, I. Y.; Shishov, M. A. Oxidative Polymerization of Aniline: Molecular
        Synthesis of Polyaniline and the Formation of Supramolecular Structures. *New polymers
        for special applications* **2012**, *740* (7), 272.

(39)   Jiang, Y.; Tang, N.; Zhou, C.; Han, Z.; Qu, H.; Duan, X. A Chemiresistive Sensor Array
        from Conductive Polymer Nanowires Fabricated by Nanoscale Soft Lithography.
        Nanoscale **2018**, *10* (44), 20578–20586. https://doi.org/10.1039/C8NR04198A.

(40)   Gooneie, A.; Hufenus, R. Hybrid Carbon Nanoparticles in Polymer Matrix for Efficient
        Connected Networks: Self-Assembly and Continuous Pathways. *Macromolecules* **2018**,
        51 (10), 3547–3562. https://doi.org/10.1021/ACS.MACROMOL.8B00585.

(41)   Dae-Geun Choi, †; Sarah Kim, ‡; Eeunsug Lee, † and; Seung-Man Yang*, ‡. Particle
        Arrays with Patterned Pores by Nanomachining with Colloidal Masks. *J Am Chem Soc*
        2005, *127* (6), 1636–1637. https://doi.org/10.1021/JA044578A.

(42)   Blaker, J. J.; Lee, K.-Y.; Li, X.; Menner, A.; Bismarck, A. Renewable Nanocomposite
        Polymer Foams Synthesized from Pickering Emulsion Templates. *Green Chemistry*
        2009, *11* (9), 1321–1326. https://doi.org/10.1039/B913740H.

(43)   Steinhart, M.; Wendorff, J. H.; Greiner, A.; Wehrspohn, R. B.; Nielsch, K.; Schilling, J.;
        Choi, J.; Gosele, U. Polymer Nanotubes by Wetting of Ordered Porous Templates.
        Science (1979) **2002**, *296* (5575), 1997.

(44)   Healey†, B. G.; Walt*, D. R. Fast Temporal Response Fiber-Optic Chemical Sensors
        Based on the Photodeposition of Micrometer-Scale Polymer Arrays. *Analytical
        Chemistry* **1997**, *69* (12), 2213–2216. https://doi.org/10.1021/AC961058S.

(45)   Tang, Q.; Wu, J.; Lin, J. A Multifunctional Hydrogel with High Conductivity, PH-
        Responsive, Thermo-Responsive and Release Properties from Polyacrylate/Polyaniline
        Hybrid.   *Carbohydrate   Polymers*   **2008**,   *73*   (2),   315–321.
        https://doi.org/10.1016/j.carbpol.2007.11.036.

(46)   Rivero, R. E.; Molina, M. A.; Rivarola, C. R.; Barbero, C. A. Pressure and Microwave Sensors/Actuators Based on Smart Hydrogel/Conductive Polymer Nanocomposite. *Sensors and Actuators, B: Chemical* **2014**, *190*, 270–278. https://doi.org/10.1016/j.snb.2013.08.054.

(47)   Kim, B. C.; Spinks, G. M.; Wallace, G. G.; John, R. Electroformation of Conducting Polymers in a Hydrogel Support Matrix. *Polymer (Guildf)* **2000**, *41* (5), 1783–1790. https://doi.org/https://doi.org/10.1016/S0032-3861(99)00308-0.

(48)   Barbetta, A.; Carnachan, R. J.; Smith, K. H.; Zhao, C.; Cameron, N. R.; Kataky, R.; Hayman, M.; Przyborski, S. A.; Swan, M. Porous Polymers by Emulsion Templating. *Macromolecular Symposia* **2005**, *226* (1), 203–212. https://doi.org/10.1002/masy.200550819.

(49)   Hoffmann, H.; Reger, M. Emulsions with Unique Properties from Proteins as Emulsifiers. *Advances in Colloid and Interface Science* **2014**, *205*, 94–104. https://doi.org/10.1016/j.cis.2013.08.007.

(50)   Abdullah; Weiss, J.; Ahmad, T.; Zhang, C.; Zhang, H. A Review of Recent Progress on High Internal-Phase Pickering Emulsions in Food Science. *Trends in Food Science & Technology* **2020**, *106*, 91–103. https://doi.org/10.1016/J.TIFS.2020.10.016.

(51)   Kim, H.; Ahn, K. H.; Lee, S. J. Conductive Poly(High Internal Phase Emulsion) Foams Incorporated with Polydopamine-Coated Carbon Nanotubes. *Polymer (Guildf)* **2017**, *110*, 187–195. https://doi.org/10.1016/J.POLYMER.2017.01.007.

(52)   Zhou, C.; Qiao, M.; Zhang, X.; Zhu, Y.; Zhang, S.; Chen, J. Production of High Internal Phase Emulsion with a Miniature Twin Screw Extruder. *ACS Omega* **2019**, *4* (6), 9957–9963. https://doi.org/10.1021/acsomega.9b01156.

(53)   Li, Y. Y.; Cunin, F.; Link, J. R.; Gao, T.; Betts, R. E.; Reiver, S. H.; Chin, V.; Bhatia, S. N.; Sailor, M. J. Polymer Replicas of Photonic Porous Silicon for Sensing and Drug Delivery Applications. *Science (1979)* **2003**, *299* (5615), 2045 LP – 2047. https://doi.org/10.1126/science.1081298.

(54)   Seo, S.; Kim, J.; Kim, B.; Vinu, A.; Kim, E. Highly Ordered Poly(Thiophene)s Prepared in Mesoporous Silica Nanoparticles. *Journal of Nanoscience and Nanotechnology* **2011**, *11* (5), 4567–4572. https://doi.org/10.1166/JNN.2011.3645.

(55)   Huang, Z. M.; Zhang, Y. Z.; Kotaki, M.; Ramakrishna, S. A Review on Polymer Nanofibers by Electrospinning and Their Applications in Nanocomposites. *Composites Science and Technology* **2003**, *63* (15), 2223–2253. https://doi.org/10.1016/s0266-3538(03)00178-7.

(56)   Xianyan Wang, †; Christopher Drew, †; Soo-Hyoung Lee, †; Kris J. Senecal, ‡; Jayant Kumar, *,† and; Lynne A. Samuelson*, ‡. Electrospun Nanofibrous Membranes for Highly Sensitive Optical Sensors. *Nano Letters* **2002**, *2* (11), 1273–1275. https://doi.org/10.1021/NL020216U.

(57)   Li, D.; Babel, A.; Jenekhe, S. A.; Xia, Y. Nanofibers of Conjugated Polymers Prepared by Electrospinning with a Two-Capillary Spinneret. *Advanced Materials* **2004**, *16* (22), 2062–2066. https://doi.org/10.1002/ADMA.200400606.

(58)   Sudha Madhugiri; Alan Dalton; Jose Gutierrez; John P. Ferraris, and; Jr.*, K. J. B. Electrospun MEH-PPV/SBA-15 Composite Nanofibers Using a Dual Syringe Method. *J Am Chem Soc* **2003**, *125* (47), 14531–14538. https://doi.org/10.1021/JA030326I.

(59)   Xie, J.; MacEwan, M. R.; Willerth, S. M.; Li, X.; Moran, D. W.; Sakiyama-Elbert, S. E.; Xia, Y. Conductive Core–Sheath Nanofibers and Their Potential Application in Neural Tissue Engineering. *Advanced Functional Materials* **2009**, *19* (14), 2312–2318. https://doi.org/10.1002/ADFM.200801904.

(60)   Hong, K. H.; Oh, K. W.; Kang, T. J. Preparation of Conducting Nylon-6 Electrospun Fiber Webs by the in Situ Polymerization of Polyaniline. *Journal of Applied Polymer Science* **2005**, *96* (4), 983–991. https://doi.org/10.1002/APP.21002.

(61)   Peterlin, A. Drawing and Extrusion of Semi-Crystalline Polymers. *Colloid & Polymer Science* **1987**, *265* (5), 357–382. https://doi.org/10.1007/BF01412215.

(62)   Lin, L.; Argon, A. S. Structure and Plastic Deformation of Polyethylene. *Journal of Materials Science* **1994**, *29* (2), 294–323.

(63)   Galeski, A. Strength and Toughness of Crystalline Polymer Systems. *Progress in Polymer Science* **2003**, *28* (12), 1643–1699. https://doi.org/10.1016/j.progpolymsci.2003.09.003.

(64)   Bartczak, Z.; Galeski, A. Plasticity of Semicrystalline Polymers. In *Macromolecular symposia*; Wiley Online Library, 2010; Vol. 294, pp 67–90.

(65)   Geil, P. H.; Ginzburg, B. M. On the Terminology and Structural Interpretation of Stress-strain Curves during Uniaxial Stretching of Soft-chain Semicrystalline Polymers. *Journal of Macromolecular Science, Part B: Physics* **2006**, *45* (2), 291–323.

(66)   Patlazhan, S.; Remond, Y. Structural Mechanics of Semicrystalline Polymers Prior to the Yield Point: A Review. *Journal of Materials Science* **2012**, *47* (19), 6749–6767.

(67)   Pawlak, A.; Galeski, A. Stability of Spherulite Growth Rate. *Journal of Polymer Science Part B: Polymer Physics* **1990**, *28* (10), 1813–1821. https://doi.org/10.1002/polb.1990.090281012.

(68)   Pawlak, A.; Galeski, A.; Rozanski, A. Cavitation during Deformation of Semicrystalline Polymers. *Progress in Polymer Science* **2014**, *39* (5), 921–958. https://doi.org/10.1016/J.PROGPOLYMSCI.2013.10.007.

(69)   Pawlak, A.; Galeski, A. Plastic Deformation of Crystalline Polymers: The Role of Cavitation and Crystal Plasticity. *Macromolecules* **2005**, *38* (23), 9688–9697.

(70)   Pawlak, A.; Galeski, A. Cavitation during Tensile Deformation of Polypropylene. *Macromolecules* **2008**, *41* (8), 2839–2851. https://doi.org/10.1021/ma0715122.

(71)   Pawlak, A.; Galeski, A. Cavitation and Morphological Changes in Polypropylene Deformed at Elevated Temperatures. *Journal of Polymer Science Part B: Polymer Physics* **2010**, *48* (12), 1271–1280. https://doi.org/10.1002/polb.22020.

(72)   Pawlak, A.; Krajenta, J.; Galeski, A. The Crystallization of Polypropylene with Reduced Density of Entanglements. *Journal of Polymer Science Part B: Polymer Physics* **2017**, *55* (9), 748–756. https://doi.org/10.1002/polb.24328.

(73)   Mohanraj, J.; Morawiec, J.; Pawlak, A.; Barton, D. C.; Galeski, A.; Ward, I. M. Orientation of Polyoxymethylene by Rolling with Side Constraints. *Polymer (Guildf)* **2008**, *49* (1), 303–316. https://doi.org/10.1016/j.polymer.2007.11.008.

(74)   Pawlak, A.; Rozanski, A.; Galeski, A. Thermovision Studies of Plastic Deformation and Cavitation in Polypropylene. *Mechanics of Materials* **2013**, *67*, 104–118.

(75)   Pawlak, A.; Galeski, A. Cavitation during Tensile Drawing of Annealed High Density Polyethylene. *Polymer (Guildf)* **2010**, *51* (24), 5771–5779.

(76)   Peterson, J. M.; Lindenmeyer, P. H. Screw Dislocations in Anisotropic Media. *Journal of Applied Physics* **1966**, *37* (11), 4051–4053. https://doi.org/10.1063/1.1707974.

(77)   Bartczak, Z.; Cohen, R. E.; Argon, A. S. Evolution of the Crystalline Texture of High-Density Polyethylene during Uniaxial Compression. *Macromolecules* **1992**, *25* (18), 4692–4704. https://doi.org/10.1021/ma00044a034.

(78)   Bartczak, Z.; Argon, A. S.; Cohen, R. E. Deformation Mechanisms and Plastic Resistance in Single-Crystal-Textured High-Density Polyethylene. *Macromolecules* **1992**, *25* (19), 5036–5053. https://doi.org/10.1021/ma00045a034.

(79)   Bartczak, Z.; Argon, A. S.; Cohen, R. E. Texture Evolution in Large Strain Simple Shear Deformation of High Density Polyethylene. *Polymer (Guildf)* **1994**, *35* (16), 3427–3441. https://doi.org/10.1016/0032-3861(94)90905-9.

(80)   Kramer, E. J. Microscopic and Molecular Fundamentals of Crazing BT - Crazing in Polymers; Kausch, H. H., Ed.; Springer Berlin Heidelberg: Berlin, Heidelberg, 1983; pp 1–56.

(81)   Bucknall, C. B. New Criterion for Craze Initiation. *Polymer (Guildf)* **2007**, *48* (4), 1030–1041. https://doi.org/https://doi.org/10.1016/j.polymer.2006.12.033.

(82)   Nowacki, R.; Kolasinska, J.; Piorkowska, E. Cavitation during Isothermal Crystallization of Isotactic Polypropylene. *Journal of Applied Polymer Science* **2001**, *79* (13), 2439–2448. https://doi.org/10.1002/1097-4628(20010328)79:13<2439::AID-APP1051>3.0.CO;2-#.

(83)   Li, J.; Nagamani, C.; Moore, J. S. Polymer Mechanochemistry: From Destructive to Productive. *Accounts of Chemical Research* **2015**, *48* (8), 2181–2190. https://doi.org/10.1021/acs.accounts.5b00184.

(84)   Göstl, R.; Clough, J. M.; Sijbesma, R. P. Optical Sensing of Stress in Polymers. *RSC Polymer Chemistry Series* **2017**, *2018-Janua* (26), 53–75. https://doi.org/10.1039/9781782623885-00053.

(85)   Argon, A. S.; Salama, M. M. Growth of Crazes in Glassy Polymers. *Philosophical Magazine* **1977**, *36* (5), 1217–1234. https://doi.org/10.1080/14786437708239790.

(86)   Kirloskar, M. A.; Donovan, J. A. Kinetics of Alcohol Assisted Craze Growth in Polycarbonate. *Polymer Engineering and Science* **1987**, *27* (2), 124–130. https://doi.org/10.1002/pen.760270205.

(87)   Marissen, R. Craze Growth Mechanics. *Polymer (Guildf)* **2000**, *41* (3), 1119–1129.

(88) Brown, H. R. A Model of Environmental Craze Growth in Polymers. *Journal of Polymer Science Part B: Polymer Physics* **1989**, *27* (6), 1273–1288. https://doi.org/10.1002/polb.1989.090270607.

(89) Kambour, R. P.; Russell, R. R. Electron Microscopy of Crazes in Polystyrene and Rubber Modified Polystyrene: Use of Iodine-Sulphur Eutectic as a Craze Reinforcing Impregnant. *Polymer (Guildf)* **1971**, *12* (4), 237–246. https://doi.org/10.1016/0032-3861(71)90048-6.

(90) Bernier, G. A.; Kambour, R. P. The Role of Organic Agents in the Stress Crazing and Cracking of Poly(2,6-Dimethyl-1,4-Phenylene Oixde). *Macromolecules* **1968**, *1* (5), 393–400. https://doi.org/10.1021/ma60005a005.

3   DEVELOPING CONTINUOUS SUBMICRON-SCALE CONDUCTIVE INTERPENETRATING HYDROGEL NETWORK IN POLYETHYLENE MATRICES THROUGH CONTROLLED CRAZING AND POLYMERIZATION

In this chapter, we examine the creation of a submicron interpenetrating network in a commodity polymer to impart it with value-added functionality, in this case, ion-conductivity. Such structures were fabricated in a high-pressure reactor, by stretching polyethylene films while immersing them in acrylic monomer, resulting in a cross-linked hydrogel. The unique goal of this work was to demonstrate, by simultaneous application of the experimental conditions, that

a percolating secondary phase can be formed in an otherwise low-cost polymer while not losing the polymer's beneficial mechanical properties. Our results show, not exceeding 7 wt.% of the initial sample mass, the hydrogel phase developed conductivity in the alloy nearly equal to that of the pure acrylic hydrogel. The chapter is based on the paper published in ACS Industrial & Engineering Chemistry Research, 2020, 59, 14, 6609–6616 (doi: 10.1021/acs.iecr.9b07010). The permission for this reproduction is granted by the American Chemical Society (ACS).

Author contributions:

The initial idea of this research appeared through valuable and inspiring discussions with Dr. Shiping Zhu and Dr. Michael R. Thompson. I was responsible for designing the experimental hardware, selecting the testing conditions, and conducting the experiment, including preparation of the samples, mechanical trials in a high-pressure reactor, and chemical synthesis. Dr. Thompson and I analyzed the obtained data and prepared the manuscript for the journal. Dr. Zhu reviewed the final manuscript before submission.

3.1   ABSTRACT

An approach is described for the synthesis of controlled submicron interpenetrating networks with distinct functional features in commodity polymers, based on a mechanism of crazing and polymerization. In this work, ion conductivity was introduced into polyethylene with only minor losses in its mechanical properties, using a highly branched acrylic hydrogel. Control over the porous network developed in the matrix was gained by the addition of a crystallizing nucleating agent, which was used to increase the number and reduce the size of crystallites.

Variation of experimental conditions, such as the degree of elongation and applied reaction pressure, produced different morphologies and conductivity for the co-continuous alloy. The samples were deformed in a liquid medium that possessed an affinity for the matrix material and acted both as a surface-active agent for the crazing, and as a reactant for the conductive phase. Without pressure, deforming by 100% strain yielded a conductivity of 5.67×10^{-7} S/cm for the polymer specimen. Simultaneously increasing system pressure while constantly straining a specimen enabled further enhancements in conductivity. As a particular example, elongation of 100% and applied pressure up to 2.76 MPa ensured conductivity nearly equal to that of the pure hydrogel at 4.43×10^{-4} S/cm.

3.2   INTRODUCTION

In recent years, hydrogels have attracted significant interest in bioengineering applications, due to their capacity to mimic biological communication. The majority of biological signaling is mediated by ions, and hydrogels function in the same way by transmitting ions via counter-ions embedded in the polymer network. Control over such processes is carried out by adjustable electrical stimuli that release molecules on-demand, with defined intensity and frequency.[7,9,107] However, applications of hydrogels are often limited due to their weak mechanical properties while swollen, which is necessary for their function.[108] In nature, gentle tissues are normally supported by an extracellular fibrous protein framework, and their mechanical properties, therefore, are less critical. Other supporting network structures applicable to synthetic hydrogels have included nanofibers,[109–111] surgical sutures,[112] or highly-porous electrospun matrices,[113,114] all expensive systems to manufacture. The present research investigates a generalized approach for introducing value-added functionality with nano-to-

micron scaled features in a broad range of matrix polymers, by polymerizing a secondary polymer phase within newly created pores produced along crystallite boundaries during plastic deformation. The introduced hydrogel in this case was polymerized within the continuous submicron network that percolated through the matrix, to demonstrate through-plane conductivity, while the matrix itself acted as a mechanically durable scaffold.

The fracture mechanism that is induced in the demonstrated method is similar to the one that occurs naturally during Environmental Stress Cracking (ESC), for which a polymer experiences crack propagation under stress while drawing in a surrounding liquid deeper into the material. This type of chemical-influenced deformation was studied earlier by Bernier and Kambour,[106] and later adopted for practical uses by Volynskii et al.,[115,116] and Rozanski et al.[117] Both of the latter research groups showed that samples subjected to tensile deformation in a liquid media, formed a large number of submicron crazes that percolated through the polymer film. Subsequent studies by Rozanski et al. reported on the significance of crystallinity on the network of crazes by this procedure.[118] The authors investigated the resulting samples by X-ray and thermal analyses, showing that the crystal fraction was unaffected by the deformation.

Attempts to use this mechanism to create two-component systems have been reported earlier. In the study by Weichold et al.[119] and Trofimchuk et al.,[120] the authors used a liquid medium, in which the samples were deformed, as a carrier for non-volatile additives that remained inside the bulk polymer after the medium evaporated. Rukhlya et al.[121,122] used a similar method to fabricate a two-component alloy by deformation of high-density polyethylene (HDPE) matrices within a solution of polyethylene oxide (PEO) in ethanol. The authors varied the deformation regimes, such as the percentage of elongation and deformation rate, and then examined how it affected the volume of absorbed PEO. Those studies did not characterize the

morphology of the alloy nor characterized the extent to which an interpenetrating structure was formed. Yarysheva et al.[123] applied the same technique, adopted from the research of Rukhlya. Using X-ray spectral analysis, the authors showed a uniform distribution of oxygen atoms throughout the bulk volume attributed to the PEO though still there was no consideration whether the filled pores were interconnected or much less, formed a percolating network which would add far more functionality to a material. For all of these reported systems, the viscosity of the fluid was increased by the dissolved or suspended secondary phase which diminished its likelihood of fully penetrating all of the pores created by crazing. It is our belief that *in situ* polymerization of the secondary phase addresses this problem and would allow co-continuous properties to be developed with little loss in the mechanical properties of the matrix.

Therefore, the present research aimed to devise a modified approach based on polymerization to attain a sub-micron interpenetrating structure to introduce new functionality in the final alloy while minimizing mechanical losses. An important criterion for the approach was the monomeric liquid medium, in this case, used to introduce ion conductivity, had to also possess a surface-active functionality with the polyethylene matrix to influence crazing so the process consisted of one step for simplicity. The study examined the extent of longitudinal elongation and reaction system pressure to achieve the chief objectives of a percolating network for the secondary phase.

3.3   EXPERIMENTAL METHODS

3.3.1   MATERIALS

Linear low-density polyethylene (LLDPE LL 8460.29 powder, ExxonMobil Chemical) and titanium dioxide nanoparticles (TiO$_2$ P25 AEROXIDE, Degussa) were used as received. The TiO$_2$ had an average particle size of 21 nm. Acrylic acid (AAc, 99%, Aldrich) was purified of its inhibitor before use. 2,2′-Azobis (2-methylpropionitrile) (AIBN, 98%, Aldrich) was recrystallized from methanol before use. N,N′-Methylenebis (acrylamide) (MBA, 99%, Aldrich) and ethanol anhydrous (EA, ≤0.005% water) were used as received.

3.3.2   PREPARATION OF P(AAC-CO-MBA)

In this study, a cross-linked poly(acrylic acid) was chosen as the model ion-conductive polymer due to its ease of synthesis and high affinity of the acrylic acid monomeric precursor to the matrix polymer (LLDPE). Along with AAc monomer, the recipe included 3 wt.% MBA as the cross-linking agent and 1 wt.% AIBN as the initiator. The resulting mixture was sonicated and cooled down to 0 °C to avoid spontaneous polymerization. Before use as a liquid medium, the recipe was premixed with 30 vol% of EA. This ratio ensured the smallest possible contact angle of 16.1 ± 0.4° to the matrix polymer surface at the highest concentration of AAc.

3.3.3   PREPARATION OF MATRIX SAMPLES

Before use, the LLDPE powder (35 mesh) was premixed with 2 wt.% of TiO$_2$ nanoparticles. Dumbbell-shaped polyethylene samples of 110±10 µm thickness, with the narrow section being 5 mm long and 5 mm wide, were molded in a hot press at 200 °C and 6 bars for 5 minutes and then cooled.

3.3.4   DEFORMATION OF SAMPLES AND POLYMERIZATION IN HIGH-PRESSURE REACTOR
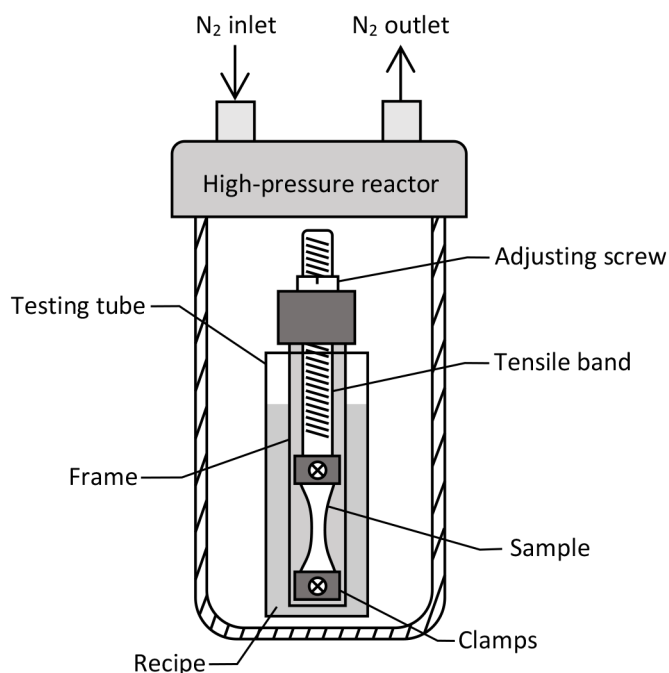
Figure 3-1. Schematic design of the tensile rig while the sample is mounted and immersed in the medium.

A tensile rig was designed to apply uniaxial strain to the samples while immersed in the monomeric medium (Fig. 3-1). The rig was contained inside a high-pressure reactor, which was

frequently depressurized to step-wise deform a sample followed by purging with nitrogen and subsequently pressurizing to an experimentally varied setpoint. For the samples deformed at atmospheric pressure, the reactor was only purged with nitrogen, without pressurization. Step changes in the extent of deformation were done at 0.25 mm per cycle increments, so that the resulting elongation rate was kept constant at 0.03 mm·min⁻¹. The deformation was carried out until the degree of longitudinal elongation reached 25, 50, 75 or 100% strain. Deformation was performed at ambient room temperature. Each set of experimental conditions was applied for a minimum of three repeats.

For polymerization, the reactor containing the tensile rig was moved into an oven set to 80 °C and heated for 3 hrs under the given pressure. Measurements inside the reactor showed that the temperature was equalized with the temperature of the oven after 15 minutes when its internal pressure was zero, and in less time when the pressure was increased. The sample remained under strain and immersed in the same medium. After polymerization, the samples were released from the tensile rig and scrapped clean of any hydrogel at the surface of the sample. Then, the samples were held under vacuum at 40 °C for 24 hours, to remove any monomer residues.

The experimental parameters for these trials are listed in Table 3-1. Samples were named according to the applied pressure (capital letters from A to E, where A is the highest pressure of 2.76 MPa, and F is atmospheric pressure) and the percent strain. For example, the sample denoted as A75 was deformed at 2.76 MPa to 75% strain. Elongation length of a sample was determined at the middle-narrowed part of the dumbbell-shaped sample, since this section experienced the highest stresses. For example, when a sample had elongated by 75% this narrowed region increased in length by 3.75 mm, while the sample increased by 8.75 mm in

total. Samples deformed while immersed in the monomer without any initiator were denoted as "NI".

Table 3-1. Conventional symbols of the samples according to the experimental conditions.

Elongation, % Pressure, MPa (psi)	25	50	75	100
2.76 (400)	A25	A50	A75	A100
2.41 (350)	B25	B50	B75	B100
2.07 (300)	C25	C50	C75	C100
1.72 (250)	D25	D50	D75	D100
1.38 (200)	E25	E50	E75	E100
atmospheric	F25	F50	F75	F100
"no initiator" 2.76 (400)	NI25	NI50	NI75	NI100

3.3.5　ION CONDUCTIVITY MEASUREMENT

After vacuum drying, samples were immersed in a 1M aqueous NaOH solution for 48 hrs, in order to neutralize the carboxylic acid groups. The samples were then washed with deionized water, dried, and weighed. Each dried sample was polished with sandpaper and cropped into a rectangular shape, to avoid ion transport circumventing the intended path through the sample. The resulting rectangular specimen was immersed for 12 hrs in the aqueous NaOH solution again for electrolyte saturation, wiped dry, and then sealed in place by molten wax over the top of a cut-out opening in a polystyrene dish. The dish was filled with aqueous NaOH and was immersed in a dish of a larger diameter, also filled with aqueous NaOH. The design of the measurement cell prevented leaks and guaranteed ion transport only through the embedded specimen.

Resistivity ρ was calculated by the formula $\rho = (R \cdot A)/L$, where R was the measured resistance for DC measurements by an Agilent 34401A 6½ Digit Multimeter. Two electrodes, both of the same area A, were made from copper foil and affixed to both exposed sides of the specimen but not sealed in place so as to hinder electrolyte wetting of the specimen. Technically, the distance between the electrodes was slightly greater than the thickness of the specimen. However, since the R of the electrolyte was much less than that of the specimen, the specimen thickness was taken as dimension L. The DC bulk conductivity σ [S·cm^{-1}] was calculated as $\sigma = 1/\rho$.

Continuous agitation of the cell, as well as the careful maintenance of pH at 13.7 by adding fresh electrolyte, minimized signal drift during the measurement. To maintain the consistency of the results, the R values were always taken ten seconds after the closure of the measurement loop.

3.3.6   MECHANICAL CHARACTERIZATION

Strain-controlled tensile testing was performed using a benchtop Model 3366 Universal Mechanical Testing System with a 5 kN load cell (Instron Corporation; Canton, MA), at ambient room temperature. Before testing, the thickness was measured with a caliper at three points in the narrow sample section. The samples were pulled longitudinally at a crosshead speed of 2.5 mm·min^{-1} until failure.

3.3.7   SURFACE MORPHOLOGY ANALYSIS

Samples were cryogenically fractured in the middle of the narrow section. Micrograph images were obtained by JEOL JSM 7000 scanning electron microscope (SEM). Platinum was used to deposit a conductive layer of 5 nm thickness. After microscopy, the SEM images were processed using ImageJ software (National Institute of Health, U.S.) to determine individual void sizes by detecting their contours based on about five hundred iterations for each image.

3.3.8   ATR-FTIR CHARACTERIZATION

Mid-range infrared spectra from 1000–3500 cm⁻¹ were recorded using a Thermo Nicolet 6700 bench with DTGS detector and diamond-window attenuated total reflectance (ATR) attachment, by scanning 64 times at a resolution of 2 cm⁻¹. The samples were progressively sectioned using a manual rotary microtome (Leica Biosystems) to an ultimate depth of 50 μm (approximately half of the total sample thickness), along the longitudinal axis. Right before scanning, the samples were immersed in deionized water for several seconds. Visible excess water was removed by using the glass surface. Water was absorbed in the acrylate phase, swollen within the void space so that the acrylate polymer was more readily detected in the scans.

3.4   RESULTS AND DISCUSSION

3.4.1   RESULTING MORPHOLOGY

According to several fracture studies,[83,98] primary voids emerge in large quantities at the crystal-amorphous interface due to chain depletion in the amorphous phase during crystallization. Bucknall[97] and later, Pawlak et al.[84] established that cavitation initiated at these primary voids during deformation will ultimately propagate as crazes. These crazes present themselves as a porous network in the deformed material. By extension of these studies,[83,84,97,98] increasing the crystal-amorphous interfacial area should increase the number of primary voids, creating circumstances where an equivalent cross-sectional cavity area is produced by smaller-sized crazes. Hypothetically, sufficiently small crazes should create a space for the conductive secondary phase in our new material with minimal influence on the stiffness of the matrix.

In order to increase the crystal-amorphous interface, the number of crystallites per unit area was increased by adding 2 wt.% of TiO_2 nanoparticles as a crystal nucleating agent during the sample preparation for all trials. Polarized light optical micrographs in Fig. 3-2 show the difference in the crystal structures of pure polyethylene versus polyethylene with added nanoparticles. As a result of the nucleating agent, instead of the large spherulites found in the original material (greater than 10 μm in size), the modified polyethylene matrix contained a larger number of smaller crystallites with sizes of 1 μm or less.

The influence of the crystal structure was noticeable on sample deformation. In preliminary testing, it was observed that only samples with the higher crystal-amorphous interfacial area (Fig. 3-2b) could possibly be stretched uniformly without necking, even for strains beyond the yield point of the matrix. Depending on whether the sample was stretched in

the air or in a medium with surface activity towards the matrix, necking occurred well beyond the yield point or not at all. According to Volynskii et al.,[116] such behavior indicates microfibrillation due to the formation of numerous crazes in the matrix. For the pure polyethylene samples, necking occurred at the yield point with noticeable whitening.
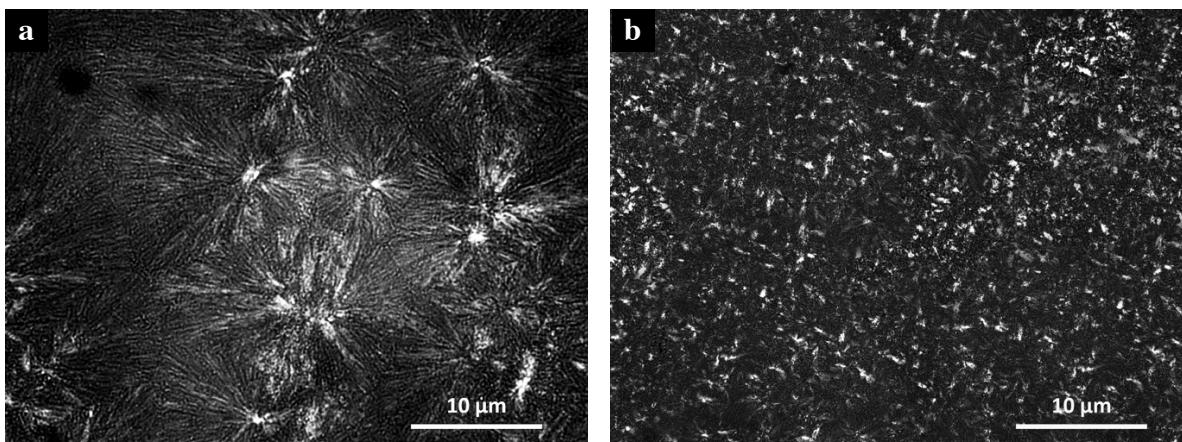
Figure 3-2. Crystal structure of (a) pure polyethylene, and (b) with the addition of 2 wt.% TiO_2 nanoparticles, obtained by polarized light microscopy.

The extent of cavitation in the matrices was examined by SEM in Fig. 3-3, comparing the morphology of F100 (no pressure) and A100 (maximum pressure). Cryo-fracturing was made perpendicular to the sample axis deformation and therefore, the craze fibril draw. Micrographs show randomly selected sections of the fracture surface, at a distance of approximately 10 µm from the edge (actual surface of the deformed sample). The micrograph for F100 shows a well-established arrangement of pores in the fractured plane being retained after deformation and polymerization of the secondary phase. Based on image analysis, the total void area was 35% for F100, with a pore size being in the order of 0.1-1.0 µm in diameter. It is expected that this structure contained some amount of dispersed hydrogel in the pore, though not seen, which

supported the cellular morphology and prevented its reversed deformation after removal from the reaction tensile rig. By contrast, the samples of trials NI (not shown) displayed noticeable shrinkage once removed from the vessel, since the monomer liquid being devoid of initiator, evaporated without forming a hydrogel to support the pores.
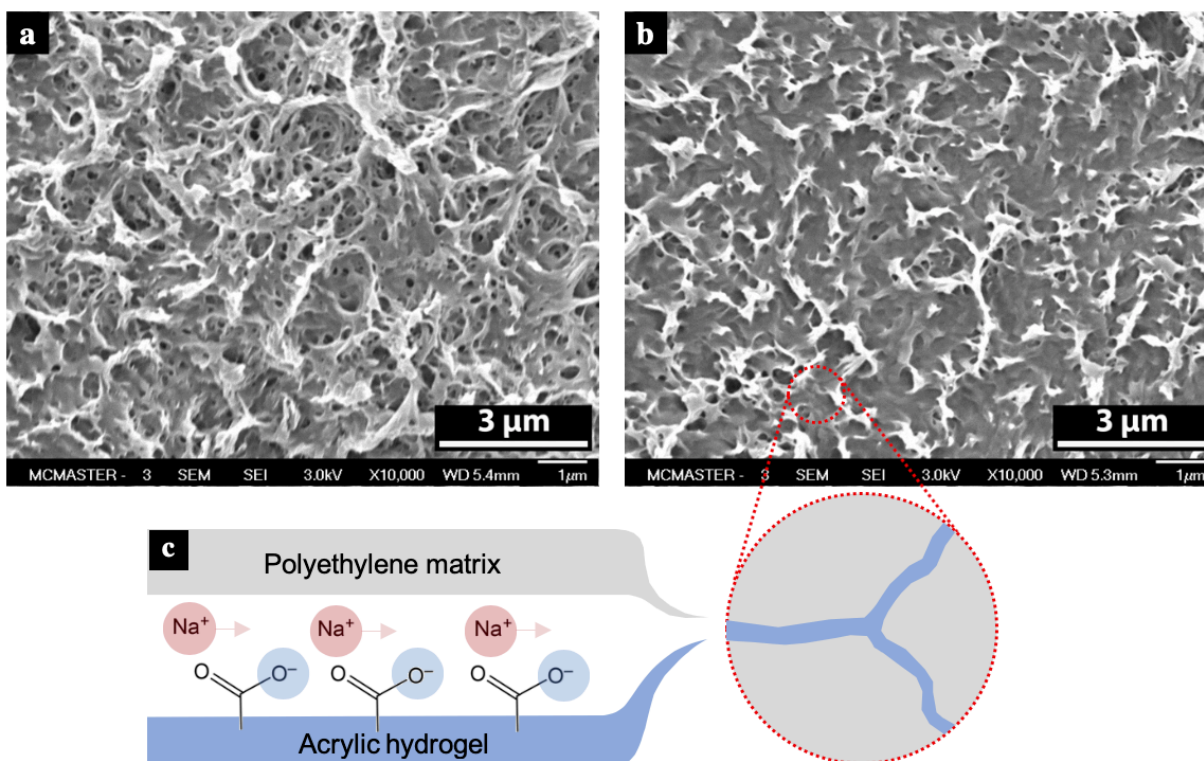
Figure 3-3. Morphology of the samples that were cryogenically fractured normal to the deformation axis: (a) F100, (b) A100, and (c) schematic representation of the ion transport through the matrix.

Unlike F100, A100 was practically devoid of visible porosity in the micrograph, with a total void area calculated at less than 3%, based on image analysis). Fewer fibrils (white protrusions in the micrographs) related to ductile fracture of the polyethylene matrix appeared in A100, replaced

with smoother regions which are believed to correspond to the more brittle dry poly(acrylic acid) phase. It appears that the high applied pressure for this reaction condition provides a more efficient movement of the monomer into the matrix compared to F100.

The micrographs demonstrate consistency in morphology, suggesting uniformity in the network being formed. Such uniformity seen in both samples is consistent with the crazing response to deformation seen by Rozanski et al.,[117] who suppressed gross failure in polymers by exposing them to penetrating liquids while undergoing deformation. The authors showed the positive effect of the liquids' compatibility with the deforming polymers by using hexane and water as the media for polyolefin and polyamide samples, respectively. These observations were taken into account in the present research; the surface energy of matrix polyethylene (0.0353 N·m^{-1} [124]) was quite close to that of the acrylic monomer (0.03 N·m^{-1} [125]).

The effect of liquid on the morphology is explicable from the mechanism of craze formation investigated by Bucknall,[97] according to which the polymer deformation may be accompanied by two processes: initiation of new crazes, and widening (and subsequent fibrillation) of existing ones. The author points out that through the mechanism of fibrillation, a newly formed craze can increase in thickness by a factor of more than 100 while maintaining mechanical stability and not turning into a crack due to the scission of fibrils. Bucknall also explains that the energy required for craze initiation varies with the size of a void, and can be evaluated through the Griffith approach, as a result of which some voids may remain inactive due to their small size. In this case, the sample elongates due to the drawing of fibrils of the existing crazes, which leads to the depletion of chains of the amorphous phase and, ultimately, the samples' failure. In the presence of contact with a liquid, the surface energy of primary voids is decreased, which facilitates their opening. It is useful to note that the contact of polymer with

any liquid promotes the new surface formation, which can be observed via Environmental Stress Cracking. However, the greater the compatibility of the penetrating liquid with the matrix polymer, the less energy that is required for craze initiation. With a sufficient decrease in the energy threshold for the opening of the primary voids, fibrillation can be suppressed with a simultaneous increase in the frequency of the newly formed crazes, due to which the elongation of the sample predominantly occurs. The inner diameter of the resulting channels remains small, which in turn contributes to higher capillary pressure and, therefore, maintains effective penetration of the liquid to the matrix.

Fig. 3-3a shows a collective effect of the expansion of the crystal-amorphous interface followed by a rise in the number of primary voids, while ensuring contact of the matrix polyethylene with the acrylic monomer. The hierarchical porous structure indicates that primary crazes worked as pathways for monomer delivery, which consequently resulted in the initiation of multiple secondary crazes. However, while wetting the inner surface of the polymer, the monomer did not appear to entirely fill the formed crazes, which is also seen in Fig. 3-3a. The elevating system pressure was necessary to increase the amount of monomer, allowing more efficient use of the emerged space for the formation of the secondary phase, which is shown by the nearly non-porous cross-section in Fig. 3-3b.

3.4.2   MASS CHANGE

Fig. 3-4 presents the sample mass change for six different pressures, including the case in which the pressure was not applied. In each case, elongations of 50, 75, and 100% are reported. Samples elongated by 25% never showed a statistically significant mass increase for any pressure, showing that the medium did not penetrate the polyethylene matrix without adequate cavitation at the surface. Due to the same lack of change in mass, no data was presented for samples of NI (no initiator) in the figure. The samples of trial F (no pressure) demonstrated the least change related to liquid penetration at any state of strain, with a 1.12% increase in mass by 100% elongation. With increasing system pressure, there was a corresponding increase in the mass change at each extent of elongation. Such behavior was attributed to induced liquid capillary flow through the restrictive void space with increasing pressure. An inflection was seen within the range of studied elongation for samples of trials C and D, and to a lesser extent for the samples of trials E. This may either suggest that the matrix material becomes more compliant above 75% elongation such that the walls of the existing crazes are being widened more easily, or that more newly initiated crazes are evolved within the cavitated volume thus creating an additional space for the secondary phase propagation. For the trials A and B, however, such an inflection point might be reached earlier (if at all), and so might not be seen within the plot area. The trend with elongation for samples of trials F was also quite linear like trials A and B, reflecting the limited penetration of the solution due to capillary forces and the dynamic viscosity of the liquid for nominal pore size.
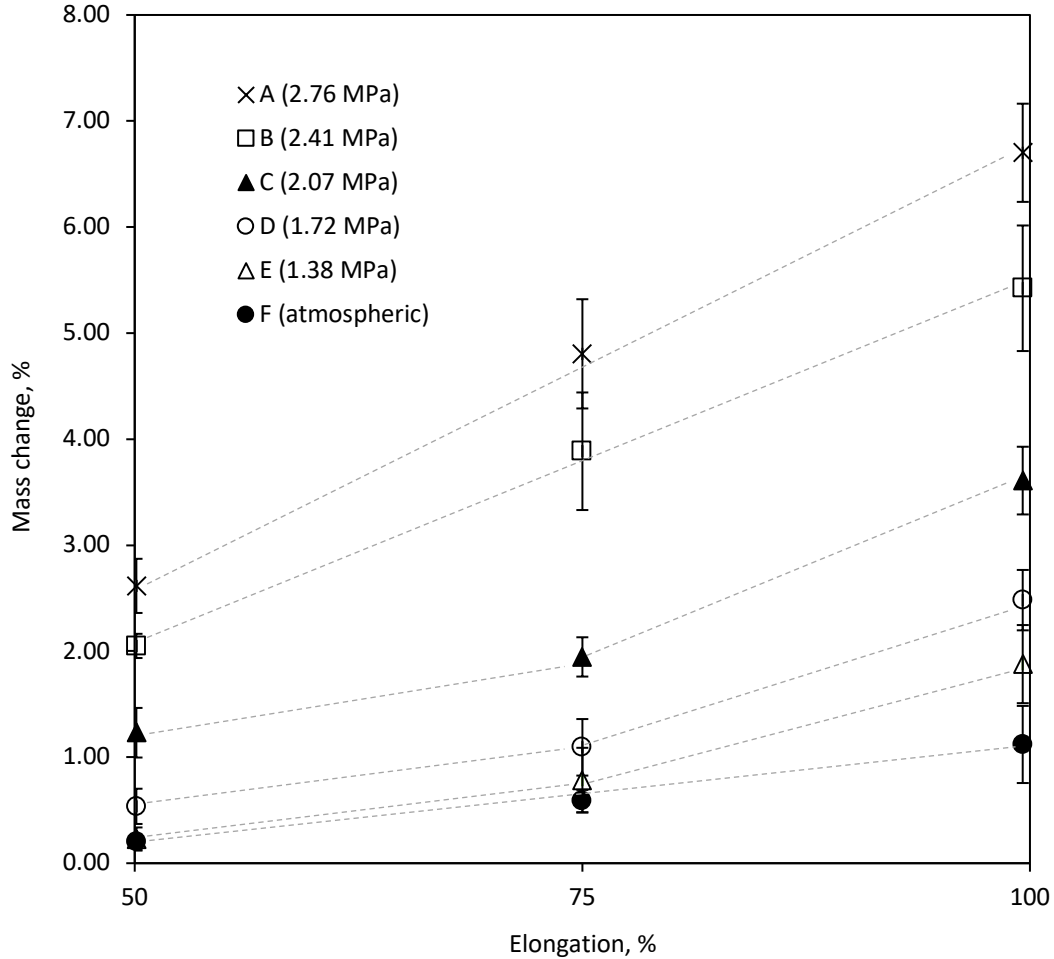
Figure 3-4. The effect of elongation on the mass change for the different system pressures (gauge). The lines are included to visually highlight transitions perceived in the data.

As a first approximation, these results of an overall mass increase, 1.12% for F100 versus 6.7% for A100, gave an estimate for the total added volume corresponding to the acrylate phase. They also presented preferable operating conditions in the preparation of the structured alloy; however, like the morphological results already presented, this data did not yet establish whether a percolating network was developed.

3.4.3   FTIR ANALYSIS

Absorbed water was used as an indicator of the hydrogel in the polyethylene matrix for the infrared analysis in Fig. 3-5, with a corresponding peak at 3000-3700 cm^{-1}. The broad absorbance peak for water was most intense for the pure hydrogel but still readily observed in the prepared samples. The band corresponding to carboxyl groups at 1652 cm^{-1} was another indicator of the interpenetrating hydrogel, in this case showing that some portion of the functional groups were not neutralized. Comparatively, the visible band for COO^- at 1557 cm^{-1} represented the portion of neutralized hydrogel in the samples.

Samples of trials A and F were microtomed to a depth of 10 μm and 50 μm, and analyzed by FTIR. All of the relevant vibrational bands showed weaker absorbances in F100 compared to A100, indicating that a greater concentration of the acrylate secondary phase penetrated the pores when a higher system pressure was used for the reaction. For both trials, a decrease in the band intensity was observed at greater depth from the surface; the reduction of the hydrogel fraction was partially compensated by higher pressure. Thus, for samples of A100 at a depth of 50 μm, the band for COO^- was still clearly distinguishable (Fig. 3-5c), while for samples F100 at the same depth, the group was not detected (Fig. 3-5e).
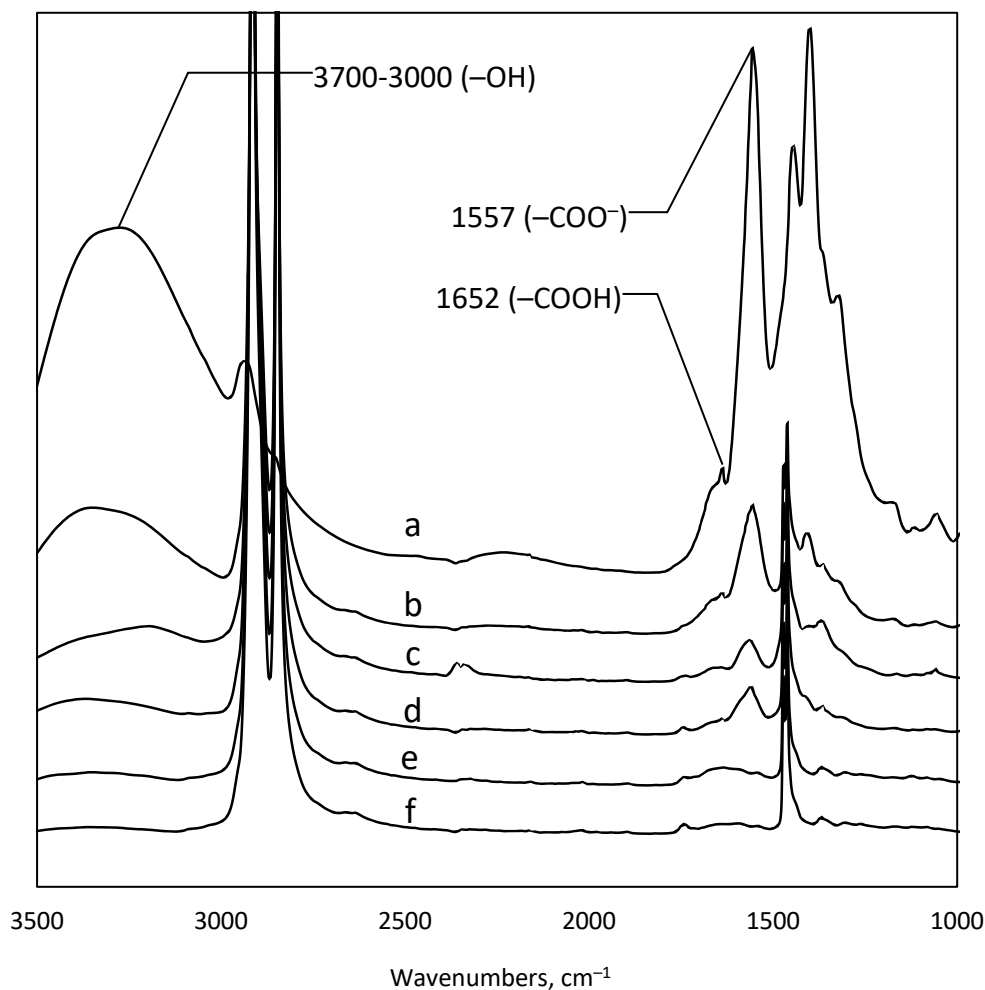
Figure 3-5. ATR-FTIR spectra: (a) for the reference hydrogel sample, (b) for the sample A100 at a depth of 10 μm, (c) for the sample A100 at a depth of 50 μm, (d) for the sample F100 at a depth of 10 μm, (e) for the sample F100 at a depth of 50 μm, and (f) for the reference matrix polymer sample.

3.4.4   ELASTIC MODULUS CHANGE

To exhibit conductivity, the acrylate phase must be impregnated with electrolyte, or in other words, the introduced secondary phase has to be swollen with water. In this state, the hydrogel is rather weak, and does not significantly affect the mechanical properties of the matrix.

To avoid variability in the measurements due to evaporation, the dry hydrogel interstitially bound within the polyethylene was tested instead, which being quite rigid might add some additional stiffness to the matrix. Since the two phases lack appreciable bonding to one another, the dispersed phase must have a certain degree of continuity in order to have a noticeable impact on the matrix mechanics. A dry acrylic hydrogel is not conductive; therefore, this data is not operational and is intended as additional information for evaluation of the morphology of the samples.

The mechanical results are presented in Fig. 3-6. An elongation of 25% was accompanied by a decrease in the elastic modulus relative to the original polyethylene, while the system pressure used at this strain had no significant effect. This suggests weak mutual percolation of initiated crazes, and as a result, a low degree of monomer penetration into the matrix. With further elongation, the modulus decreased by as much as 30% without the secondary phase (based on the results of samples for trial NI), but this loss in stiffness could be compensated with the increasingly interpenetrating polyacrylate structure. This is especially noticeable for the samples of trials A and B, at 75% and 100% elongation, which demonstrated moduli similar or as much as 26% higher than the original polyethylene matrix. Dry PAA itself has a quite high Young's modulus ensured by strong intermolecular interaction and varies from 4.5 to 4.67 GPa. For the neutralized form of PAA, this number has reached as high as 10 GPa.[126]
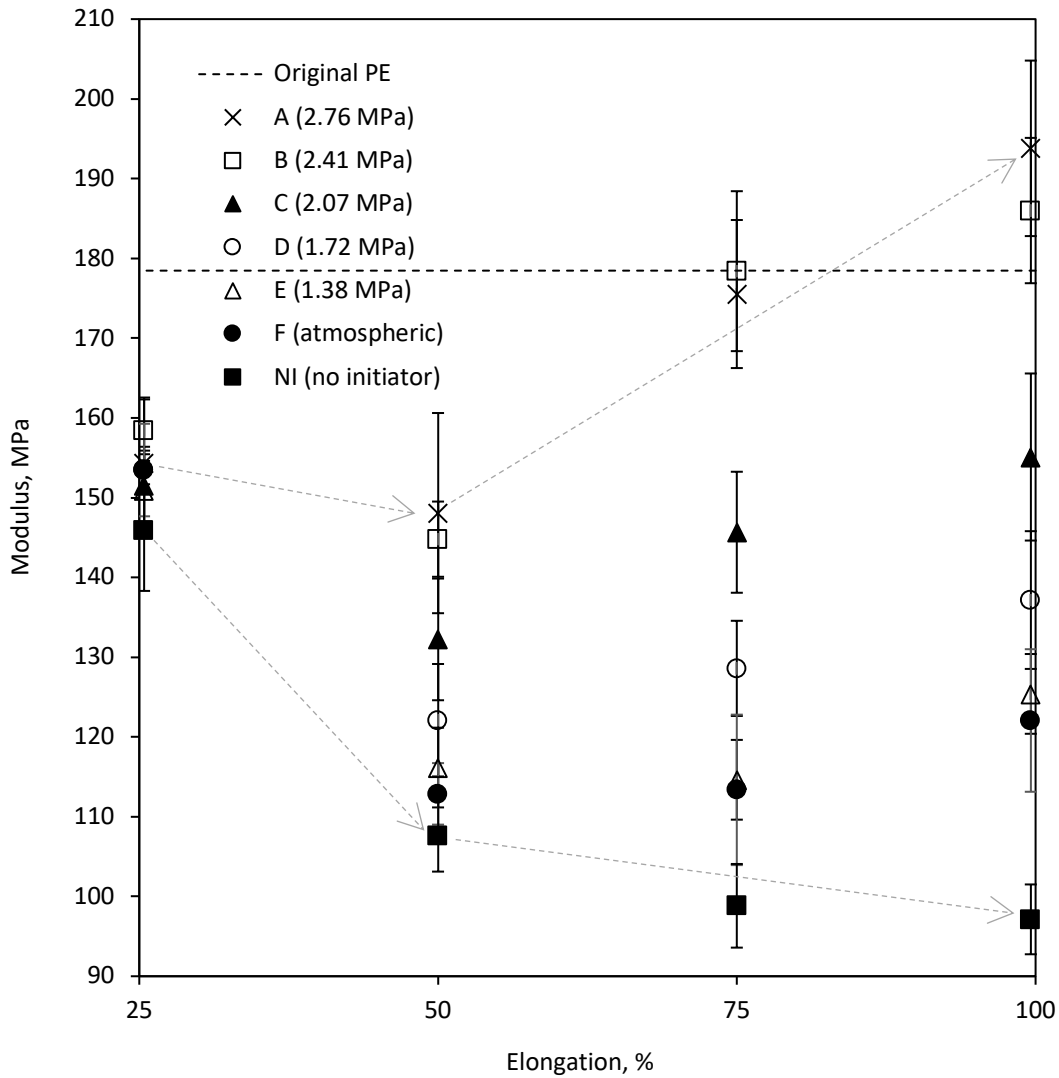
Figure 3-6. Effect of the elongation and system pressure on Young's modulus of the material. The arrows highlight two extremal results: the upper trend shows the maximum impact of the dispersed phase on stiffness; the lower trend shows the absence of an impact by the dispersed phase for the non-polymerized samples for batch NI.

Slowing down the decrease in the modulus for trial NI could indicate a partial hardening of the matrix due to fibrillation. However, given the presence of a secondary phase for trial A (deformed under the same conditions), it may suggest that fibrillation for trial NI was to a large

extent suppressed, as also indicated by the absence of a visible neck of the samples. In this case, the deformation of the samples occurred predominantly due to the formation of secondary crazes, rather than due to the widening of existing ones, as was described in the Morphology section.

The mechanical response of the materials showed evidence of an interpenetrating secondary phase at higher pressures and elongation, but this characterization, along with the morphology and mass change assessments, were insufficient to show the porous system produced by deformation exhibited percolation.

3.4.5   ION CONDUCTIVITY

While demonstrating the new functionality of the modified polyethylene, the characterization of through-plane ion conductivity was also meant to prove that a co-continuous network (acrylic hydrogel) had been developed throughout the material from one surface to another. The measure of conductivity was considered to be revealing the quality of the percolating network. The hydrogel was not highly conductive but suitable for the measurement technique, with an inherent conductivity of $5.68 \cdot 10^{-4}$ S·cm^{-1}. The reported value is comparable to other studies in the literature.[127]

The ion conductivity of the acrylic hydrogel network within the polyethylene samples is shown in Fig. 3-7, varying based on the influence of elongation and system pressure during their preparation. The highest conductivity of $4.43 \cdot 10^{-4}$ S·cm^{-1} (median value of three samples tested) was recorded for samples of A100, which was nearly equal to the conductivity of pure hydrogel. The relative standard deviation (RSD) proportionally increased with conductivity and applied pressure, and was 12% nominally. The high value for A100 corresponded with all other analyses that indicated it had the least unfilled voids of all trial conditions, but now there was evidence

that those poly(acrylic acid) filled crazes formed a percolating network across the polyethylene substrate, through which the electrolyte could diffuse. The result also allows for the conclusion that the increased modulus of elasticity seen for A100 was indicative of the high level of acrylic phase continuity in polyethylene. Conductivity for the samples of B100 was nearly equal to that for the samples of A100, being $3.93 \cdot 10^{-4}$ S·cm^{-1}. In fact, the difference between A100 and B100 was within statistical error. The same trend was observed when comparing the modulus for these two samples, though A100 showed a higher mass change. Thus, a further increase in mass with a certain elongation of the sample does not significantly affect the percolation of the phase; therefore, the additional elevation of pressure was not deemed effective.

It should be noted that conductivity was measured for the undeformed samples, as well as for the samples elongated to 25%, at highest pressure (i.e., A0 – not listed in the table, and A25). However, the results showed no conductivity for these two conditions and were thus not included in the graph. Since there was no network formed in the matrix, no through-plane conductivity was measured. The samples of trial NI also remained nonconductive at the elongation to 50% and less. Some conductivity was detected only at 75% and 100% elongation, though at the lower detection threshold of the multimeter, which might suggest either trace amounts of monomer, or slight diffusion of electrolyte through cavitated matrices.
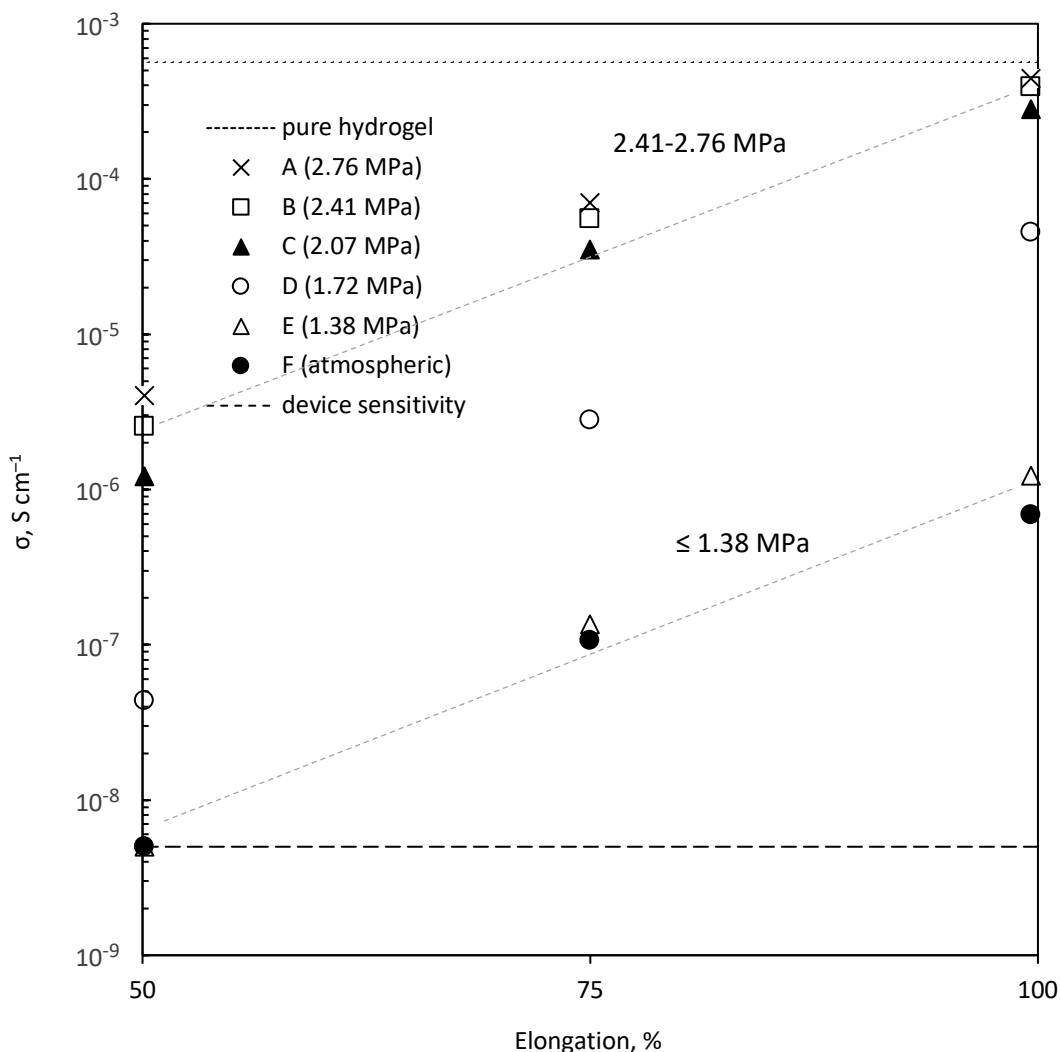
Figure 3-7. Conductivity of the samples deformed at different pressures as a function of elongation. Gray lines show two distinctive extremal trends in conductivity and the transition region between them. RSD proportionally increased with conductivity and applied pressure, and was 12% on average.

The transition in the experimental conditions between trials A/B/C versus D produced a decline in conductivity. Based on the results, trial C was considered to represent the lowest structural variation to produce an interpenetrating network, though its modulus and mass change

was notably lower; a plateau in performance is expected for properties reliant on a percolation network once sufficient continuity in the hydrogel across the polyethylene was reached.

3.5   CONCLUSION

The mechanism of crazing in polymers under tensile deformation was used to form continuous submicron-size channels in the matrix of a commodity polymer, enabling the material to exhibit through-plane conductivity by a newly polymerized hydrogel phase. The liquid monomeric medium was found to function as both a surface-active agent for craze initiation, as well as the secondary phase for the subsequent polymerization. Elevated pressures were found beneficial to overcome capillary forces and promote deep penetration of the medium into the crazed matrix, to ensure continuity in properties while minimizing the extent of mechanical losses in the new material. Collectively, these results demonstrate the potential of modifying regular semicrystalline polymers, such as commodity polyethylene, so as to impart them conductivity.

3.6   ACKNOWLEDGEMENT

Government Guiding Local Science and Technology Development: Environmental Purification

Functional Materials Research Platform.

3.7   REFERENCES

(1)   Jonsson, A.; Song, Z.; Nilsson, D.; Meyerson, B. A.; Simon, D. T.; Linderoth, B.; Berggren, M. Therapy Using Implanted Organic Bioelectronics. *Science Advances* **2015**, *1* (4), e1500039. https://doi.org/10.1126/sciadv.1500039.

(2)   Simon, D. T.; Kurup, S.; Larsson, K. C.; Hori, R.; Tybrandt, K.; Goiny, M.; Jager, E. W. H.; Berggren, M.; Canlon, B.; Richter-Dahlfors, A. Organic Electronics for Precise Delivery of Neurotransmitters to Modulate Mammalian Sensory Function. *Nature Materials* **2009**, *8* (9), 742–746. https://doi.org/10.1038/nmat2494.

(3)   Jonsson, A.; Sjöström, T. A.; Tybrandt, K.; Berggren, M.; Simon, D. T. Chemical Delivery Array with Millisecond Neurotransmitter Release. *Science Advances* **2016**, *2* (11), e1601340. https://doi.org/10.1126/sciadv.1601340.

(4)   Hoare, T. R.; Kohane, D. S. Hydrogels in Drug Delivery: Progress and Challenges. *Polymer* **2008**, *49* (8), 1993–2007. https://doi.org/10.1016/J.POLYMER.2008.01.027.

(5)   Shin, S. R.; Bae, H.; Cha, J. M.; Mun, J. Y.; Chen, Y.-C.; Tekin, H.; Shin, H.; Farshchi, S.; Dokmeci, M. R.; Tang, S.; Khademhosseini, A. Carbon Nanotube Reinforced Hybrid Microgels as Scaffold Materials for Cell Encapsulation. *ACS Nano* **2012**, *6* (1), 362–372. https://doi.org/10.1021/nn203711s.

(6)   Saez-Martinez, V.; Garcia-Gallastegui, A.; Vera, C.; Olalde, B.; Madarieta, I.; Obieta, I.; Garagorri, N. New Hybrid System: Poly(Ethylene Glycol) Hydrogel with Covalently Bonded Pegylated Nanotubes. *Journal of Applied Polymer Science* **2011**, *120* (1), 124–132. https://doi.org/10.1002/app.33095.

(7)   Maranchi, J. P.; Trexler, M. M.; Guo, Q.; Elisseeff, J. H. Fibre-Reinforced Hydrogels with High Optical Transparency. *International Materials Reviews* **2014**, *59* (5), 264–296. https://doi.org/10.1179/1743280414Y.0000000032.

(8)   Eslami, M.; Vrana, N. E.; Zorlutuna, P.; Sant, S.; Jung, S.; Masoumi, N.; Khavari-Nejad, R. A.; Javadi, G.; Khademhosseini, A. Fiber-Reinforced Hydrogel Scaffolds for Heart

Valve Tissue Engineering. *Journal of Biomaterials Applications* **2014**, *29* (3), 399–410. https://doi.org/10.1177/0885328214530589.

(9)   Visser, J.; Melchels, F. P. W.; Jeon, J. E.; van Bussel, E. M.; Kimpton, L. S.; Byrne, H. M.; Dhert, W. J. A.; Dalton, P. D.; Hutmacher, D. W.; Malda, J. Reinforcement of Hydrogels Using Three-Dimensionally Printed Microfibres. *Nature Communications* **2015**, *6* (1), 6933. https://doi.org/10.1038/ncomms7933.

(10)   Pati, F.; Jang, J.; Ha, D.-H.; Won Kim, S.; Rhie, J.-W.; Shim, J.-H.; Kim, D.-H.; Cho, D.-W. Printing Three-Dimensional Tissue Analogues with Decellularized Extracellular Matrix Bioink. *Nature Communications* **2014**, *5* (1), 3935. https://doi.org/10.1038/ncomms4935.

(11)   Bernier, G. A.; Kambour, R. P. The Role of Organic Agents in the Stress Crazing and Cracking of Poly(2,6-Dimethyl-1,4-Phenylene Oixde). *Macromolecules* **1968**, *1* (5), 393–400. https://doi.org/10.1021/ma60005a005.

(12)   Volynskii, A. L.; Aleskerov, A. G.; Grokhovskaya, T. Y.; Bakeyev, N. F. Mechanical Behavior of Glassy Polyethylene Terephthalate Deformed in Liquid Adsorption Active Media. *Polymer Science USSR* **1976**, *18* (9), 2419–2426.

(13)   Volynskii, A. L.; Bakeev, N. F. *Solvent Crazing of Polymers*; Newnes, 2012; Vol. 13.

(14)   Rozanski, A.; Galeski, A. Plastic Yielding of Semicrystalline Polymers Affected by Amorphous Phase. *International Journal of Plasticity* **2013**, *41*, 14–29. https://doi.org/10.1016/J.IJPLAS.2012.07.008.

(15)   Rozanski, A.; Galeski, A. Controlling Cavitation of Semicrystalline Polymers during Tensile Drawing. *Macromolecules* **2011**, *44* (18), 7273–7287.

(16)   Weichold, O.; Goel, P.; Lehmann, K.-H.; Möller, M. Solvent-Crazed PET Fibers Imparting Antibacterial Activity by Release of Zn^{2+}. *Journal of Applied Polymer Science* **2009**, *112* (5), 2634–2640. https://doi.org/10.1002/app.29818.

(17)   Trofimchuk, E. S.; Nikonorova, N. I.; Chagarovskii, A. O.; Volynskii, A. L.; Bakeev, N. F. Crystallization of Silver Chloride in Crazed Porous Polymers. **2005**. https://doi.org/10.1021/JP051920C.

(18)   Rukhlya, E. G.; Litmanovich, E. A.; Dolinnyi, A. I.; Yarysheva, L. M.; Volynskii, A. L.; Bakeev, N. F. Penetration of Poly(Ethylene Oxide) into the Nanoporous Structure of the

Solvent-Crazed Poly(Ethylene Terephthalate) Films. *Macromolecules* **2011**, *44* (13), 5262–5267. https://doi.org/10.1021/ma200812c.

(19) Rukhlya, E. G.; Karpushkin, E. A.; Yarysheva, L. M.; Volynskii, A. L. Special Features of Crazing of Glassy Poly(Ethylene Terephthalate) in Poly(Ethylene Oxide) Solutions. *Macromolecules* **2017**, *50* (14), 5459–5465. https://doi.org/10.1021/acs.macromol.7b01084.

(20) Yarysheva, A. Y.; Bagrov, D. V.; Bakirov, V. A. V.; Tarasevich, B. N.; Grohovskaya, T. E.; Yarysheva, L. M.; Chvalun, S. N.; Volynskii, A. L. Polyethylene–Poly(Ethylene Oxide) Hybrid Films Obtained by Crazing and Their Structural Peculiarities. *Macromolecules* **2017**, *50* (7), 2881–2888. https://doi.org/10.1021/acs.macromol.6b02512.

(21) Pawlak, A.; Galeski, A. Stability of Spherulite Growth Rate. *Journal of Polymer Science Part B: Polymer Physics* **1990**, *28* (10), 1813–1821. https://doi.org/10.1002/polb.1990.090281012.

(22) Nowacki, R.; Kolasinska, J.; Piorkowska, E. Cavitation during Isothermal Crystallization of Isotactic Polypropylene. *Journal of Appl Polymer Science* **2001**, *79* (13), 2439–2448. https://doi.org/10.1002/1097-4628(20010328)79:13<2439::aid-app1051>3.0.co;2-#.

(23) Bucknall, C. B. New Criterion for Craze Initiation. *Polymer (Guildf)* **2007**, *48* (4), 1030–1041. https://doi.org/https://doi.org/10.1016/j.polymer.2006.12.033.

(24) Pawlak, A.; Galeski, A.; Rozanski, A. Cavitation during Deformation of Semicrystalline Polymers. *Progress in Polymer Science* **2014**, *39* (5), 921–958. https://doi.org/10.1016/j.progpolymsci.2013.10.007.

(25) Federal Republic of Germany. *Surface Tension Values of Some Common Polymers/Test Liquids for Surface Energy Analysis*. www.surface-tension.de.

(26) Gokel, G. W.; Dean, J. A. *Dean's Handbook of Organic Chemistry*; McGraw-Hill handbooks; McGraw-Hill, 2004.

(27) Cappella, B. *Mechanical Properties of Polymers Measured through AFM Force-Distance Curves*; Springer Laboratory; Springer International Publishing: Cham, 2016. https://doi.org/10.1007/978-3-319-29459-9.

(28)   Pochard, I.; Couchot, P.; Foissy, A. Potentiometric and Conductometric Analysis of the Binding of Barium Ions with Alkali Polyacrylate. *Colloid & Polymer Science* **1998**, *276* (12), 1088–1097. https://doi.org/10.1007/s003960050350.

3.8   GRAPHICAL ABSTRACT
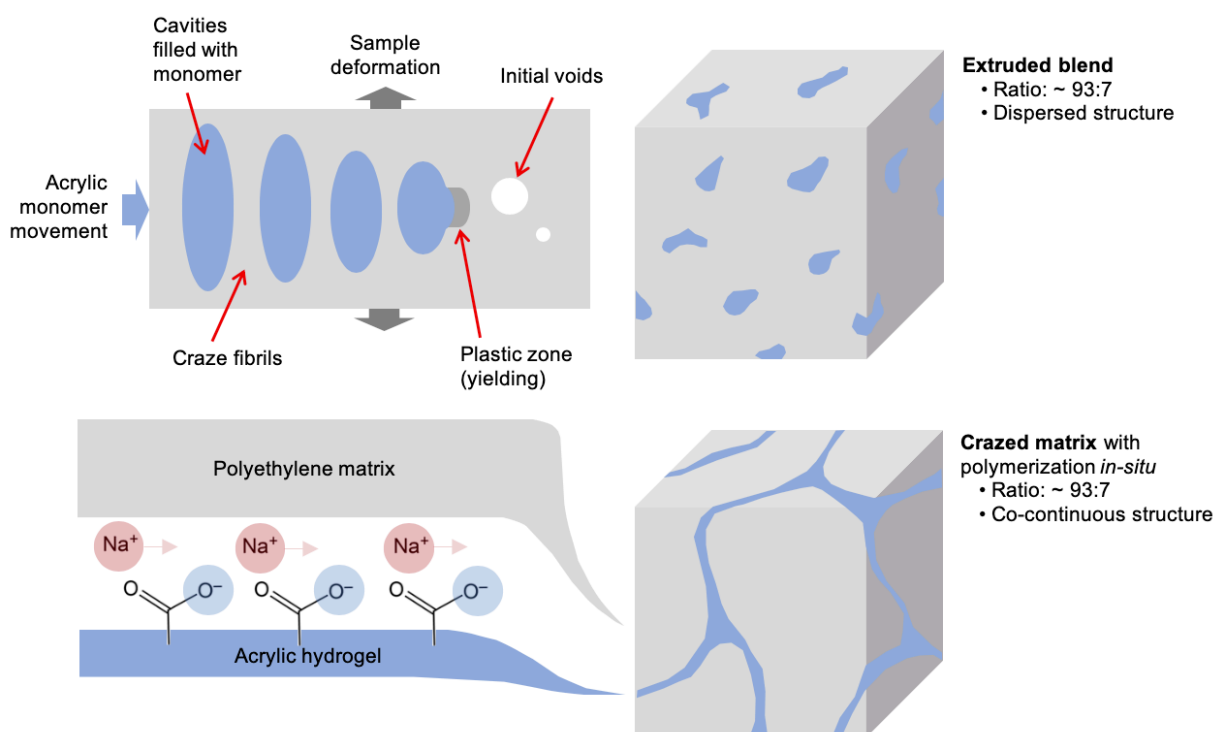
4   FLEXIBLE CONDUCTIVE SUBSTRATE INCORPORATING SUBMICRON CO-CONTINUOUS POLYANILINE PHASE WITHIN POLYETHYLENE BY CONTROLLED CRAZING

In this chapter, we investigate the possibility of creating a submicron co-continuous structure based on a commodity polymer to impart it with value-added functionality, in this case, electron conductivity. Such structures were fabricated in a high-pressure reactor by stretching polyethylene films while immersing them in an emulsified medium of aniline in chloroform, which resulted in the formation of transverse crazes filled with doped polyaniline. The craze frequency was controlled by varying the matrix polyethylene crystallite size, using different

nucleating agents. The unique goal of this work was to use pre-synthesized polyaniline fibers as nucleating particles, which first resulted in a reduction of the matrix crystallite size and then enabled the enhancement of the material conductivity due to the subsequent integration of the fibers into the emerging polyaniline network. It was also shown that the excessively high craze frequency resulted in a decrease in the craze diameter, making it difficult for the emulsion droplets to penetrate the matrix. The chapter is based on the paper published in ACS Applied Polymer Materials, 2021, 3, 4, 1880-1889 (doi: 10.1021/acsapm.0c01416). The permission for this reproduction is granted by the American Chemical Society (ACS).

Author contributions:

After a discussion with Dr. Zhu, we were looking to apply the approach of the previous work to make materials electron-conductive. While designing the experiment described in this chapter, I was inspired by the publication of M.R. Thompson et al. "Multiple Percolation in a Carbon-Filled Polymer Composites via Foaming" *Journal of Applied Polymer Science* **2010**, *115* (2), with the replacement of carbon conductors with *in situ* polymerized PANI network. I was responsible for conducting all the experiment steps, including the sample preparation, which required casting the films and the preliminary synthesis of conductive PANI fibers. Based on the results obtained in the previous work, I selected the testing conditions and performed the mechanical trials in a high-pressure reactor, followed by the final polymerization of the continuous conductive networks. Under the supervision of Dr. Thompson, I troubleshot the experiment, analyzed the obtained data, and prepared the manuscript. Dr. Zhu did the final revision and controlled the quality of the manuscript before its submission to the journal.

4.1   ABSTRACT

A polyethylene film with an incorporated nano-dispersed polyaniline conductive network was developed by controlled crazing in a high-pressure reactor while immersed in an emulsified medium of aniline in chloroform. The resulting conductive material exhibited an average through-plane electron conductivity of 2×10^{-2} S·cm^{-1}, within an order of magnitude of brittle doped polyaniline (1.2×10^{-1} S·cm^{-1}) yet retained the ductility of the polyethylene matrix. It was also shown that 90% of the original conductivity was retained after 1% elongation. Embedded polyaniline fibers acted both as a nucleating agent to reduce the size of crystallites for controlled crazing and as submicron conductive nodes, connecting neighboring conductive conduits formed inside the crazing voids, with both effects contributing to the increasing electrical permeability of the secondary phase. For comparison, montmorillonite and TiO_2 particles were tested as alternative nucleating agents to verify the effect of the preliminary embedded polyaniline fibers on the matrix morphology and, consequently, the conductivity acquired.

4.2   INTRODUCTION

Among the familiar group of intrinsically conductive polymers, polyaniline (PANI) has become a focal point of interest due to its combination of properties such as stability in aggressive chemical environments, extremely low solubility in water and most known solvents, thermal stability, and non-toxicity.[128] The mechanism of synthesis and oxidizing (doping) of PANI is well-studied,[129–131] with its high conductivity notably reversible by adjusting its surrounding pH.[132] Such characteristics have made doped PANI highly attractive as a material for adjustable sensing of acids,[133,134] alkalis,[135] and various organic substances,[136,137] via

monitoring the electrical conductivity of PANI, while it is in contact with the investigated chemicals.

However, PANI has a variety of disadvantages such as a tendency to decompose at ~200 °C,[138] below its melting temperature, and its known brittleness and low strength,[139] which greatly limit its utility and reliability as a material for flexible sensors fabrication. One of the ways to balance this mechanical weakness and expand the scope of application of PANI is to embed it into a mechanically durable and elastic matrix but there are significant challenges with establishing a percolating secondary phase for conductivity without high loadings such that the flexible nature of the matrix is not lost.[29]

The conventional method for imparting conductivity to non-conductive matrices by admixing them with conductive solid fillers is not always an adequate long-term solution. PANI has such a high melting temperature that it is usually considered a solid filler in most compounded polymer systems. The dispersed particles form permeable structures in the matrix volume only at relatively high content, which produce very high processing viscosities during their preparation and present solid-state property sensitive to deformation. Ideally, co-continuity of a conductive secondary phase at relatively low content is envisioned as a more desirable material system. Such an alternative approach could consist of polymerizing conductive liquid reactants within the cavitated space of a matrix to form nano-to-micron scaled channels in an otherwise ductile material. The mixture of reactants serves an added role in the method, foreseeably acting as a surface-active liquid medium to facilitate controlled cavitation along the crystallite boundaries during matrix plastic deformation.

The described alternative approach above is based on the mechanism of crazing in polymers in the presence of liquids, similar to the damaging phenomenon that occurs naturally

during part service via Environmental Stress Cracking (ESC).[140,141] In our previous research,[2] we extended the approach of Volynskii et al.,[115,116] and Rozanski et al.[117] by adjusting the experimental parameters. For our purposes of developing a functional cross-linked network within a polyethylene matrix, we included a post-polymerization of the surrounding liquid in which the matrices were stretched. To increase the efficiency of the method, nucleating particles were added into the matrix polymer, thereby reducing the crystallite size and expanding the crystal-amorphous interfacial area, which, in turn, caused a rise in the number of primary voids[83,98] followed by growth in the density of crazes.[84,97] Three different nucleating agents: TiO_2, polyaniline, and montmorillonite, were investigated to determine their effect on the resulting conductivity properties of the material after their function of controlling the crystallinity of the matrix. TiO_2 was used in the previous research and had predominantly been selected due to it yielded a larger number of small crystallites in the initial matrices, with sizes of 1 μm or less. Its particles were also chemically inert to the secondary phase precursors and were not washed out by the solvents used. The use of pre-synthesized polyaniline fibers was one of the elements of the novelty in this research. Having performed their nucleating function, they integrated into the post-polymerized polyaniline phase, forming a highly conductive network within the polyethylene matrix. The montmorillonite particles produced crystallites of the same size as the polyaniline fibers and were therefore used to elucidate the role of PANI fibers conductivity in the overall conductivity of the final materials.

The resulting material possessed submicron channels that percolated through the matrix, consisting of the secondary polyaniline phase at a low volume fraction. Since thin or narrow structures tend to be more prone to displaying a flexible nature compared to bulk materials, it

was hypothesized that this approach may be suitable for creating flexible electronic components, something very attractive in the field of wearable technology. Therefore, the present research aimed to advance further the approach investigated earlier for the purpose of now producing a highly conductive yet ductile polymer alloy featuring a percolating network of PANI within a polyethylene matrix.

4.3   EXPERIMENTAL METHODS

4.3.1   MATERIALS

Linear low-density polyethylene (LLDPE LL 8460.29, ExxonMobil Chemical), titanium dioxide nanoparticles (TiO$_2$ P25 AEROXIDE, Degussa, composition of anatase/rutile/amorphous),[142] and montmorillonite particles (Cloisite 30B, Southern Clay Products) were used as received. The TiO$_2$ had a quoted particle size of 21 nm by the supplier. Fractions of the montmorillonite with a particle size of less than or equal to 2, 6, and 13 μm were of 10, 50, and 90%, respectively. Aniline (≥99.5%, Aldrich), 4-dodecylbenzenesulfonic acid (DBSA) (DBSA, mixture of isomers ≥95%, Aldrich), ammonium persulfate (APS, ≥98%, Aldrich), lithium chloride (LiCl, ≥99%, Aldrich), xylene (≥98.5%, mixture of the isomers, Aldrich), and chloroform (≥99%, Aldrich) were used as received.

4.3.2   PREPARATION OF PANI FIBERS

Traditionally, aniline is polymerized in an aqueous solution. In this research, polymerization for both the pre-synthesized polyaniline fibers and the subsequently introduced secondary polyaniline phase in polyethylene were carried out in the weakly polar solvents of xylene and chloroform, respectively. The monomer and surface-active agent (DBSA) formed an anilinium-DBSA complex, as shown in Fig. 4-1, which presented itself as micelles in the solvents;[143] the DBSA hydrophobic tails were directed outward to the highly compatible solvent molecules and subsequently, to the matrix polyethylene.
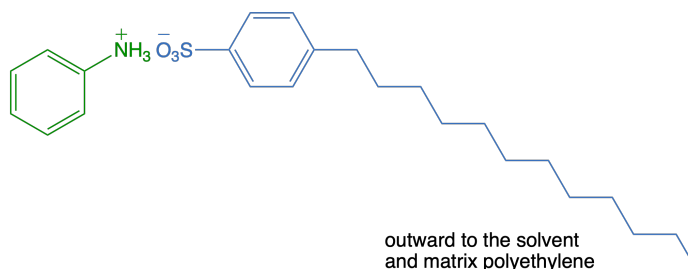
Figure 4-1. Structure of intermediate anilinium-DBSA complex as a preliminary step in the polymerization of aniline for PANI fibers.

The recipe for pre-synthesized polyaniline fibers as a nucleating agent in the polyethylene was mainly adopted from the research by Osterholm et al.[130] A solution of 4.65 ml of aniline, and 24.48 g of DBSA in xylene (Aldrich) was cooled down to 0 °C. Polymerization was initiated by the addition of 4.68 g of APS into 20 ml distilled water, introduced dropwise over 30 min

under vigorous agitation, as the reaction is quite exothermic. The total polymerization time was 24 hrs. After synthesis, the precipitate was centrifuged and stored for further use.

Some portion of the precipitate was washed and dried as a film to measure the conductivity of the pure material, which was found to be $1.2 \times 10^{-1} \pm 3.5 \times 10^{-2}$ S·cm⁻¹. The color of the precipitate was dark green, which corresponds to the emeraldine salt form, with a slight blue tint that indicates the partial inclusion of the deprotonated emeraldine base form.[144]

4.3.3 PREPARATION OF MATRIX SAMPLES

Fabricating the films of LLDPE, powder was dissolved in xylene at 132 °C and then premixed with one of three types of nucleating agents: pre-synthesized PANI-DBSA fibers in the amount of 5% (w/w) to pure LLDPE (denoted as P); Cloisite 30B particles in the amount of 5% (w/w) to pure LLDPE (denoted as C); or TiO_2 nanoparticles in the amount of 2% (w/w) to pure LLDPE (denoted as T). The solution was cast on aluminum substrates and then kept in an oven at 80 °C under vacuum overnight to remove xylene residues.

The final cast film had a thickness of 110±10 μm. Dumbbell-shaped samples were cut out of the film with a middle-narrowed section being 5 mm long and 5 mm wide, and larger ends for mounting in the tensile rig mentioned below.

4.3.4 DEFORMATION OF SAMPLES AND POLYMERIZATION

The deformation procedure was basically adopted from the previous research.[2] The tensile rig with the mounted sample, while immersed in the prepared emulsion, was placed inside a high-pressure reactor with a maintained temperature controlled by a circulating refrigerant fluid. The tensile strain was applied to the samples step-wise at 0.25 mm per cycle increments, so as

to maintain the resulting rate of deformation constant at 0.03 mm·min⁻¹. A pressure of 2.76 MPa was created inside the reactor with high-purity nitrogen gas after preliminary purging. The deformation was performed until the degree of longitudinal elongation of the middle-narrowed section reached 25, 50, 75 or 100% strain. The percent elongation was used following the capital letters, P, C, and T, in the naming convention of completed samples. The capital letters were selected based on the nucleating agents used: P for polyaniline fibers, C for montmorillonite (clay) particles, and T for titanium dioxide particles. For example, the sample denoted as T50 contained TiO_2 nucleating particles and its middle-narrowed section increased in length by 2.5 mm, up to 7.5 mm in total.

The emulsion, within which the samples were deformed, was prepared as follows. Under vigorous agitation, 0.285 g of aniline was added dropwise to a solution containing 1.53 g of DBSA in chloroform, after which the total volume of the emulsion was brought up to 16 ml with chloroform. After emulsion homogeneity was achieved, its temperature was decreased to –17 °C. 0.3 g of APS was dissolved in 1.25 ml of distilled water, with the addition of 2.623 g of LiCl to keep the solution unfrozen. The solution was cooled down to –17 °C and then added dropwise to the emulsion under vigorous agitation.

Chloroform, as a weakly polar solvent, has proven to be an effective penetrating liquid; its surface energy is of 0.0299 N·m⁻¹,[125] which is fairly close to that of polyethylene, 0.0353 N·m⁻¹.[124] This was in agreement with the research by Rozanski et al.[118] who suppressed gross failure in polymers by exposing them to chloroform while undergoing deformation. Chloroform was also used due to the ease of its removal from the final composites, as compared to xylene. The lower emulsion viscosity was also an advantage giving the solution a higher

penetration capacity, as well as the facilitated agitation of the reaction mixture while the sample is saturated at deformation, as well as while the mixture is polymerized, especially in the later stages, when its viscosity increased.

The low reaction temperature was due to the need to inhibit the decay of APS and thus ensure that the cavitated matrix was fully impregnated with the reaction mixture before polymerization began. After the sample deformation was completed, the temperature of the reaction cell was elevated up to 0 °C and maintained at this condition for 24 hrs, enabling APS to decay and initiate polymerization directly in the cavitated space of the matrix.

4.3.5   ELECTRICAL CONDUCTIVITY MEASUREMENT

After vacuum drying at 80 °C for 24 hrs, elongated dumbbell samples were polished with sandpaper on both sides to remove any polyaniline-deposited film on their surfaces. The edges of the samples, possibly more enriched by polyaniline, were also cropped to avoid electrical current circumventing a path through the sample.

The probes, both with faces of the same contact area A, were formed by depositing a conductive nickel paste on both surfaces of the obtained specimens. Silver-plated wires were embedded into the probes and connected to an Agilent 34401A 6½ Digit Multimeter. Direct current (DC) resistivity was calculated as $\rho = (R \cdot A)/L$, where R was the measured resistance. The specimen thickness, which is equivalent to the distance between the probes, was taken as dimension L in the resistivity calculation. The DC conductivity σ [S·cm^{-1}] was then calculated by the formula $\sigma = 1/\rho$. To maintain consistency, the resistance was always taken ten seconds after the closure of the measurement loop.

4.3.6   MECHANICAL CHARACTERIZATION

A benchtop Model 3366 Universal Mechanical Testing System (Instron Corporation; Canton, MA) was used for the strain-controlled tensile tests and stretchable conductivity response measurements. The system was equipped with a 500 N load cell and operated at ambient room temperature. For each sample, the thickness was measured with a digital caliper at three points in the narrowed section. Testing was performed at a strain rate of 2.5 mm·min⁻¹ until failure. At least three repeated measurements were performed for each test.

4.3.7   STRETCHABLE CONDUCTIVITY RESPONSE

The flexibility of the PANI secondary phase within samples was evaluated for both through-plane and in-plane conductivity, as schematically shown in Fig. 4-2a and Fig. 4-2b, respectively, by measuring resistance R while simultaneous stretching the samples in the same mechanical testing system, at a strain rate of 2.5 mm·min⁻¹, until the conductivity dropped below the limit of the measurement device.
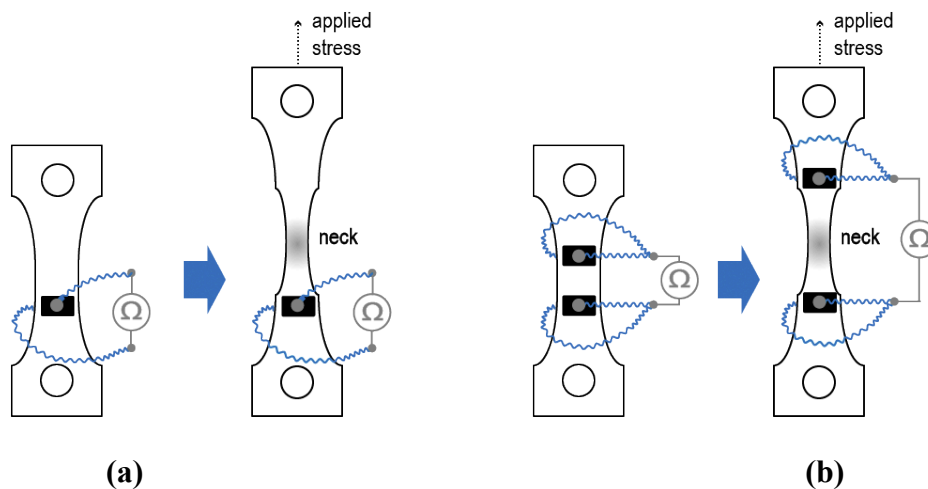
Figure 4-2. Specimens for (a) through-plane and (b) in-plane conductivity measurements.

For through-plane conductivity, the measurement was carried out through a couple of contralateral probes mounted on opposite sides of the specimen. For in-plane conductivity, the measurement used the second set of probes mounted at an initial distance of L, which then increased with stretching. Dimension A for the resistivity was equal to the product of the probe width (the length of the probe edge perpendicular to the specimen) and the thickness of the specimen, before stretching. Since the dimension A cannot be assumed to be fixed during stretching of the specimen, the reported values cannot be considered an accurate value of conductivity, but served well to demonstrate the persistence of electron pathways as the PANI channels were distressed.

The results revealed an inflection point on the through-plane conductivity curve corresponding to a specimen elongation of ~1% strain, until which conductivity remained almost unchanged. In this range, deformation was close to elastic, as indicated by the nearly linear behavior of the stress-strain curve. Based on this, the specimens were subjected to cyclic loading, at the same strain rate of 2.5 mm·min⁻¹, with subsequent relaxation, for 10 cycles in total, with simultaneous measurement of through-plane conductivity.

4.3.8   MORPHOLOGICAL CHARACTERISATION

A JEOL JSM 7000 scanning electron microscope (SEM) was used to obtain micrographs for morphology analysis. A sample was cryogenically fractured in its narrowed section, and the exposed cross-section was sputter-coated with a 5 nm thick layer of platinum. To determine the individual pore sizes and secondary phase distribution, the original images with the analyzing area of 5×6 μm were processed using ImageJ software (National Institute of Health, U.S.). The processing results were based on five hundred occurrences of pores in each image.

A Zeiss Axioplan 2 light microscope was used to characterize the pre-synthesized PANI fibers dispersed in xylene, and evaluate the effect of the different nucleating agents on the crystallinity of the matrix. To prepare a specimen of the fibers, a drop of non-centrifuged suspension was placed on a slide, under a coverslip and immediately examined. Specimens of the matrix were prepared by placing a drop of heated (132 °C) solution of polyethylene with a corresponding nucleating agent, placed on a slide, under a coverslip, and then kept at 80 °C overnight under vacuum before examination.

4.4   RESULTS AND DISCUSSION

4.4.1   PRE-SYNTHESIZED PANI FIBERS

The emulsion polymerization method produced a threadlike structure of PANI in suspension. This fibrous form was similarly reported by other researchers using this polymerization method.[139,145] The aligned chain arrangement of PANI results in high electrical conductivity due to a low impedance to interchain charge diffusion along the final fiber [146,147].
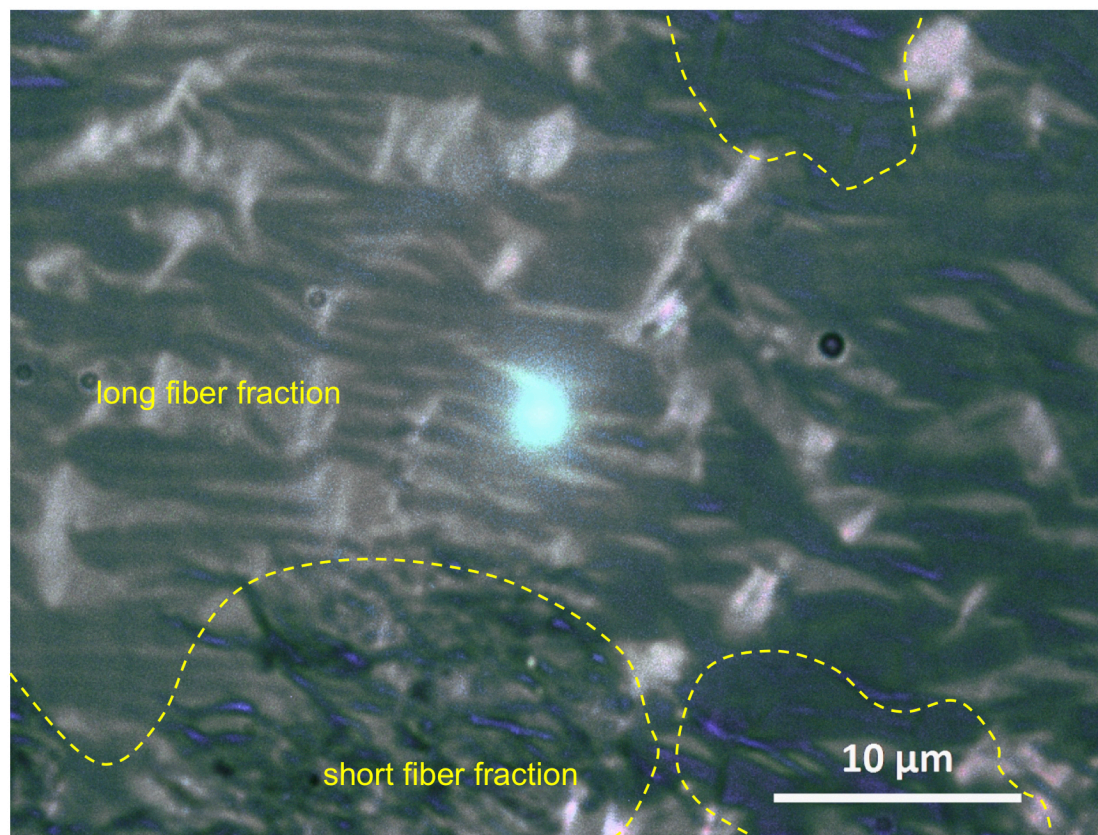
Figure 4-3. Pre-synthesized PANI fibers in xylene with two distinguishable lengths of fiber present. Dashed lines indicate the boundaries of clusters with fibers of different lengths.

The emeraldine-colored PANI fibers in xylene, prepared by the technique described in section 2.8, are shown in Fig. 4-3. The image shows the presence of comparable fractions of both short (2-3 µm) and long (up to 10 µm) fibers in the suspension, which can be attributed to uneven distribution of DBSA during the synthesis.[148,149] Long hydrophobic tails of DBSA stabilize and orient PANI chains with the formation of a fiber. Accordingly, a low concentration of DBSA yields the short fiber regions in the image, which are characterized by a blue tint due to insufficient protonated polyaniline emeraldine base.

When choosing the initial nucleating agent content for the fibers, a balance between conductivity of the final samples and their mechanical characteristics was considered. With an increase in the content of fibers, the yielding behavior of the matrix showed much more fragmentary plastic damage. Microscopic analysis showed visible agglomerations of polyaniline fibers between crystallites at higher than 5 wt.% content, which apparently led to the mechanical instability of the matrices. Conversely, at a lower percentage of fibers, a noticeable drop in conductivity of the final samples was observed, probably due to an insufficiently developed distribution of junctions for the subsequent polyaniline network, which could not effectively contribute to the percolation requirements of the secondary polyaniline phase.

4.4.2   EFFECT OF NUCLEATING PARTICLES ON MATRIX MORPHOLOGY

All three nucleating agents showed good dispersion in the polyethylene solution with xylene. Few aggregates were seen in the solution itself or in the cast films. The organic coating of Cloisite 30B was beneficial in this regard. Similarly, for the PANI fibers, the embedded DBSA with its protruding alkyl tails from the surfaces of the fibers ensured their compatibility with the polyethylene matrix, improving the van der Waals interactions.

The size of the polyethylene crystallites was shown in a previous study to be reduced by the addition of TiO_2 nucleating nanoparticles, which results in an increased crystal-amorphous interfacial area.[2] Crystallites of approximately 1 μm or less in size, are shown in the optical micrograph in Fig. 4-4a with TiO_2 as a nucleating agent. For comparison, pure polyethylene displayed larger crystallites of about 100 μm (Fig. 4-4b). Montmorillonite and PANI fibers were tested as alternative nucleating agents, and both found to yield similar average sized polyethylene crystallites of about 5 μm, shown by optical micrographs in Fig. 4-4c and 4d, respectively. The crystallite sizes found in sample type C with montmorillonite were, however, more homogeneous while sample type P had distinct regions of larger and smaller crystallites (visually separated by a yellow dotted line). The variation in crystallite size was attributed to the presence of two size fractions of polyaniline fibers, which is explained in the next section. The micrograph for sample type P shows that the green polyaniline fibers are displaced along the inter-crystalline boundaries. The fibers that are not well connected by the alignment along the boundaries was enough to result in a low, but detectable conductivity of undeformed matrices, equal to about 6×10^{-9} S·cm^{-1}. Neither the pure polyethylene or samples type C and T showed any detectable conductivity within the sensitivity of the multimeter.
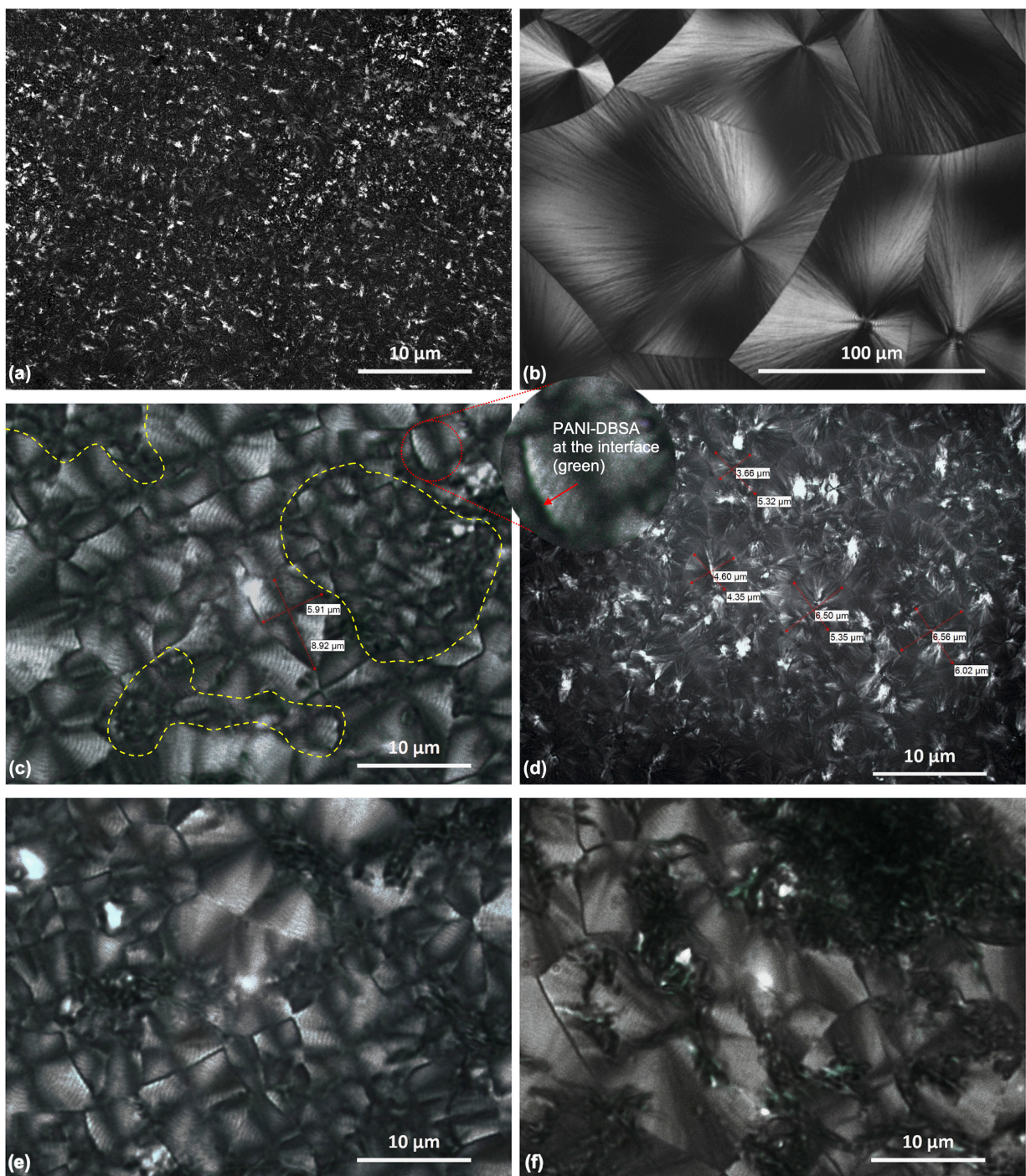
Figure 4-4. Morphology of LLDPE matrix with TiO_2 (a) (Reproduced from [2]. Copyright 2020 American Chemical Society), pure LLDPE matrix (b), LLDPE matrix with 5 wt% of PANI fibers [type P] (c), and Cloisite 30B [type C] (d). For comparison, morphology of LLDPE matrices with 10 wt% (e) and 30 wt% (f) of PANI fibers are provided. Magnification differences due to the scale of morphological detail to be shown.

4.4.3   RESULTING MORPHOLOGY AND MASS CHANGE

The morphologies of P100, C100 and T100 were examined by SEM and are respectively shown in Fig. 4-5a, 4-5b, and 4-5c. The micrographs presented were representative of the entire fractured surface, focused at a distance of approximately 10 μm from one of the specimens' edges for consistency.
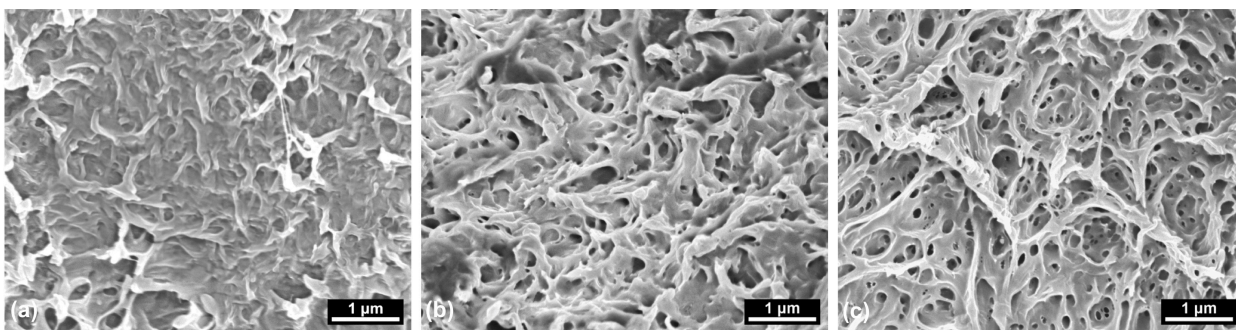
Figure 4-5. SEM morphology of samples (a) P100, (b) C100 and (c) T100 exposed by cryogenically fractured normal to the deformation axis. A varying degree of porosity was evident as the PANI secondary phase filled in the cavitated network formed by stretching polyethylene in aniline-DBSA emulsion in chloroform.

A network of PANI effectively filled the cavitated structure of the polyethylene in the case of P100. The smooth dark regions seen in the SEM image for P100 were believed to correspond to the brittle polyaniline phase, while the white rough regions were considered to be fibril protrusions corresponding to the ductile polyethylene phase; PANI is a brittle polymer and the least likely of the two polymers to fail via fibrillation during cryofracturing. Based on image analysis of these micrographs, the cross-section for P100 showed the least porosity, estimated at 5% based on the displayed surface area. For C100, the total porous area found was 11%, while

for T100 it was 35%, with hierarchical porosity and a pore area variation being in the order of 0.001-0.1 μm². The characteristics of porosity for each sample type are summarized in Table 4-1.

Table 4-1. The results of the SEM micrographs' image analysis for P100, C100, and T100 (calculated for the area 5×6 μm).

	Total unfilled area, %	Total number of pores
P100	5	18
C100	9	129
T100	35	308

There were considerable concerns for the pore size in this study, controlling the mass fraction of the secondary phase, as well as influencing the conductivity and flexibility of the final material. In regards to mass gain, the physical size of the micelles formed by the anilinium-DBSA complex would limit their entry into the strain-developed crazes until the pore was large enough, making the pores a significant factor in the extent of PANI-filled regions seen in the micrographs. The micelle size and structure can vary significantly depending on the ratio of aniline to surfactant. Several other research groups conducted the synthesis under similar conditions, and reported that the micelles can be up to 250 nm in size,[150] but can also form agglomerates up to ~1 μm in diameter.[143] In order to estimate the approximate size of emerging crazes, the crystal fraction should be considered unaffected while the polymer matrix is stretched in a thermodynamically compatible liquid medium, as established by Rozanski et al.[118] and later by our previous research.[2] The matrix is elongated only due to uniform cavitation of its amorphous fraction, as a result of which, the finer crystal structure of the matrix results in the smaller diameter of the emerging crazes, for equal elongations.

Accordingly, the cavitated structure of matrices P and C with their average initial crystallite size of 5 μm (Fig. 4-4) crazed, yielding pore sizes better to accommodate the emulsion micelles than matrix T with an average crystallite size of 1 μm and less. Low molecular weight chloroform, being highly compatible with polyethylene, freely penetrated all types of matrices and decreased the mechanical energy threshold for craze initiation,[97] regardless of the total amount of absorbed emulsion. This was evident for T100, shown in Fig. 4-5c, with a visible absence of dark areas associated with the secondary polyaniline phase but still showing a high number of evenly distributed small cavities.

This cavitation behavior of T100 is in a good agreement with the previous research results.[2] The matrices that were cast with the use of the same nucleating agent, TiO_2, stretched under the same conditions, but in acrylic acid, which surface energy (0.0300 N·m^{-1} [125]) was similar to that of chloroform, and quite close to that of the matrix polyethylene, demonstrated approximately the same scale of cavitation.

Fig. 4-6 shows changes in mass of the three sample types prepared in the study, at different degrees of elongation. The case in which an effectively cavitated sample showed insignificant mass increase corresponding to the introduced secondary phase of PANI is shown by sample type T; preliminary tensile testing of the matrix has shown that any strain greater than 1% will result in plastic deformation and hence all tested states in this figure correspond to permanent damage. A noticeable improvement in mass gain was only seen upon reaching an elongation of 75% (denoted as A in the figure) for type T, indicating an adequate change in the diameter of crazes for which penetration of the emulsion into the matrix increased. The lower PANI phase content of this sample type noted by this mass gain was similarly attributed to the very ductile

nature of the final sample in Fig 4-5, noted by the substantial fibrillation in the micrograph. Furthermore, shrinkage was notably higher for T100 than seen for P100, once the sample was removed from the reactor, which again confirmed our conclusion that sample type T included less of the PANI secondary phase. Interestingly, the shrinkage for T100 specimens was similar to C100, which would not be expected from the mass gain data. We believe this can be attributed to the enriched PANI outer layers seen for T100, adding rigidity and hence resistance to shrinkage until it was eventually removed by sanding.
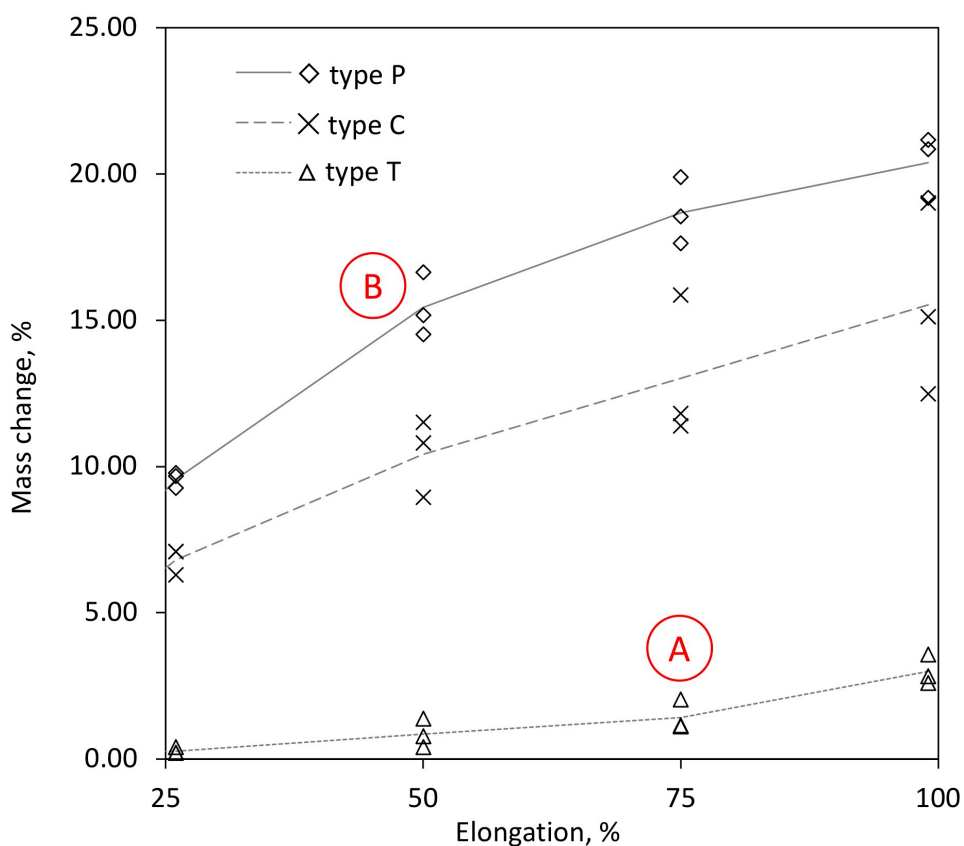
Figure 4-6. The effect of different degrees of elongation on the sample mass change due to formation of the secondary phase of PANI. The lines are included to visually highlight trends. Maximum standard deviation was of 1.14% for P, 3.28% for C, and 0.52% for T.

Samples of types P and C showed a substantial mass gain in Fig. 4-6, with type P showing the greatest mass gains of all the three types prepared in the study. Mass changed rapidly up to 10wt% for type P by an elongation of 25%, and then up to 15wt% at 50% elongation (denoted as B on the graph). As discussed above, the larger diameter of crazes for this sample type led to a higher absorption rate of the anilinium-DBSA emulsion, even at a low extent of deformation. The fibers initially embedded in the matrix additionally promoted movement of the emulsion micelles through crazes due to high thermodynamic compatibility, as discussed below. The rate of further mass gain decreased slightly and reached 20wt% for P100. Taking into account the mass of the fibers initially embedded into the matrix, the amount of PANI-DBSA secondary phase in the completed blends yielded 25wt%. Samples of type C showed less mass gain in the graph and underwent more noticeable shrinkage after removal from the reactor, compared with samples of type P. The shrinkage mentioned is attributed to stress relaxation upon removal from the reactor and no longer being subject to fixed strain, with the dimensional change being greater when less polyaniline was present to fill the voids created by cavitation. Compared with samples of type P, the mass gains for samples of type C were lower, reaching only to 15wt% for C100. Given the same average crystallite size for samples P and C (Fig. 4-4a and 4-4b), we can expect an equal diameter of the opening crazes, and therefore a similar pattern of matrix saturation by the emulsion droplets. The obtained difference is explained by lower compatibility of the emulsion micelles with the matrix material containing embedded montmorillonite particles rather than embedded PANI fibers. The high degree of fibrillation on the surface of C100 in Fig. 4-4 and Fig. 4-5 had a quite significant ductile fraction, but at the same time exhibited a fairly low porosity.

The size of matrix crystallites (influenced by the nucleating agent) and penetrating liquid collectively influenced the intensified formation of a crazed network. A higher frequency of crazes decreased the potential for increased pore sizes at the same degree of sample elongation, which in turn mitigated the loss of the matrix mechanical properties. It was determined, however, that an excessively developed network forms crazes with a diameter insufficient for the passage of the emulsion micelles, resulting in poor absorption of the secondary phase material by the matrix. The use of PANI fibers as nucleating particles provided the optimal crystallite size, as well as ensured better affinity of the matrix cavitated interior to the emulsion micelles, which, in turn, resulted in the highest mass increase at equal degrees of sample elongation, with the formation of the visually homogeneous composite.

4.4.4   ELASTIC MODULUS CHANGE

Fig. 4-7 shows the Young's modulus of samples of types P, C, and T, produced at differing degrees of elongation after being immersed in the emulsion. Samples of type T showed higher elastic moduli for all levels of elongation compared to the other types, due to its finer crystallite structure and reinforcement by TiO_2. The undeformed samples of type C showed a larger modulus than type P, due to the higher mechanical strength of montmorillonite particles and their correspondingly better reinforcement of the LLDPE matrix than PANI fibers.

While matrices were deformed, uniform cavitation occurred due to the penetration of chloroform, which resulted in a decline in modulus for all the samples. At 100% elongation, the modulus of samples had decreased by 53%, 70%, and 52% corresponding to sample type P, C, and T, respectively. Cavitation had a much more significant effect on mechanical properties for samples of type C, with a drop in modulus by 47% at only 25% strain. For the same strain and

average crystallite size of type P, its modulus decreased by only 32% due to comparatively improved bonding with its filler as a result of the hydrophobic tails of DBSA molecules. The more moderate decrease in modulus for P compared with C may also be related to the reinforcing nature of a fiber versus a particle, resulting in more effective stress transmission. Compared with C and P, type T demonstrated a more moderate decrease in modulus at 25% strain. This was due to the finer crystallites, which appears to be more stable during matrix deformation than the reinforcing effect of embedded particles.

At deformations higher than 50% strain, all the three types show a decline in the rate of strength loss. Type P demonstrates a smaller rate of loss at higher strain due to the continuous polyaniline phase connecting the originally added fibers to add rigidity to the sample. The onset of this described plateau began at lower strain compared to the other sample types due to this continuous secondary phase (as demonstrated by the results for through-plane conductivity, next section).

Type C samples, according to the mass change results, acquired a certain amount of PANI, but this secondary phase did not form many continuous channels (as evident by its low conductivity) to add reinforcement to the matrix. Subsurface material accumulation was possible, which ensured some reinforcement at high deformations, but at the same time, resulted in considerable scatter in the results. For type T, the PANI phase did not appear to penetrate the matrix in any significant quantities, which is consistent with the results for mass change and conductivity.
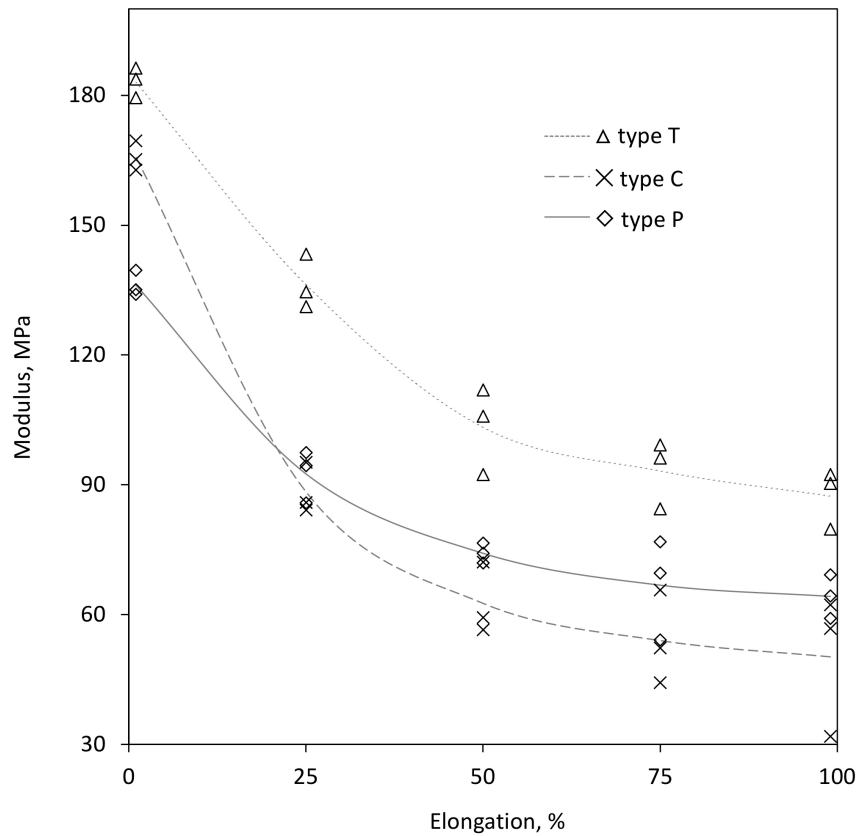
Figure 4-7. Effect of the elongation and particle type on Young's modulus of the material. The lines are included to visually highlight trends. Maximum standard deviation was of 10.0 for T, 16.2 for C, and 11.6 for P.

4.4.5   THROUGH-PLANE CONDUCTIVITY

Electrical conductivity is a relatively simple and reliable way to determine continuity of the secondary phase within the polyethylene matrix. The bulk through-plane measurement was calculated based on the apparent volume of the tested samples, without taking into account the morphology of the conducting phase, as DC conductivity depends only on the total secondary phase cross-section and does not depend on the diameter of its individual channels. The conductivity of the three sample types is shown in Fig. 4-8, based on the extent of elongation

during their preparation. Samples of type T demonstrated negligible conductivity relative to the sensitivity of the multimeter until the elongation reached 75%. This matches the measured mass gains in the previous sections where it was concluded that the emulsion micelles had difficulty passing into the crazes until the pores were large enough, and so could not effectively be deposited with formation of the conductive secondary phase. From 75% to 100% elongation (denoted as A in the graph), there was a subtle increase in conductivity, up to 10^{-8} S·cm^{-1}. The low mass gain and low conductivity together suggest that the formed percolative network was poorly developed, though interference by the TiO_2 was a possible contributing factor.
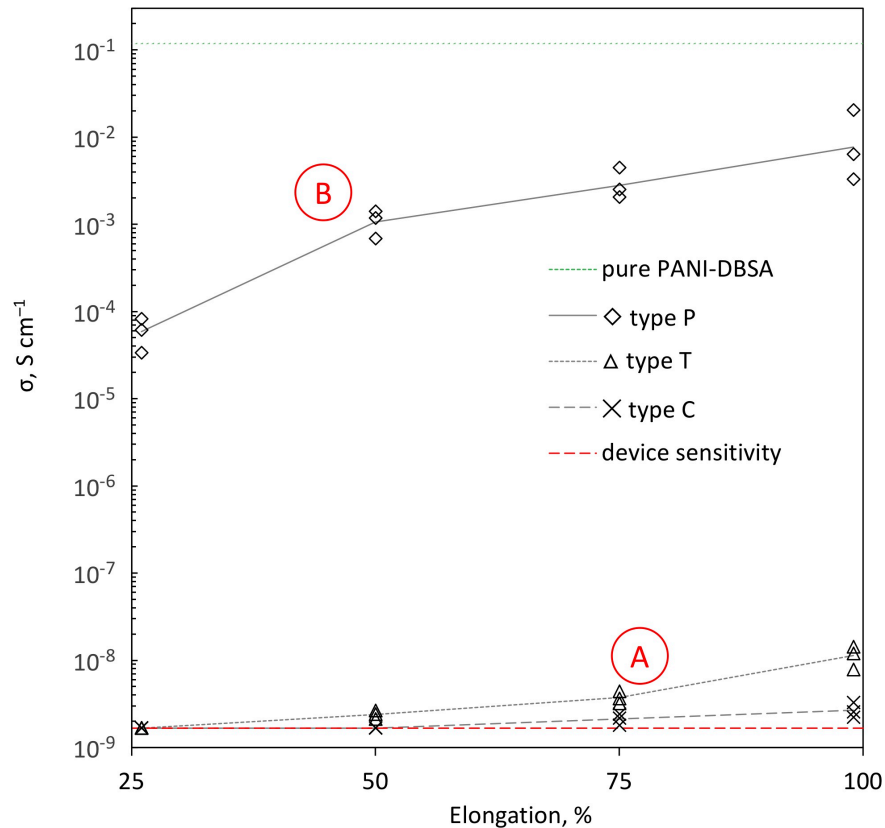
Figure 4-8. Through-plane conductivity of the samples with the different types of particles as a function of elongation.

Samples of types P and C had similar crystallite sizes and hence would have been expected to craze similarly. Both sample types showed significant mass gains to indicate adequate deposition of the conductive secondary phase in the cavitated matrix of polyethylene as a result of elongation. It was, therefore, interesting how different in conductivity these two sample types were in testing. At 50% elongation, the measured average conductivity for P50 (denoted as B in the graph) was 1.06×10^{-3} S·cm^{-1}, whereas it was only 1.67×10^{-9} S·cm^{-1} for C50. At 100% elongation, P100 showed an average conductivity of 2×10^{-2} S·cm^{-1}, which was close enough to the conductivity of the reference sample of pure PANI-DBSA, 1.2×10^{-1} S·cm^{-1}. In contrast, the conductivity for C100 conductivity showed no significant change compared with C50. The two curves representing the results for type C and P appear to be demonstrating the effects of the embedded nucleating agent as junctions in a conductive network since the mass gains results would have predicted better conductivity for sample type C, especially considering sample type T performed better despite how little PANI was deposited. The PANI fibers appeared to be contributing to electrical percolation of the secondary phase whereas the montmorillonite disrupted the conductive pathway. Accepting this analysis, the result indicates that the pathways of PANI within the crazes, in almost all the cases, only formed where a nucleating particle was present.

4.4.6   STRETCHABLE CONDUCTIVITY RESPONSE

Durability of the conductive network is an important property of flexible sensors, in expanding the scope of their application. Through-plane and in-plane conductivity for the new, highly conductive P100 sample was monitored while undergoing deformation up to a strain of 15% to quantify the ability of the secondary phase to move without fracturing inside the

stretching polyethylene matrix. Fig. 4-9 presents both conductivity measurements and includes a tensile stress-strain curve obtained for P100 so that the elastoplastic response of the polymer can be related to the trend in conductivity. The in-plane conductivity, even undeformed, was more than three orders of magnitude lower than through-plane, indicating that the crazes forming the secondary phase network were mostly oriented transversely to the direction of elongation, likely due to the relatively small crystallites. The drop in in-plane conductivity occurred progressively while the polymer displayed an elastic response, reflecting brittle failures in the inter-connecting conductive pathways (i.e., branching pathways formed transversely to the direction of crazing).
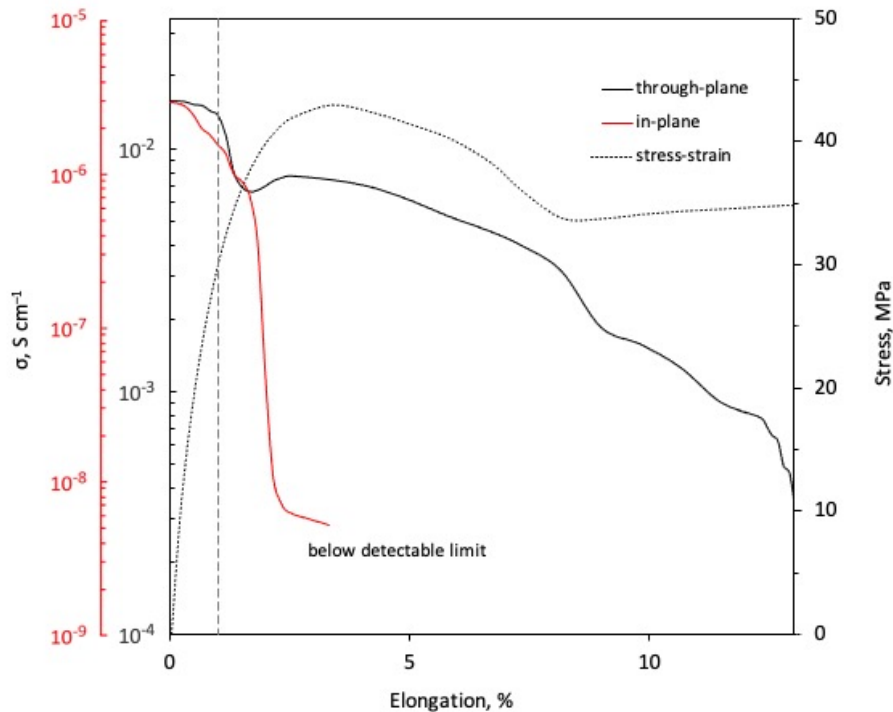
Figure 4-9. Change of through-plane and in-plane electrical conductivities during deformation of P100 with an average tensile stress-strain curve. The dotted vertical line limits a stable range of about 1% strain within which the through-plane conductivity varies insignificantly.

The near asymptotic decline in in-plane conductivity seen at 2-3% strain corresponded to yielding of the samples, after which the appearance of visible necking was seen.

The through-plane conductivity endured tensile deformation better, probably because the original crazing forming the secondary phase was largely transversely oriented and the tensile stresses therefore became concentrated at the polyethylene-PANI interface rather than in the PANI phase. At least while the polymer exhibited an elastic response, these transversely oriented PANI pathways were unaffected by the tensile deformation (less than 1% strain). Between 1% and 2% strain, through-plane conductivity decreased in a similar manner to in-plane conductivity. We believe the inter-connecting pathways (branches) were failing at the junction with the transversely oriented pathway, rather than in the middle of the branching pathway, causing a loss of conductivity in both the in-plane and through-plane direction for those pathways. Some plastic reorganization related to crystal slip was occurring in the sample structure,[151,152] though complete yielding had not yet occurred. Beyond the yielding point, further plastic deformation of the matrix polyethylene resulted in a slower yet gradual fragmentation of the conductive channels. However, even at 15% strain, the polymer remained quite conductive in the order of 10^{-3} S·cm^{-1}.

Cyclic deformation of P100 within the elastic limits (1% strain) showed a subtle irreversible change in conductivity per loading cycle, with a total decline of 5 mS·cm^{-1}, after ten cycles (Fig. 4-10).
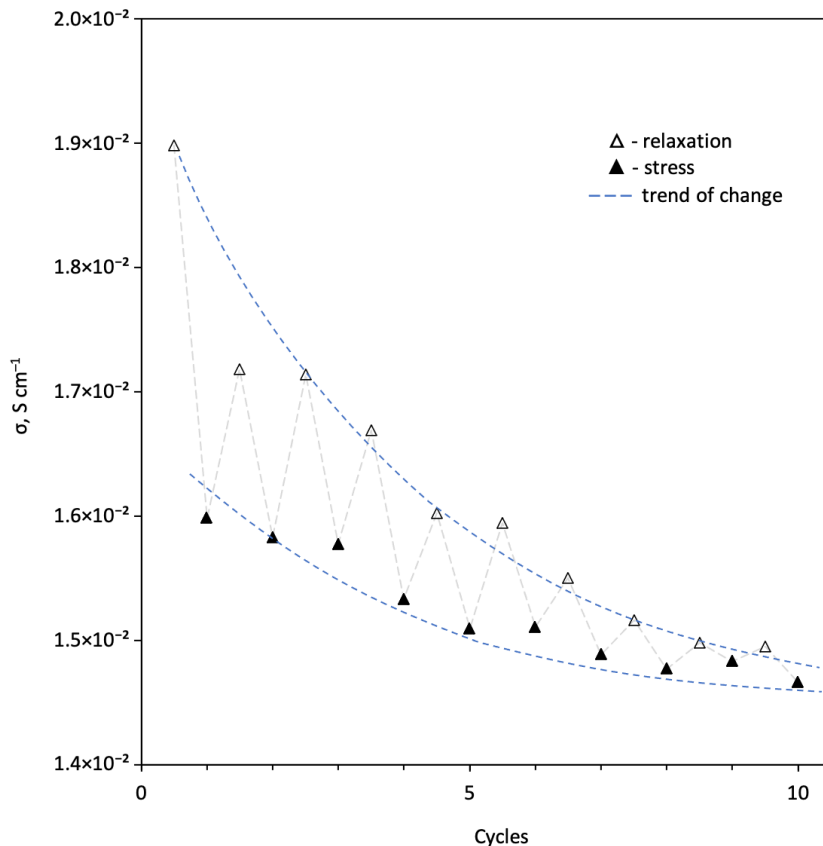
Figure 4-10. Cyclic deformation of P100 within the elastic limit of 1% strain for 10 cycles.

The difference in conductivity between the stress and relaxation stages decreased from cycle to cycle, reaching a value of 300 μS·cm⁻¹ by the end of the test. This decrease was probably due to rearrangements in the brittle polyaniline phase and the consequent reduction of the influence from the deformed polyethylene matrix on the phase integrity. After the test, the samples remained visually unchanged. Based on these results, cyclic deformation of the new conductivity polymer within 1% strain was considered adequately flexible in terms of both conductivity and elastic recovery.

4.5   CONCLUSION

The results in this paper demonstrate introducing advanced properties into otherwise inexpensive materials, based on establishing controlled percolative pathways from intercrystalline crazing and polymerizing a secondary phase within those channels. In this regard, controlled crazing is associated with penetration of a secondary phase monomer while retaining much of the physical nature of the matrix. Being inherently conductive, polyaniline was used to determine phase network continuity by measuring the in-plane and through-plane electrical properties of the resulting samples. Different types of nucleating particles were examined in the study to vary the size of crystallites in the matrix prior to deformation. Montmorillonite and pre-synthesized PANI fibers produced similar size crystallites and correspondingly, crazes large enough for the ingress of the emulsified monomer; however, only the latter was effective in percolation. The merging of the PANI fibers with the polymerized in-situ polyaniline, formed a continuous, highly conductive network with overall composite conductivity of 2×10^{-2} S·cm^{-1}, close in magnitude to the pure doped polyaniline (1.2×10^{-1} S·cm^{-1}). This sub-micron conductive network within polyethylene showed good retention of its electrical properties under cyclic stretching, indicating potential for flexible electronics.

4.6   ACKNOWLEDGEMENT

4.7   REFERENCES

(1)   Mozafari, M.; Chauhan, N. P. S. *Fundamentals and Emerging Applications of Polyaniline*; Elsevier, 2019.

(2)   Heeger, A. J. Polyaniline with Surfactant Counterions: Conducting Polymer Materials Which Are Processible in the Conducting Form. *Synthetic Metals* **1993**, *57* (1), 3471–3482. https://doi.org/10.1016/0379-6779(93)90462-6.

(3)   Osterholm, J.-E.; Cao, Y.; Klavetter, F.; Smith, P. Emulsion Polymerization of Aniline. *Polymer* **1994**, *35* (13), 2902–2906.

(4)   Adams, P.; Laughlin, P.; Metals, A. Synthesis of High Molecular Weight Polyaniline at Low Temperatures. *Elsevier* **1996**, *76* (1–3), 157–160.

(5)   Kohlman, R. S.; Epstein, A. J. Insulator-Metal Transition and Inhomogeneous Metallic State in Conducting Polymers. *Handbook of conducting polymers* **1998**, *2*, 85–122.

(6)   Ayad, M. M.; Salahuddin, N. A.; Alghaysh, M. O.; Issa, R. M. Phosphoric Acid and PH Sensors Based on Polyaniline Films. *Current Applied Physics* **2010**, *10* (1), 235–240. https://doi.org/10.1016/J.CAP.2009.05.030.

(7)   Virji, S.; Kaner, R. B.; Weiller, B. H. Hydrogen Sensors Based on Conductivity Changes in Polyaniline Nanofibers. *The Journal of Physical Chemistry B* **2006**, *110* (44), 22266–22270. https://doi.org/10.1021/jp063166g.

(8)   Kim, M.-S.; Kim, S.; Kong, H. J.; Kwon, O. S.; Yoon, H. Tunable Electrical-Sensing Performance of Random-Alternating Layered Graphene/Polyaniline Nanoarchitectures. *The Journal of Physical Chemistry C* **2016**, *120* (32), 18289–18295. https://doi.org/10.1021/acs.jpcc.6b03705.

(9)   Segal, E.; Tchoudakov, R.; Narkis, M.; Siegmann, A.; Yen Wei. Polystyrene/Polyaniline Nanoblends for Sensing of Aliphatic Alcohols. *Sensors and Actuators B: Chemical* **2005**, *104* (1), 140–150. https://doi.org/https://doi.org/10.1016/j.snb.2004.05.002.

(10)   Kar, P.; Choudhury, A. Carboxylic Acid Functionalized Multi-Walled Carbon Nanotube Doped Polyaniline for Chloroform Sensors. *Sensors and Actuators B: Chemical* **2013**, *183*, 25–33. https://doi.org/10.1016/J.SNB.2013.03.093.

(11)   Yang, C. Y.; Reghu, M.; Heeger, A. J.; Cao, Y. Thermal Stability of Polyaniline Networks in Conducting Polymer Blends. *Synthetic Metals* **1996**, *79* (1), 27–32. https://doi.org/https://doi.org/10.1016/0379-6779(96)80126-3.

(12)   Bhadra, S.; Khastgir, D.; Singha, N. K.; Lee, J. H. Progress in Preparation, Processing and Applications of Polyaniline. *Progress in Polymer Science* **2009**, *34* (8), 783–810. https://doi.org/https://doi.org/10.1016/j.progpolymsci.2009.04.003.

(13)   Thompson, M. R.; Motlagh, G. H.; Oxby, K. J.; Hrymak, A. N. Multiple Percolation in a Carbon-Filled Polymer Composites via Foaming. *Journal of Applied Polymer Science* **2010**, *115* (2), 646–654. https://doi.org/10.1002/app.30177.

(14)   Schilling, M.; Niebergall, U.; Alig, I.; Oehler, H.; Lellinger, D.; Meinel, D.; Böhning, M. Crack Propagation in PE-HD Induced by Environmental Stress Cracking (ESC) Analyzed by Several Imaging Techniques. *Polymer Testing* **2018**, *70*, 544–555. https://doi.org/https://doi.org/10.1016/j.polymertesting.2018.08.014.

(15)   Saad, A. K.; Abdulhussain, H. A.; Gomes, F. P. C.; Vlachopoulos, J.; Thompson, M. R. Studying the Mechanism of Biodiesel Acting as an Environmental Stress Cracking Agent with Polyethylenes. *Polymer* **2020**, *191*, 122278. https://doi.org/https://doi.org/10.1016/j.polymer.2020.122278.

(16)   Kornberg, A. B.; Thompson, M. R.; Zhu, S. Developing Continuous Submicron-Scale Conductive Interpenetrating Hydrogel Network in Polyethylene Matrices through Controlled Crazing and Polymerization. *Industrial & Engineering Chemistry Research* **2020**, acs.iecr.9b07010. https://doi.org/10.1021/acs.iecr.9b07010.

(17)   Volynskii, A. L.; Aleskerov, A. G.; Grokhovskaya, T. Y.; Bakeyev, N. F. Mechanical Behavior of Glassy Polyethylene Terephthalate Deformed in Liquid Adsorption Active Media. *Polymer Science USSR* **1976**, *18* (9), 2419–2426.

(18)   Volynskii, A. L.; Bakeev, N. F. *Solvent Crazing of Polymers*; Newnes, 2012; Vol. 13.

(19)   Rozanski, A.; Galeski, A. Plastic Yielding of Semicrystalline Polymers Affected by Amorphous Phase. *International Journal of Plasticity* **2013**, *41*, 14–29. https://doi.org/10.1016/J.IJPLAS.2012.07.008.

(20)   Pawlak, A.; Galeski, A. Stability of Spherulite Growth Rate. *Journal of Polymer Science Part B: Polymer Physics* **1990**, *28* (10), 1813–1821. https://doi.org/10.1002/polb.1990.090281012.

(21)   Nowacki, R.; Kolasinska, J.; Piorkowska, E. Cavitation during Isothermal Crystallization of Isotactic Polypropylene. *Journal of Applied Polymer Science* **2001**, *79* (13), 2439–2448. https://doi.org/10.1002/1097-4628(20010328)79:13<2439::AID-APP1051>3.0.CO;2-#.

(22)   Bucknall, C. B. New Criterion for Craze Initiation. *Polymer (Guildf)* **2007**, *48* (4), 1030–1041. https://doi.org/https://doi.org/10.1016/j.polymer.2006.12.033.

(23)   Pawlak, A.; Galeski, A.; Rozanski, A. Cavitation during Deformation of Semicrystalline Polymers. *Progress in Polymer Science* **2014**, *39* (5), 921–958. https://doi.org/10.1016/J.PROGPOLYMSCI.2013.10.007.

(24)   Ohtani, B.; Prieto-Mahaney, O. O.; Li, D.; Abe, R. What Is Degussa (Evonic) P25? Crystalline Composition Analysis, Reconstruction from Isolated Pure Particles and Photocatalytic Activity Test. *Journal of Photochemistry and Photobiology A: Chemistry* **2010**, *216* (2–3), 179–182. https://doi.org/10.1016/j.jphotochem.2010.07.024.

(25)   Han, Y.-G.; Kusunose, T.; Sekino, T. One-Step Reverse Micelle Polymerization of Organic Dispersible Polyaniline Nanoparticles. *Synthetic Metals* **2009**, *159* (1–2), 123–131. https://doi.org/10.1016/J.SYNTHMET.2008.08.011.

(26)   Stejskal, J.; Kratochvíl, P.; Jenkins, A. D. The Formation of Polyaniline and the Nature of Its Structures. *Polymer* **1996**, *37* (2), 367–369. https://doi.org/10.1016/0032-3861(96)81113-X.

(27)   Gokel, G. W.; Dean, J. A. *Dean's Handbook of Organic Chemistry*; McGraw-Hill handbooks; McGraw-Hill, 2004.

(28)   Federal Republic of Germany. *Surface Tension Values of Some Common Polymers/Test Liquids for Surface Energy Analysis*. www.surface-tension.de.

(29)   Rozanski, A.; Galeski, A. Controlling Cavitation of Semicrystalline Polymers during Tensile Drawing. *Macromolecules* **2011**, *44* (18), 7273–7287.

(30) Shreepathi, S.; Holze, R. Spectroelectrochemical Investigations of Soluble Polyaniline Synthesized via New Inverse Emulsion Pathway. *Chemistry of Materials* **2005**, *17* (16), 4078–4085. https://doi.org/10.1021/cm050117s.

(31) Zheng, W.-Y.; Levon, K.; Taka, T.; Laakso, J.; Österholm, J.-E. Doping-Induced Layered Structure in N-Alkylated Polyanilines. *Polymer Journal* **1996**, *28* (5), 412–418. https://doi.org/10.1295/polymj.28.412.

(32) Levon, K.; Ho, K.-H.; Zheng, W.-Y.; Laakso, J.; Kärnä, T.; Taka, T.; Österholm, J.-E. Thermal Doping of Polyaniline with Dodecylbenzene Sulfonic Acid without Auxiliary Solvents.   *Polymer*   **1995**,   *36*   (14),   2733–2738. https://doi.org/https://doi.org/10.1016/0032-3861(95)93650-B.

(33) Kumar, A.; Kumar, V.; Sain, P. K.; Kumar, M.; Awasthi, K. Synthesis and Characterization of Polyaniline Membranes with – Secondary Amine Additive Containing N,N′-Dimethyl Propylene Urea for Fuel Cell Application. *International Journal   of   Hydrogen   Energy*   **2018**,   *43*   (47),   21715–21723. https://doi.org/10.1016/J.IJHYDENE.2018.04.083.

(34) Zhang, F.; Halverson, P. A.; Lunt, B.; Linford, M. R. Wet Spinning of Pre-Doped Polyaniline into an Aqueous Solution of a Polyelectrolyte. *Synthetic Metals* **2006**, *156* (14–15), 932–937. https://doi.org/10.1016/J.SYNTHMET.2006.06.002.

(35) Hassan, P. A.; Sawant, S. N.; Bagkar, N. C.; Yakhmi, J. V. Polyaniline Nanoparticles Prepared   in   Rodlike   Micelles.   *Langmuir*   **2004**,   *20*   (12),   4874–4880. https://doi.org/10.1021/la0498096.

(36) Seguela, R.; Elkoun, S.; Gaucher-Miri, V. Plastic Deformation of Polyethylene and Ethylene Copolymers: Part II Heterogeneous Crystal Slip and Strain-Induced Phase Change.   *Journal   of   Materials   Science*   **1998**,   *33*   (7),   1801–1807. https://doi.org/10.1023/A:1004340902180.

(37) Gomes, F. P. C.; West, W. T. J.; Thompson, M. R. Effects of Annealing and Swelling to Initial Plastic Deformation of Polyethylene Probed by Nonlinear Ultrasonic Guided Waves.   *Polymer*   **2017**,   *131*,   160–168. https://doi.org/https://doi.org/10.1016/j.polymer.2017.10.041.

4.8   GRAPHICAL ABSTRACT
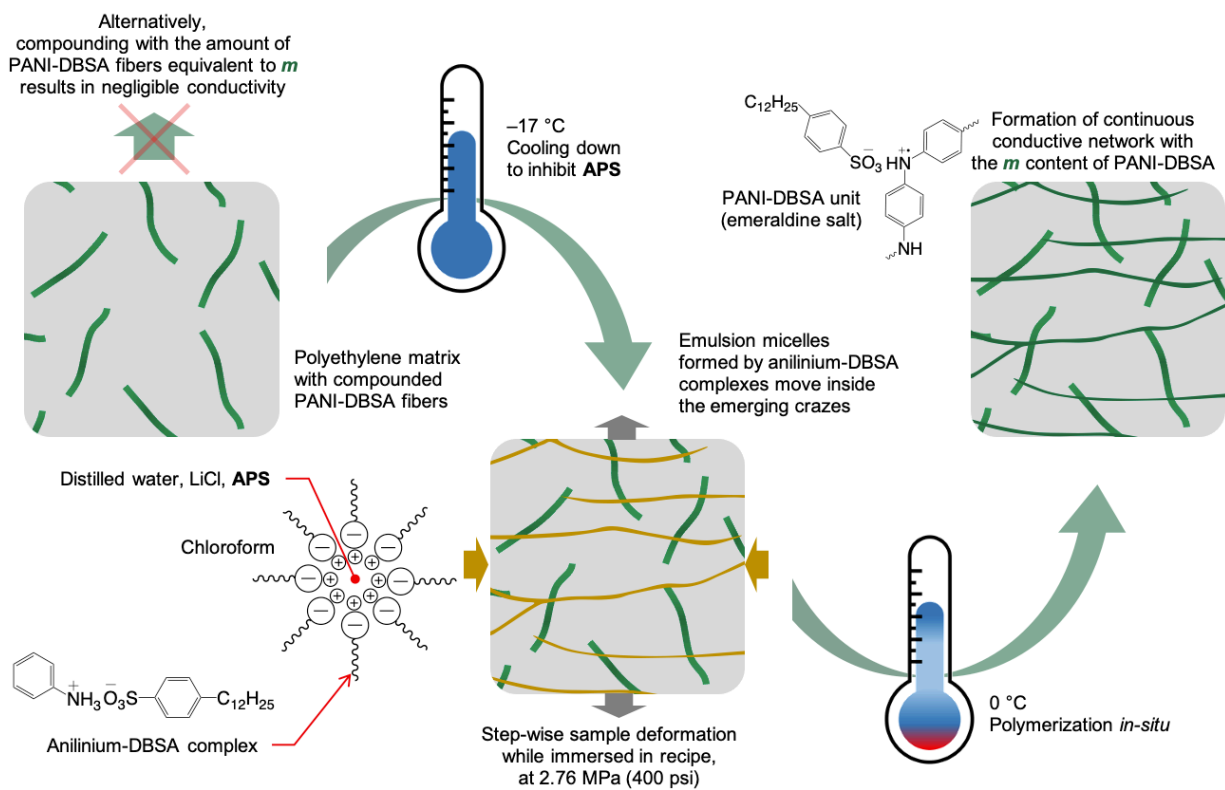
5   FLEXIBLE NANOSCALE CO-CONTINUOUS STRUCTURES PREPARED BY CONTROLLED CRAZING OF ETHYLENE-OCTENE ELASTOMERS AND IN SITU POLYMERIZATION OF CONDUCTIVE NETWORKS

In this chapter, we attempted to replace polyethylene with materials from the polyolefin elastomer (POE) family. The study considers the initial morphology of the matrix elastomers, specifically the size and frequency of the crystalline domains distributed in the elastomer volume, as a factor that determines the materials' cavitation behavior and, accordingly, the quality of the conductive network polymerized *in situ*. Acrylic hydrogel was chosen as the

conductive material at the stage of selecting the most suitable POE. The final material needed to exhibit electron conductivity, so after numerous unsuccessful attempts, a working method was found to replace the hydrogel with an electron-conductive phase of polyaniline. The chapter is based on the paper published in The Canadian Journal of Chemical Engineering, 2022 (doi:10.1002/cjce.24796). The permission for this reproduction is granted by Wiley.

Author contributions:

The preliminary idea of this research was generated from the discussion with Dr. Thompson; he proposed using polyurethane domains to replace the semi-crystalline morphology of olefinic materials. Subsequently, polyurethanes were replaced by polyolefin elastomers since they did not require additional safety approvals. I was responsible for conducting all the experiment steps, including the sample preparation, which also required the chemical compatibilization of two immiscible polymers. Additionally, I synthesized matrix polycaprolactone, not only because I ran out of it but also because it gave me joy. Based on the results obtained in the previous works, I selected the experimental conditions and performed the mechanical trials in a high-pressure reactor, followed by the final polymerization of the continuous conductive networks. The success of Dr. Zhu's students in his laboratory at the Chinese University of Hong Kong encouraged me to keep up, so I spent a lot of extra time developing a method for producing an electron-conductive material by partially replacing matrix phases during polymerization. Under the supervision of Dr. Thompson, I troubleshot this method and analyzed the data, especially those obtained from DMA. Finally, Dr. Thompson and I prepared the manuscript, and Dr. Zhu did its final revision before including it in this thesis.

5.1   ABSTRACT

An approach based on controlled crazing and post-polymerization was used to incorporate a nanoscaled conductive co-continuous network into a commercial polyolefin elastomer (POE). Three POE films of differing crystallinity and phase morphology were stretched in a reactive mixture of acrylic polymerization precursors that possessed an affinity for the olefinic materials and acted as a surface-active agent for craze promotion. As a result, a rigid acrylic hydrogel phase was grown in the void space associated with crazing which prevented the formed channels from collapsing after mechanical stresses were removed. The hydrogel phase offered ion conductivity properties to the POE. Simply replacing the acrylic monomer with an aniline emulsion for polymerization did not lead to the same outcome in terms of a continuous network; the materials became insulative after removal of mechanical stresses due to fragmentation of the polyaniline channels from the unrestrained elastic relaxation of the POE. This problem was overcome by solution casting POE with polycaprolactone (PCL) into films and subsequently, partially dissolving and leaching PCL from the blend while a sample was stretched in an aniline emulsion medium containing formic acid. The residual PCL left in the crazes reinforced the polyaniline to prevent fragmentation and allowing the formation of a highly electron conductive secondary phase.

5.2   INTRODUCTION

Elastomers are a class of engineering materials that have found wide application in various industries such as automotive, footwear, cable, construction, medical, and many others.[153] The hallmark of elastomers is that they are highly flexible and can be deformed to at least twice their original size, regaining their shape when the stress is released. Many elastomers

are, in fact, three-dimensional networks resulting from entanglements and crosslinking of the linear or branched molecules. Thermoplastic polyolefin elastomers (POEs), however, are not crosslinked. Structurally, they are block copolymers consisting of at least two immiscible comonomers, which define their morphology. A wide variety of property combinations can be achieved by altering the molecular weight, ratio, and chemical type of the segments formed by these comonomers.

As in the case of semicrystalline polymers, mechanical and viscoelastic properties of POEs are derived from a combination of their crystalline and amorphous regions, formed by linear and branched segments, respectively. The linear segments in a POE structure tend to form bundled crystallites without well-developed spherulites (hard domains), surrounded by a fringe of amorphous chains of branched units (soft domains).[154] This concept of domain structure, with hard domains acting as stress-concentrating points within soft domains, was taken as a basis for analysis of the crazing behavior of POEs. In previous studies, we demonstrated that the crazes in regular semicrystalline polyolefins were initiated at primary voids formed at the crystal-amorphous interface due to mechanical stresses. The voids originate from crystallization when chains are consumed from the amorphous phase in the forming of crystals, resulting in depleted areas at the interface.[2,53] The crystalline and amorphous fractions in POEs, in contrast, are formed from the different chain segments (ethylene and octene, respectively) without causing chain depletion at the interface and, therefore, resulting in a void-free initial material morphology. However, while a POE is stretched, the hard domains act as stress-concentrators on which the primary voids to initiate crazing are formed.

In order to conceive the mechanisms of void appearance and establish the effect of this mechanism on the resulting morphology, the domains in the original elastomeric structures can

be considered as interlinked elastic inclusions (particles) within an elastoplastic polymer environment (matrix). The strength of the particle-matrix interface in a POE is insured thermodynamically by dispersion forces and covalently by transition polymer chains. As shown in the theoretical research by Eshelby,[155–157] then Thompson and Hancock,[158] and later by Wilner,[3] cavitation in such systems can be predicted by analysis of their stress fields. According to the derivations established by those authors, for a hard particle well-bridged with a soft matrix, maximum plastic flow occurs in the matrix volume at some distance from the particle boundary, above and below the particle in the direction of uniaxial tensile deformation, as shown in Fig. 5-1a. The size and location of the flow areas are dependent on the particle radius, as well as Young's moduli and Poisson ratios of both particle and matrix. With progressive deformation, the flow areas yield, forming two voids, on which crazes are initiated and propagated perpendicular to the axis of the applied stress.
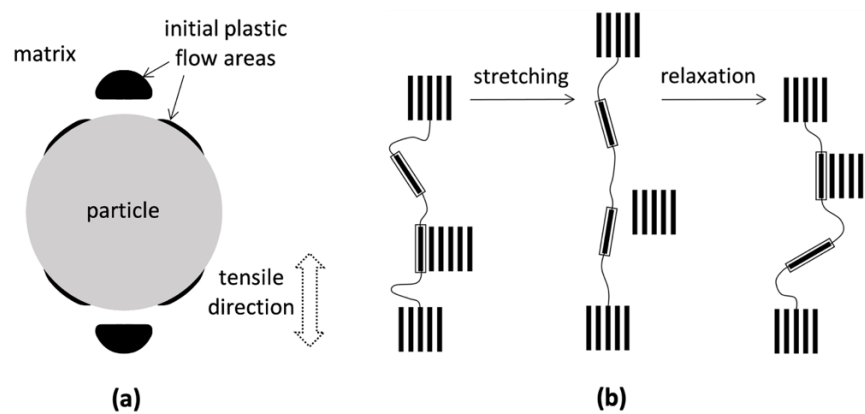
Figure 5-1. Initial plastic flow in the system by Eshelby (a),[9] with permission from Elsevier, and schematic illustration of defragmentation of crystallites by Bensason (b),[10] with permission from ACS.

Another essential factor influencing materials' crazing behavior is described in Bensason et al.[10] The authors studied the mechanism of fragmentation and recombination of crystals (detachment-attachment of chains) at cyclic stress, as shown in Fig. 5-1b., and compared the behavior of materials with different initial morphologies. According to their results, materials with smaller crystals were more susceptible to such chain rearrangements, therefore having a greater potential for self-recovery, which can not only suppress their plastic deformation but can potentially increase their crystallinity.

With the general trends described above, different crazed networks can be formed under uniaxial deformation based on the initial elastomer morphology of a POE: the number and size of hard domains, as well as the distance between them, which is determined by the ethylene-octene fractions ratio and the sequence lengths of the ethylene and octene segments. The mechanism of formation of such networks under mechanical stress is well-studied in the research by Pawlak et al.[11] The network is used to introduce a conductive phase in otherwise commodity materials. The experimental conditions (such as applied pressure, stretching rate, matrix-medium thermodynamical compatibility, and mechanical deformation parameters) will influence the formation of a network within a matrix. Various monomeric liquids can serve as a penetrating agent while simultaneously enabling *in situ* synthesis of a conductive phase within the craze network. The novel focus of the present research was evaluating the effectiveness of craze initiation with differing hard domains in polyolefin elastomers. We aimed for the first time to engineer a flexible conductor by taking advantage of the domain-like morphology related to the chemical composition of the commercial POEs used. The percolating networks' architectures, which resulted from the effectiveness of crazing, were implicitly evaluated by conductivity of an introduced secondary phase.

5.3   EXPERIMENTAL METHODS

5.3.1   MATERIALS

POEs Engage 8003, Engage 8137, and Engage 8180 were purchased from the Dow Chemical Company, and Luperox A98 benzoyl peroxide (BPO, ≥98%) was supplied by Arkema (Burlington, Canada). The following chemicals were purchased from Sigma-Aldrich (Mississauga, Canada) and used as received: cyclohexane (≥99.5%, anhydrous), 1-methyl-2-pyrrolidinone anhydrous (NMP, ≥99.5%), tin(II) 2-ethylhexanoate (≥95%), N,N′-Methylenebis (acrylamide) (MBA, 99%), ethanol anhydrous (≤0.005% water), methanol anhydrous (≥99.8%), aniline (≥99.5%), 4-dodecylbenzene sulfonic acid (DBSA, mixture of isomers ≥95%), ammonium persulfate (APS, ≥98%,), lithium chloride (LiCl, ≥99%), formic acid (≥95%), chloroform (≥99%).

Additional chemicals purchased from Sigma-Aldrich (Mississauga, Canada) included ε-Caprolactone (≥97%) which was dried over CaH_2 and distilled under reduced pressure; Iron(III) bromide anhydrous (≥98%; Sigma-Aldrich) was vacuum dried prior to use and stored under nitrogen; acrylic acid (AAc, 99%) was purified of its inhibitor; and 2,2′-Azobis (2-methylpropionitrile) (AIBN, 98%) was recrystallized from methanol.

5.3.2   PREPARATION OF MATRIX SAMPLES

For the preparation of a POE film, beads of the corresponding material were dissolved in cyclohexane at 85 °C. The solution was cast onto an aluminum substrate and then kept in an oven at 30 °C under vacuum overnight to remove cyclohexane residues. The final cast film had a thickness of 100 ± 10 μm. Dogbone-shaped samples were cut out of a film with the middle-narrowed section being 5 mm long and 5 mm wide, and their larger ends used for mounting in the tensile rig.

Polycaprolactone was synthesized in bulk by ring-opening polymerization (ROP) of ε-caprolactone with tin(II) 2-ethylhexanoate as an initiator and iron(III) bromide as a catalyst, according to the mechanism described by Storey et al.[12] The components were added at a molar ratio of 200:1:5 (monomer to catalyst to initiator), as proposed in the study by Hege et al.[13] A 50 ml two-neck round-bottom flask was sealed, heated up to 110 °C in an oil bath and purged with dry nitrogen. 0.34 g catalyst and 25 ml ε-caprolactone monomer were added to the flask. 1.83 ml of the initiator was added to start the reaction. The reaction mixture was continuously agitated with a stir bar and kept under a nitrogen atmosphere throughout the synthesis until the reaction mixture became solid. The synthesized polymer was dissolved in chloroform, precipitated in methanol, and then dried.

To prepare the POE-PCL blend, 2 g of POE was first mixed into cyclohexane at 85 °C for 2 hrs until the POE was completely dissolved. Then 0.2 g BPO was added to the flask and left at 85 °C for another 4 hrs with continuous agitation; the benzoyl peroxide was used to generate carbonyl or ketone functional groups along the POE chains via free-radical oxidation to improve compatibility with the PCL.[14] PCL was added to the mixture at a 50:50 ratio with the POE at

85 °C and constantly agitated for 24 hrs, after which the solution was deposited onto a PTFE sheet and dried in an oven at 30 °C overnight under vacuum until the cyclohexane was evaporated. The deposited film was then compression molded at 85 °C to remove residual bubbles and achieve an overall film thickness of 100 μm. The final film had a cloudy-whitish appearance, without visible heterogeneities and agglomerated particles.

5.3.3   PREPARATION OF REACTIVE MIXTURES FOR CONDUCTIVE PHASES (PAA & PANI-DBSA)

As in our previous study,[4] a cross-linked PAA was used as the ion-conductive secondary phase for a co-continuous network due to its low toxicity, ease of synthesis, and high affinity of the monomeric precursor for the elastomeric matrices. Along with the acrylic acid monomer, the resulting mixture included 3 wt% MBA as a cross-linking agent and 1 wt% AIBN as a thermally sensitive initiator. After premixing with 30 vol% ethanol and subsequent sonication, the reactive mixture was cooled down to 0 °C to avoid spontaneous polymerization. *In-situ* synthesis of PAA was done in the presence of the deformed POE film, as described below.

In the present research, we used DBSA-dopped polyaniline (PANI-DBSA, emeraldine salt form) as an electron-conductive material. The reactive aniline emulsion was prepared as follows. Under vigorous agitation, 0.285 g of aniline was added dropwise to a solution containing 1.53 g of DBSA in formic acid, after which the total volume of the reactive mixture was brought up to 16 ml with formic acid. After emulsion homogeneity was achieved, its temperature was decreased to –10 °C. 0.3 g of APS was dissolved in 1.25 ml of distilled water, with the addition of 2.623 g of LiCl to keep the solution unfrozen. The solution was also cooled down to –10 °C and then slowly added dropwise to the emulsion under vigorous agitation.

5.3.4   DEFORMATION OF POE AND POE-PCL MATRICES IN A LIQUID MEDIUM

The general deformation procedure was basically adopted from the two previous studies.[3,4] The custom tensile rig was contained inside a high-pressure reactor, which was frequently depressurized to carry out a step-wise deformation of the sample followed by purging and subsequent re-pressurizing to 2.76 MPa (400 psi) with dry nitrogen. Step changes in the extent of deformation were done at 10% per cycle increment and held constant with each step for 1000 sec so that the resulting elongation rate was 0.03 mm·min⁻¹. Deformation was performed at ambient room temperature. Each set of experimental conditions was applied for a minimum of three repeats.

For POE dogbone samples, the deformation was carried out until the degree of longitudinal elongation reached 50, 100, 200, or 300% strain. This distinguished the present research from the previous two studies, in which the stiffer, less elastic polyethylene matrix only needed to be stretched up to 100% strain to induce sufficient crazing with through-plane microcracks propagating from one side to the other of a film sample. After deformation, the reactor containing the sample that remained stretched in the rig and immersed in the monomer, without depressurizing, was heated to 60 °C overnight in the case of Engage 8003, and 30 °C for a week in the cases of Engage 8137 and Engage 8180, due to the different melting points of the elastomers.[15] After polymerization was completed, the samples were released from the tensile rig and scrapped clean of any hydrogel at the surface of the sample. Then, the sample was vacuum dried for 24 hours to remove any monomer residues.

To introduce polyaniline as the secondary phase in POE, the more rigid POE-PCL sample was mounted in the tensile rig in the presence of an emulsion of aniline, with the

subsequent polymerization being partially adopted from a previous study[3] but was customized as follows. Formic acid was chosen as the medium due to its ability to dissolve the PCL domains without significantly compromising other process parameters, and as a weakly polar liquid, it has proven to be an effective penetrating agent; its surface energy is 0.0398 N·m⁻¹,[16] which is fairly close to that of PCL, 0.0378 N·m⁻¹,[17] and branched polyethylene, 0.0353 N·m⁻¹.[18] A POE-PCL blend sample was pre-stretched up to 100% strain in pure formic acid and left overnight (primary stage of deformation). Then, the medium was replaced with an aniline emulsion formic acid as a medium in the tensile rig (secondary stage of deformation), while the blend sample was stretched up to 300% strain; the low viscosity of the emulsion based on formic acid was an advantage giving the medium a higher penetration capacity.[16–18] The reaction temperature was lowered to –8 °C to inhibit the decay of APS and thus ensure that the deforming sample was fully impregnated with the reaction emulsion before polymerization began. After the stretching was completed, the temperature of the reaction mixture was elevated up to 0 °C and maintained at this condition for 24 hrs, enabling APS to decay and initiate the reaction *in situ*, directly in the cavitated matrix network. After polymerization, the samples were released from the tensile rig and scrapped clean of any polyaniline at the surface of the sample. Then, the sample was vacuum dried at 40 °C for 24 hrs to remove any residues.

5.3.5 DSC CHARACTERIZATION

Thermal analysis was performed for the Engage 8003, Engage 8137, and Engage 8180 raw materials using a differential scanning calorimeter (DSC) model Q200 (TA Instruments) with nitrogen purge. The thermal history of the specimens, each of about 5.0-7.0 mg, was first removed by heating them to 160 °C and holding at that temperature for 5 min. The specimens

were then cooled down to −20 °C at a rate of 10 °C/min. This temperature was maintained at −20 °C for 5 min and was then elevated up to 160 °C at the same rate, 10 °C/min.

5.3.6   DMA CHARACTERIZATION

The stress relaxation test was conducted using Dynamic Mechanical Analysis (DMA) in tensile mode with the bench device DMA 2980 (TA Instruments). The strain by 10% increments was applied stepwise instantaneously and held constant with each step for 1000 sec. while the stress was monitored as a function of time, allowing for detection of viscoplastic flow in the matrix material. The samples were first deformed in air and then immersed in a sealed sleeve filled with ethanol, a non-hazardous substitution for the acrylic monomer used in the actual experiment. The penetrating capacities of these two liquids were similar due to their close surface energies; for ethanol, this value was only slightly lower (0.0245 N·m⁻¹) than that of the acrylic monomer (0.0281 N·m⁻¹).[16] In other words, these trials by DMA mimicked the actual deformation of the samples in our tests, with and without immersion in the penetrating agent, showing its effect on the mechanical behavior of the tested materials.

5.3.7   CONDUCTIVITY MEASUREMENT

Measurement of ion conductivity was accomplished by measuring resistivity across an area of samples that contained the acrylic conductive phase. The samples were immersed in an electrolyte, 1M aqueous lithium hydroxide solution, for 48 hrs to neutralize the carboxylic groups in the acrylic material, repeatedly washed with DI water, dried, and weighed. The edges and the topmost layers on both sides of the samples that might be excessively enriched with the acrylic material and result in circumventing ion transport, were taken off. The resulting

rectangular specimens were placed over the opening notched out in a polystyrene container and sealed in place with melted paraffin. Two polished copper electrodes were attached to the two exposed sides of a specimen but not sealed to enable electrolyte wetting of the specimen surfaces. The electrodes were connected to the measuring device by silver-plated wires. The container with the embedded specimen was inserted into a container of larger diameter, forming an electrochemical cell, where the specimen acted as an ion-exchange separator. Both containers were filled with the same aqueous alkaline electrolyte and left for 12 hrs to saturate the specimens. The electrolyte pH was maintained at 13.7 by continuous agitation and frequent addition of fresh electrolyte to minimize signal drift during measurements. The measured values were always taken ten seconds after the measurement circuit's closure, maintaining the results' consistency. The cell design precluded any leaks between the upper and lower parts and, with careful assemblage, ensured ion transport only through the embedded specimen.

Conductivity for the materials based on the POE-PCL framework with a polyaniline electron-conductive phase (POE-PCL-PANI) was measured dry during stepwise stretching of the specimens, which were prepared by cutting off the edges that might be excessively enriched with polyaniline. The tests were performed with a benchtop Universal Mechanical Testing System (Model 3366, Instron Corporation, Canton, MA). An overall stretching rate was 2.5 mm·min⁻¹. The electrodes were not permanently affixed to the specimen. Instead, the specimen was compressed with a clamp equipped with two copper electrodes after each stretching step. The measured values were taken immediately after the clamp was attached to avoid a decline in signal due to specimen relaxation.

The DC bulk resistance R was measured by an Agilent 34401A 6½ Digit Multimeter, followed by calculating resistivity by considering the total amount of both fractions (contact area

of the electrode faces *A* and thickness of the specimen *L*) by $\rho = (R \cdot A)/L$. The DC conductivity σ was calculated in $S \cdot cm^{-1}$ by the formula $\sigma = 1/\rho$.

5.3.8   RESPONSE IN CONDUCTIVITY TO CYCLIC MECHANICAL DEFORMATION

Electron conductivity of the POE-PCL-PANI samples was also measured in response to multiple stress-relaxation cycles by the procedure developed for our previous research.[3] The test specimens were prepared as described in the previous section. They were elongated within the so-called survival range determined from the previous test. Within the range, the specimens' conductivity decreased moderately and remained above 10^{-1} $S \cdot cm^{-1}$. The resistance value *R* was measured twice for each cycle, before and after the specimens were stretched for 100 cycles in total. The DC conductivity σ was calculated as described in the previous section.

5.3.9   MORPHOLOGY ANALYSIS

SEM images were obtained by a scanning electron microscope (JSM 7000, JEOL, Japan) operated at 3.0 kV. Samples were cryogenically fractured in the middle of the narrow section, or sectioned on a manual rotary microtome (Leica Biosystems). The exposed surfaces were then sputter-coated with a 5 nm thick layer of platinum. The obtained micrographs were optionally analyzed using ImageJ software (National Institute of Health, U.S.) to determine the area after removal of the conductive secondary phase, by detecting the contours based on about five hundred iterations for each image.

5.4   RESULTS AND DISCUSSION

5.4.1   INITIAL DOMAIN MORPHOLOGY OF POE SAMPLES DETERMINED BY DSC

As noted above, each POE exhibits a unique combination of hard and soft domains, which enables control of its deformation behavior with a high level of accuracy.[1] Knowing the morphology enables one to choose the proper matrix material by predicting its crazing behavior in the subsequent experiments.
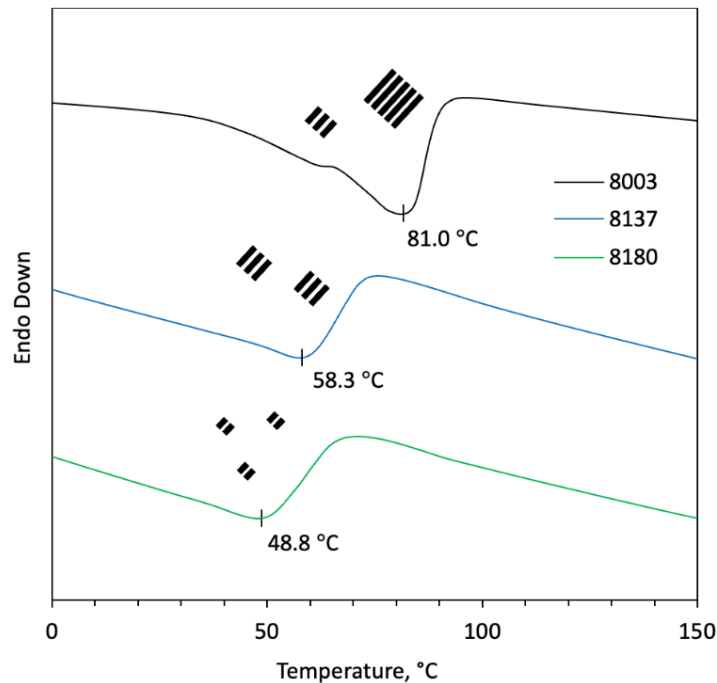
Figure 5-2. DSC melting curves for Engage 8003, Engage 8137, and Engage 8180, with a schematic representation of the hard domain structure for each material.

Fig. 5-2 shows the DSC curves for three POEs: Engage 8003, Engage 8137, and Engage 8180. The narrowness of an endotherm is typically attributed to more consistent crystal size, whereas the melting temperature indicates the size of the crystals that consume more heat

122

during the phase change (within the same family of polymers). On the basis of assumed equivalent crystallinity, materials with larger crystals will have higher melting temperatures. Engage 8003 exhibits a melting peak at 81 °C due to the larger crystals, the highest temperature of the three materials tested. The melting temperature of Engage 8003 (as well as Engage 8137 and Engage 8180 mentioned below) is slightly different from the value provided by DOW.[15] This insignificant inconsistency is likely due to differences in sample preparation procedures, calorimetric cell designs, purge gas purity, and other factors. The material density is 0.885 g/cc, which is close to the upper limit for polyolefin elastomers.[19] The crystallinity of Engage 8003 is 25%,[15] with its 30 wt.% (90.4 mol%) of linear ethylene segments fraction.[20] This means that a significant amount of the ethylene segments does not crystallize and, therefore, belong to the amorphous material volume. The melting temperatures of the second and third selected materials, Engage 8137 and Engage 8180, were 58 and 49 °C, respectively, which evidences that Engage 8137 contains larger crystals. These materials have the same linear ethylene segments fraction, 42 wt.% (84.7 mol%).[21] According to DOW Chemical's technical specification, the density of Engage 8137, 0.864 g/cc, is only slightly higher than that of Engage 8180, 0.863 g/cc.[15] The provided densities of the elastomeric materials are narrowly consistent with their linear and branched segment ratios, implying that both parameters are related. The crystallinity of Engage 8180, however, is higher than that of Engage 8137, being 16% and 13%, respectively.[15] This appears counterintuitive, given that both materials have nearly the same densities and crystal-amorphous ratios. This difference might be attributed to the comonomer distribution in the elastomer chains. In the research by Sanchez and Eby, the authors found that the elastomers with thicker crystals had lower crystallinity than those with thinner crystals, with the equivalent fraction of linear sequences for both materials. This phenomenon was due to the

ability of long sequences to form lamellas even while capturing amorphous inclusions, which resulted in accumulating defects and decreased the total crystalline fraction volume.[22] Similarly, the higher crystallinity of Engage 8180, compared to Engage 8137, can be attributed to shorter and more frequently alternating sequences, which result in thinner and hypothetically more homogeneous (i.e., contain fewer crystal defects) crystals, spaced closer and more frequently interconnected by transition chains. The concept is in good agreement with the DSC data and explains the relationship between the size of crystals and the total crystallinity of the materials.

The peak of the endotherm of Engage 8180 is approximately 3% broader than that of Engage 8137, suggesting greater variation in the crystal size. The influence of the initial crystal size on the increase in crystallinity is explained in the research by Minick et al., in which the authors investigated the morphology of crystallizable sequences in POEs obtained on different catalyst systems.[23] They found the tendency of thinner crystals to thicken with time due to the linear chain unit's reorganization by the following mechanism. The transition chains move through the crystals, energetically occupying more favorable positions. As a result, the defects are gradually ejected from the crystals, increasing their homogeneity and, therefore, calorimetric response. The crystals of Engage 8180 favor the passage of the chains, increasing the material crystallinity. This process appears uneven (i.e., crystals grow at a different speed), as evidenced by the broader melting peak of the material. Thicker crystals of Engage 8137 impede the movement of chains through the lamellar volume. The material's melting peak is narrower, indicating a more consistent crystal size and suggesting that their growth is inhibited.

5.4.2   SELF-RECOVERY POTENTIAL OF POE SAMPLES DETERMINED BY DMA

The potential for self-recovery was evaluated by DMA for the three POEs, with results at 29 °C shown in Fig. 5-3.
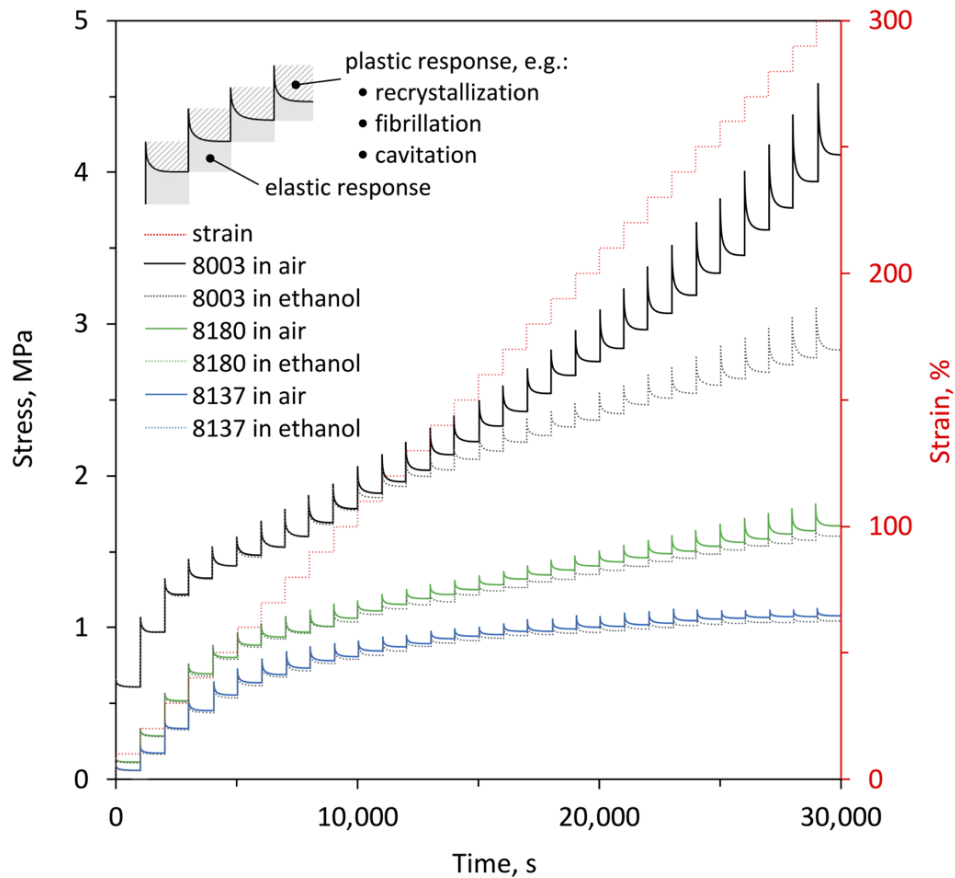
Figure 5-3. Stress-relaxation DMA curves for Engage 8003, Engage 8180, and Engage 8137, taken at 28-31 °C. Each material was tested in the air (solid lines) and immersed in ethanol (dotted lines).

For Engage 8003, the beginning of deformation in the figure was characterized by a high proportion of elastic response up to achieving ~50% strain. The difference between the samples tested in air and immersed in ethanol was negligible, suggesting that penetration of ethanol into

the volume was either near-surface or very local and had little effect on the bulk strength of the elastomer. With further deformation, the detected stresses for the sample deformed in air were noticeably increased, which corresponds to hardening via micronecking. In contrast, the sample deformed in ethanol demonstrated a decrease in stress, which was likely the result of intensive penetration of ethanol into the volume through the newly formed crazes.

Initially translucent, the sample deformed in air turned whitish as a result of evident fibrillation (micronecking) throughout the entire sample part subjected to deformation. After the test, the sample's ability to recover its shape was mainly lost. In contrast, once removed from the testing cell, the sample deformed in ethanol partially recovered its shape. The material structure was preserved due to an increase in the frequency of the newly formed crazes, resulting from the penetration of ethanol through the primary pathways during sample stretching. With the increase in frequency, the inner diameter of the emerging crazes remained small, which ensured high capillary pressure and, as a consequence, effective delivery of the ethanol inside the material. The sample was practically devoid of visible whitening, suggesting that the scale of fibrillation was significantly decreased, resulting in less severe material damage.

Based on the assumption that larger crystalline domains generate voids of larger diameter, which are cavitated more efficiently when the sample is stretched, the process of primary crazing and consequent saturation of a sample volume with ethanol in Engage 8137 was expected to be more intense than in Engage 8180. By analogy with Engage 8003, it would be seen from the greater difference in stress required to maintain an equivalent strain of the samples tested in air and immersed in ethanol. In reality, Engage 8180 demonstrated a more noticeable response to the immersion in ethanol. At first, this appeared counterintuitive but was later explained by the following mechanism. Since smaller and frequently distributed domains

resulted in narrow opening crazes in Engage 8180, it was hypothesized that the small craze diameter contributed to higher capillary pressure, leading to more effective penetration of ethanol into the matrix. The behavior, shown by Engage 8003, which has even larger domains than Engage 8137, can be explained by the material bimodality. It appears that the material linear segments have two different sequence lengths, with some portion of shorter inclusions. As shown in the research by Liu et al., such intrachain sequence heterogeneity results in segregation into crystal domains of different sizes and can be detected by the multi-modality of DSC curves of ethylene-octene elastomers.[24] The manufacturer does not explicitly indicate this property of Engage 8003, and yet, bimodality was seen in its thermogram in Fig. 5-2; a large endo-peak is preceded by a small peak with a lower melting point, indicating a second crystalline fraction.

It is worth noting that the stress responses of these three tested materials, regardless of the environment in which they were deformed, was not strictly a function of the crystal size, but appeared to be a result of the combination of factors such as the spacing between crystals, the frequency of transition chains between them, the total material crystallinity, the presence of crystal defects, and distribution in the crystal size (multimodality).

5.4.3   MORPHOLOGY OF THE POE-PAA SAMPLES AFTER DEFORMATION

Unlike the DMA tests conducted in ethanol, the actual experiment implied stretching the samples in the acrylic medium with its subsequent polymerization. The extent of cavitation in the material samples, deformed in the presence of acrylic acid to preserve the formed channels, was examined by SEM and shown in Fig. 5-4. Cryo-fracturing was made perpendicular to the sample axis of deformation and in parallel to the emerging crazes.
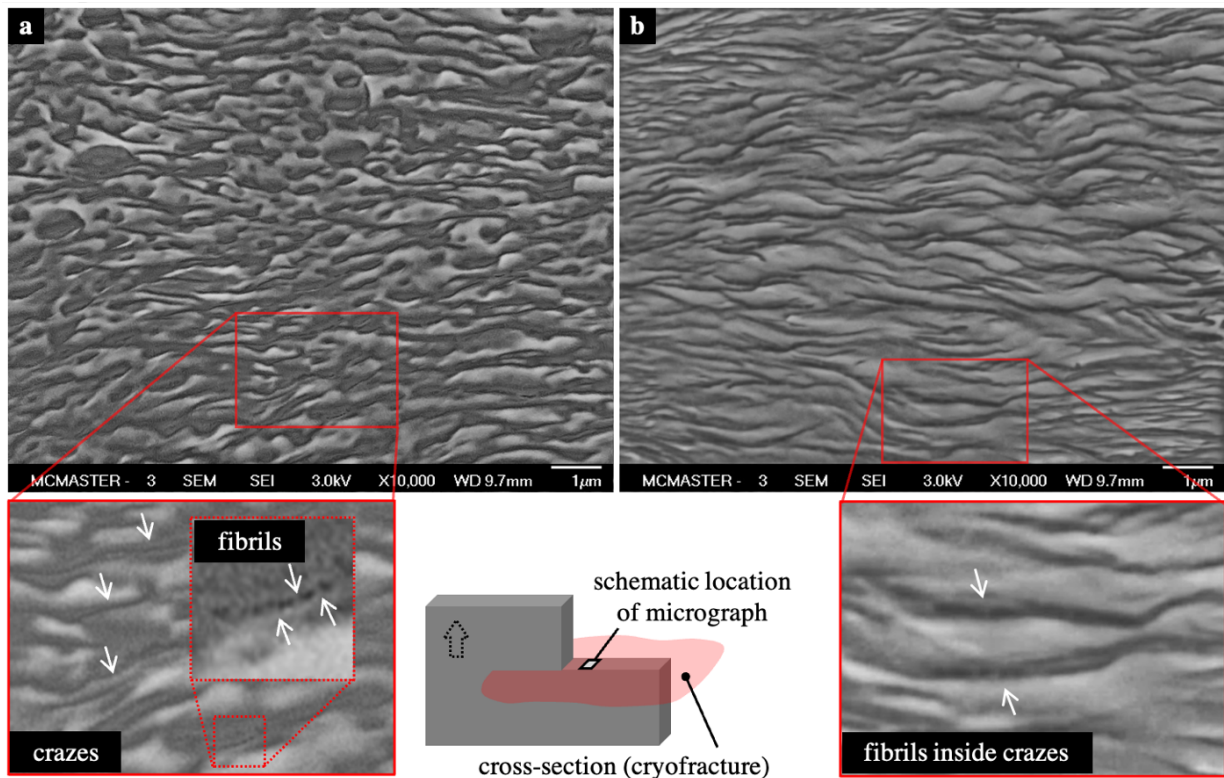
Figure 5-4. Morphology of Engage 8003 (a) and Engage 8180 (b), deformed by 300% strain in acrylic monomer with its subsequent polymerization, and then cryogenically fractured normal to the axis of sample deformation (black dashed arrow). Crazes are shown by white arrows.

The micrographs represent the entire fractured surface; in this case, focused at a distance of approximately 10 μm from the edge. For both samples seen in the figure, their morphologies were similar with white protrusions that correspond to ductile fractures of the elastomeric matrix and black smooth regions which are believed to correspond to the brittle dry poly(acrylic acid) phase.

The cavitation modes of Engage 8003 and Engage 8180 were distinctly different, as expected from the DSC results. Based on the micrographs, cavitation in Engage 8003 occurred with the formation of the broader crazes producing internal channels in the order of 0.1-0.5 μm in diameter. The acrylic phase was well-distinguished and appeared to exhibit a co-continuous morphology. The crazes for Engage 8137 (not shown here) and Engage 8180 were similar, appearing narrower with diameters no greater than 0.1 μm. The main difference between the POEs, however, was not in the width of the crazes but in their morphology. For Engage 8003, the crazes were characterized by noticeable local node-like thickenings of the acrylic phase. This is unlike the other two materials, in which crazes were poorly filled with the acrylic material, resulting in relaxation and partial collapse of the voids associated with crazing after the tensile stresses were removed. Enlarged sections of both micrographs in Fig. 5-4 show the internal fibrillar structure of the crazes. For Engage 8003, the fibrils were barely detectable in the acrylic fraction volume, while for Engage 8180, the fibrils were visibly exposed due to intermittent discontinuity of the acrylic-filled channels.

Similar to the ethanol used in the DMA tests, acrylic monomer also proved to be an effective surface-active liquid medium in the research by Kornberg et al.[4] Driven by capillary pressure and applied external pressure, the monomer penetrates the material volume through the primary crazes formed due to the deformation of the sample, thereby lowering the energy of any

available internal surfaces and facilitating further material cavitation. As a result, a synergistic effect of the primary voids homogeneity and the surface activity of the monomer is achieved, leading to uniform material cavitation. Capillary pressure in the narrow primary crazes of Engage 8180 was important. However, as seen from the SEM micrographs, initial cavitation intensity determined by the size of the primary voids was more vital since it ensured effective delivery of the medium throughout the Engage 8003 sample volume. Unlike the DMA tests conducted at atmospheric pressure, the lack of capillary pressure due to the wider primary crazes of Engage 8003, in this case, was compensated by deforming the samples in a high-pressure reactor.

The node-like thickenings of Engage 8003 were believed to act as buffer reservoirs for the monomer during stepwise deformation of the sample, being saturated with the medium while the stress was applied and preventing the matrix from being elastically recovered due to hydrostatic pressure while the stress was gradually dissipated. After the experiment was completed and the acrylic environment had polymerized to offer a rigid supportive framework, the acrylic thickenings could have also prevented the collapse of the internal crazed matrix structure due to elastic recovery and recombination of crystallites. In contrast, Engage 8180 had a fine but open-textured morphology with craze fibrils seen due to a lack of acrylic phase. Despite the high capillary pressure ensured by the narrow crazes initiated by its small crystals, the monomer was squeezed out of the Engage 8180 matrix during each stepwise deformation cycle, when the matrix elastically recovered. The low melting temperature of the elastomer also contributed to poor saturation by the medium. When the reactor was heated up to initiate polymerization, the elastic matrix recovery further accelerated due to an increase in mobility of the elastomeric chains.

It is worth noting that the micrographs demonstrated high uniformity in morphology for both elastomers, regardless of the crazing response to deformation. This is consistent with the research by Bucknall,[25] in which the author established the thermodynamic similarity of craze initiation with the opening of voids depending on their size. While the gradual tensile strain is applied to the matrix with voids of different diameters (e.g., in a regular olefinic material such as polyethylene), smaller voids can remain inactive, and the polymer elongates due to the initiation and widening of crazes on the larger voids. As shown in the Introduction section, in POEs with their hypothetically homogeneous domain structure, the size of primary voids that emerge in areas of maximum plastic flow is consistent. Thermodynamically, this ensures the opening of voids at approximately the same time, resulting in a uniform crazed network.

5.4.4   MASS CHANGE AND ION CONDUCTIVITY OF POE-PAA SAMPLES

Fig. 5-5 shows mass change due to acrylic phase inclusion and through-plane ion conductivity as a function of elongation for all three materials. Dotted trendlines were added for clarity in the measured characteristics. The resulting ion-conductive composite materials are potentially of great practical importance. In this study, however, conductivity and its relationship with the change in mass were aimed at evaluating the effectiveness of craze formation in the deforming matrices, from the level of electrical percolation depending on the initial domain-based elastomeric morphology.

It appears that the penetration capacity of matrices of Engage 8137 and Engage 8180 by acrylic monomer was insignificant up to ~100% strain; the samples did not show an increase in mass and, correspondingly, no conductivity. Yet, the DMA results demonstrate a noticeable increase in the plastic response of all three samples in the range ~50-100% strain, suggesting

that their elastomeric structures might have undergone sufficient cavitation to absorb some amount of the acrylic medium. Such a discrepancy might likely be due to the internal cavitation when the initiated crazes had no way out and couldn't deliver the medium inside the volume. Also, the samples' recovery response was still high at these elongations, causing the monomer to be squeezed out during steps of relaxation from the crazes. The reason might also be the inhibition or complete lack of crazing with nevertheless a sufficient level of local cavitation on the hard domains, which might also result from the absence of a liquid medium in the internal matrix volume. If the crystallites in a POE are too thin, cavitation may be suppressed entirely. In the research by Pawlak et al., the authors showed that crystallites with thickness less than a particular critical value might begin to deform through crystallographic slip before the stress exceeds the strength of the amorphous phase.[11]

Beyond ~100% strain, the mass of both samples slowly raised, with Engage 8137 showing a larger increase than Engage 8180. The conductivity of Engage 8180 became detectable by ~200% strain and even slightly increased by ~300% strain (still being marginally low, $9.2 \cdot 10^{-9}$ S·cm^{-1}). This indicates that, with the less amount of absorbed monomer, the crazes in Engage 8180 propagated more efficiently and were able to continuously pass through the matrix, likely due to their narrowness and, as a result, higher capillary pressure, as was discussed in the section with the results obtained by DMA. For Engage 8137, the applied pressure in the reactor did not compensate for the drop in capillary pressure due to the wider crazes, resulting in no detectable electrical percolation.
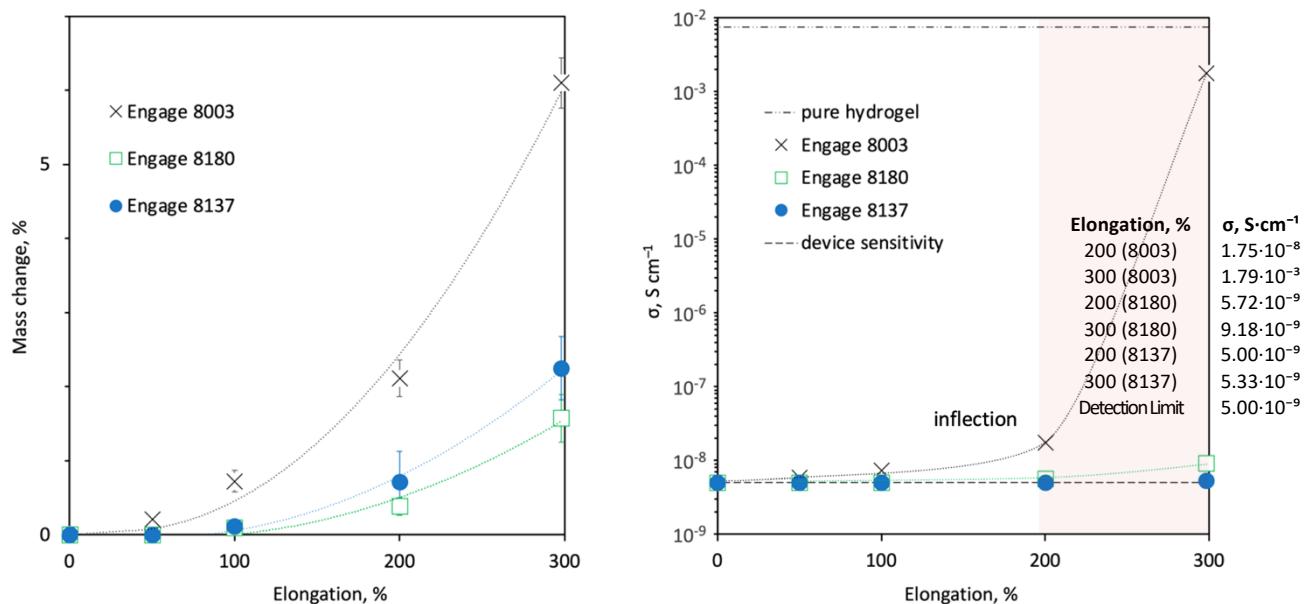
Figure 5-5. Effect of elongation on mass change and ion conductivity for three tested materials. The trendlines were included to visually highlight the difference in the dynamics of changes between these two parameters. For the conductivity graph, RSD proportionally increased with elongation and was ~5% on average. Values of conductivity are provided for 200% and 300% elongations (region shown in pale red).

In contrast with Engage 8137 and Engage 8180, Engage 8003 showed a slight increase in mass by ~50% strain and gained 0.8% of its initial weight by ~100% strain. All three Engage 8003 trial samples exhibited ion conductivity above the threshold of the measuring device sensitivity, indicating percolation was present for all four strain conditions. The overall trend in mass change of Engage 8003 resembled an exponential behavior. As mentioned, the node-like thickenings in the cavitated space may be essential in growing the acrylic phase, acting as buffer reservoirs, and preserving the monomer during elastic matrix recovery. The thickenings may emerge at ~100% strain and, getting filled with the monomer, may account for the additional

mass. An abrupt increase in conductivity, seen by the visible inflection point on the curve, occurred due to intense craze propagation resulting in a significant rise in percolation throughout the matrix, ultimately giving an average mass gain of 6% at a matrix strain of 300% and conductivity of $1.8 \cdot 10^{-3}$ S·cm^{-1}, close to the inherent conductivity of the pure hydrogel, $7.5 \cdot 10^{-3}$ S·cm^{-1}.

5.4.5 PRELIMINARY ATTEMPTS TO CREATE ELECTRON-CONDUCTIVE POE-PANI MATERIALS

Due to its domain structure, Engage 8003 exhibits the ability to effectively form crazes in thermodynamically compatible liquid media, which made it suitable for creating a continuous acrylic network. However, the need for an electrolyte limits the possible use of such materials as flexible conductors. The use of electrolyte-free materials for the conductive phase overcomes this limitation but, at the same time, introduces additional technological difficulties in engineering the composites.

Polyaniline doped with DBSA, an electrolyte-free intrinsically conducting polymer that can transmit both ions and electrons, is well-soluble in NMP. The solution exhibits quite a low surface energy and, at first glance, seemed suitable for use as the liquid medium for stretching elastomers. After deformation of the samples and evaporation of NMP, polyaniline was expected to solidify and form a continuous conductive network within the matrix. However, this approach appeared to be impracticable. Due to the relatively low melting point of Engage 8003 (81.0 °C, as shown in Section 3.1), the complete removal of the solvent from the obtained materials took quite a long time, even under vacuum. But the most critical restriction was in the tendency of PANI to lose the dopant, which made the final material non-conductive. Re-doping was nearly

impossible since the PANI network, embedded into the elastomeric volume, was insulated from any doping agent.

In our previous research, *in situ* emulsion polymerization of aniline in the polyethylene matrix yielded a highly conductive secondary phase of PANI-DBSA.[3] This resembles the approach of stretching the samples in the acrylic monomer, only replacing the hydrogel secondary phase with polyaniline to achieve electron conductivity. However, an attempt to follow this approach with pure Engage 8003 failed since the partial elastic recovery of the matrix displaced the incorporated polyaniline conductive phase when the deformed samples were taken out of the rig, causing the conductivity to drop to an undetectable level. In contrast to polyaniline, the acrylic hydrogel was rigid and acted as an additional framework, preserving crazes from their elastic collapse. Following this, the idea arose to incorporate supplementary rigid material, such as PCL, into an elastomeric matrix for reinforcement. The presence of PCL dramatically increased the continuity of the conductive PANI phase in the final POE-PCL-PANI materials.

5.4.6   MORPHOLOGY OF THE ENGAGE 8003-BASED POE-PCL-PANI SAMPLES AFTER DEFORMATION

The morphology of the final POE-PCL-PANI material in two planes, perpendicular and parallel to the axis of deformation, was examined by SEM and is respectively shown in Fig. 5-6 and 7. The micrographs were representative of the entire cross-sectioned surfaces. A network of PANI was extracted from the matrix with NMP to reveal the matrix morphology.
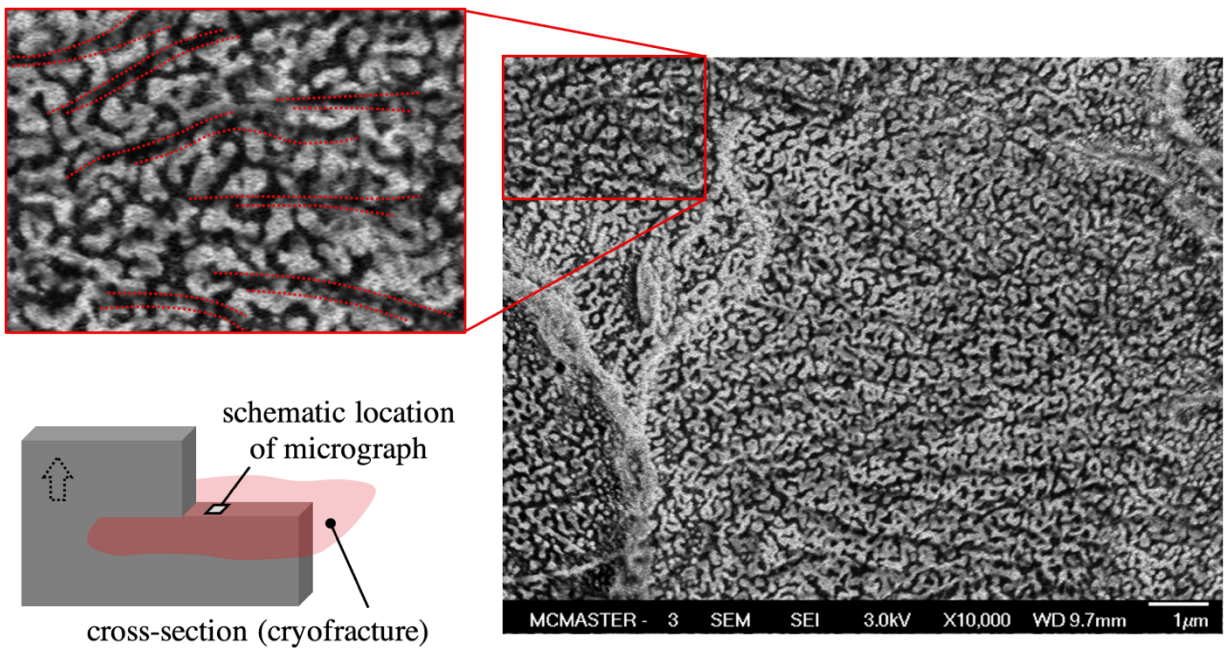
Figure 5-6. Morphology of the sample cryogenically fractured normal to the axis of tensile sample deformation and after dissolving the PANI phase with NMP.

The first micrograph shown in Fig. 5-6, obtained on the surface after perpendicular cryo-fracturing, evaluated the sample's through-plane percolation. The hierarchical cavitated structure is clearly distinguished, consisting of microscale crazes (dashed red lines on the zoomed-in fragment) and nanoscale voids that emerged after dissolving PCL. Low molecular weight formic acid, highly compatible with POE and PCL, could freely penetrate a matrix material while a sample was deformed. Not only did it dissolve PCL and work as a carrier for the aniline emulsion droplets, but it also acted as a surface-active liquid medium, decreasing the mechanical energy threshold for further craze propagation. Based on image analysis, the cross-section showed the continuous secondary phase network accounted for an estimated 37.5-44% of the displayed surface area.
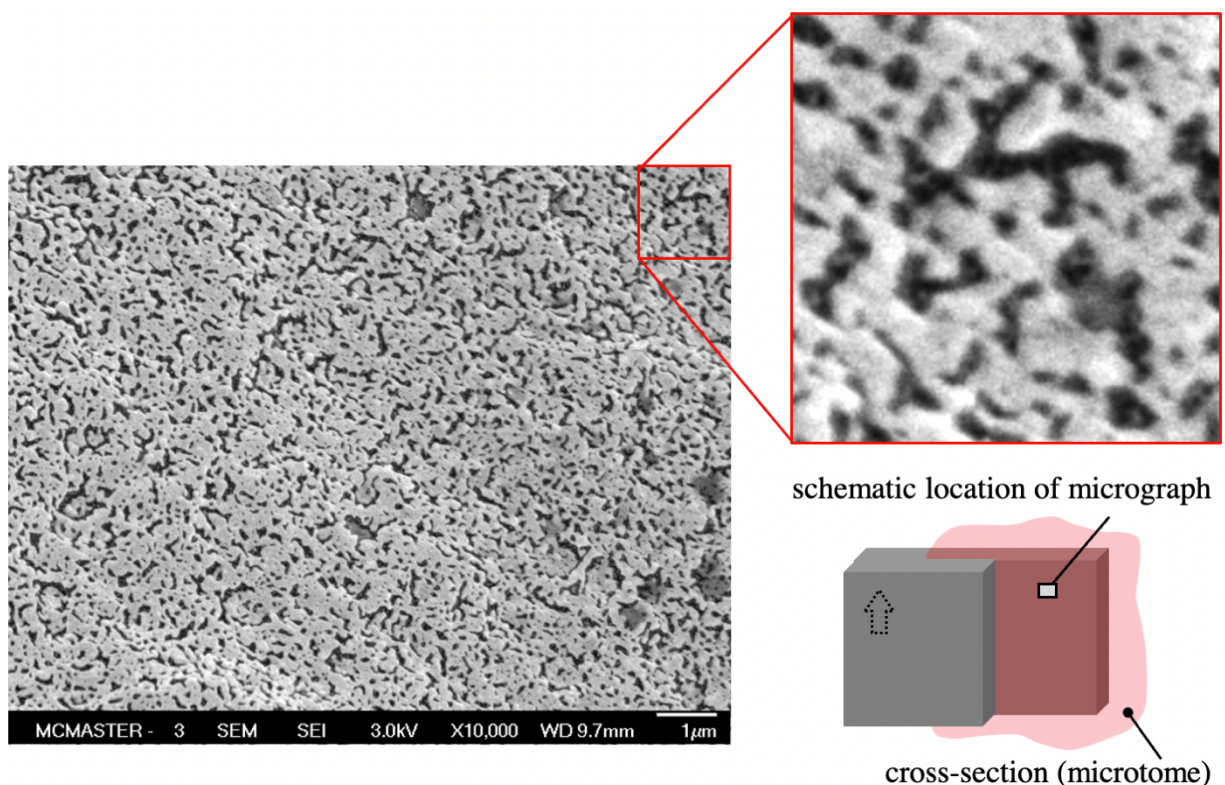
Figure 5-7. Morphology of the sample sectioned with a microtome along the axis of tensile sample deformation and after dissolving the PANI phase with NMP.

The second micrograph shown in Fig. 5-7, obtained after sectioning along the deformation axis, at 90° to the surface of the previous micrograph, evaluates the sample's in-plane percolation. The structure had limited continuity, with the crazed space resulting from both dissolved PCL and crazes, which propagated perpendicular to this surface plane, as confirmed by the presence of fibrils visible at the zoomed-in fragment.

The initial morphology of a POE (ensured by its chemical composition) and the approach of replacing a sacrificial fraction of PCL with a conductive fraction of PANI-DBSA, collectively

with the method of controlled crazing in a surface-active environment, influenced the formation of a co-continuous structure. It was determined that co-continuity was homogeneously formed normal to the sample drawing axis. Comparatively, cross-section made vertically, perpendicular to the formed crazes, showed a lack of continuity of the conductive phase, which likely limits the suitability of these materials in applications that require in-plane electrical percolation.

5.4.7   RESPONSE OF CONDUCTIVITY TO CYCLIC MECHANICAL DEFORMATION OF THE ENGAGE 8003-BASED POE-PCL-PANI SAMPLES

The durability of the conductive network and consistency in conductivity at moderate tensile strain were considered essential properties of the newly created POE-PCL-PANI material. Through-plane conductivity was measured while undergoing deformation to evaluate the capacity of the matrix to retain its percolating network morphology and quantify the ability of the secondary phase to move without fracturing inside the cavitated matrix space. Fig. 5-8a presents through-plane conductivity measurements under tensile strain. The in-plane conductivity (not provided), even for the undeformed samples, was more than five orders of magnitude lower than through-plane, confirming the observation made based on the SEM images (Section 3.6) that the crazes forming the secondary phase network were mainly oriented transversely to the direction of the sample stretching axis. The decline in in-plane conductivity to an undetectable level occurred at the onset of deforming the material. A slight decrease in through-plane conductivity was observed up to approximately 2.1% strain, after which a progressive drop happened. As mentioned, this diapason was denoted as a survival range of the POE-PCL-PANI samples, within which the specimens' conductivity decreased moderately and remained above 10^{-1} S·cm^{-1}.

The through-plane conductivity endured tensile deformation due to the transversely oriented crazing and, consequently, the orientation of the polyaniline network formed inside. While the sample was deformed, the tensile stresses concentrated at the matrix-PANI interface rather than in the PANI phase. Transverse compression of PANI resulting from longitudinal matrix stretching usually increases its conductivity due to the compaction of the PANI fibers.[26] However, the typically high Poisson's ratio for POEs, ~0.5,[27] suggests that the matrix material was substantially thinned during stretching. As a result, the transversely oriented PANI pathways likely were not significantly affected by the tensile deformation. However, up to 2.1% strain, through-plane conductivity slightly decreased. We believe the inter-connecting channels (side pathways) were failing at the junction with the transversely oriented channels rather than in the middle of the branching channels, causing a decrease of conductivity in the through-plane direction and an immediate loss of conductivity in the in-plane direction. After ~2.1% strain, further plastic deformation of the matrix elastomer resulted in a slower yet gradual fragmentation of the conductive channels, resulting in a noticeable drop in the through-plane conductivity. Nevertheless, even at 2.5% strain, the polymer remained relatively conductive in the order of 10^{-3} S·cm^{-1}.
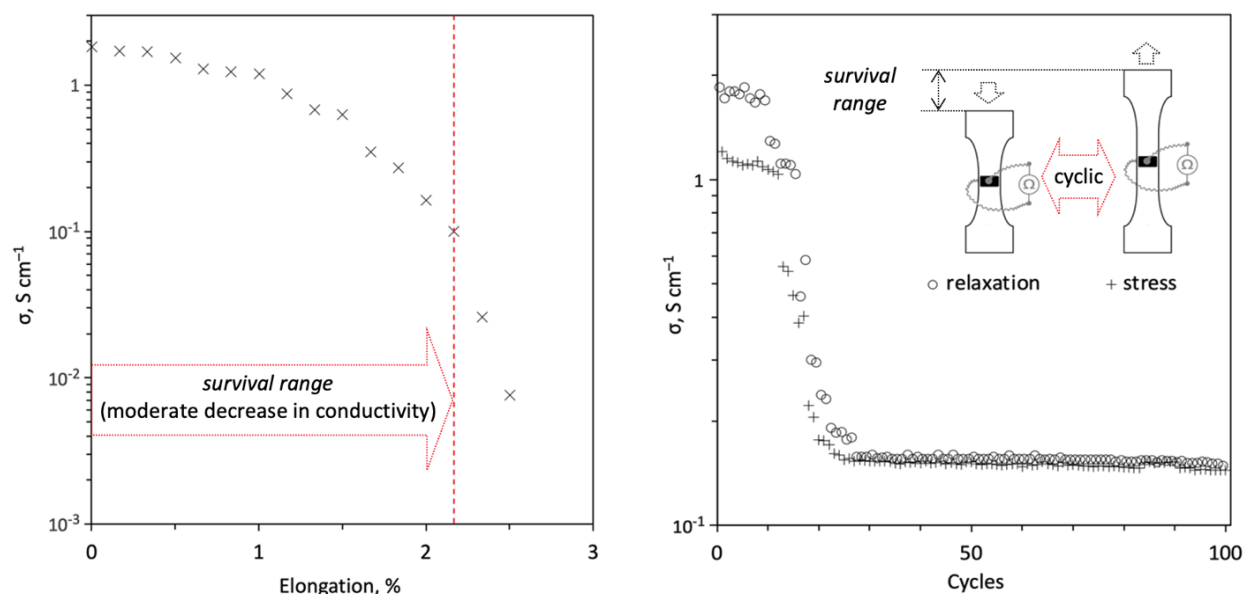
Figure 5-8. Change of through-plane electron conductivity during tensile deformation and cyclic deformation of POE-PCL-PANI. The red dotted vertical line limits a stable range of about 2.1% strain within which the conductivity varies insignificantly.

Cyclic deformation of the obtained material within the safe survival range showed a subtle irreversible change in conductivity per loading cycle, with a total decline of about 1.1×10^{-1} S·cm^{-1}, after 30 cycles, with a subsequent stabilization (Fig. 5-8b). The decrease was probably attributed to rearrangements in the brittle polyaniline phase and the consequent reduction of the influence from the deformed matrix on phase integrity. After the test, the samples remained visually unchanged. Based on these results, cyclic deformation of the new material at 2.1% strain was considered adequately stretchable in terms of conductivity.

5.5   CONCLUSION

In this paper, we described the lateral detachment of crystallites near the crystal-amorphous interface as a response to stress, which resulted in uniform cavitation through the samples. More importantly, we described the mechanism of recovering in the POEs' structure upon stress relaxation, hypothesizing the return of crystallites to their initial locations and noting the nearly absent neck formation phase, which is always present on the stress-strain curves for semicrystalline polymers. Based on the results of cavitation of the POE matrices, facilitated in thermodynamically compatible media, we chose the most suitable material with the most advantageous combination of large and small domains that resulted in the effective formation of crazed networks. We incorporated a continuous electron-conductive phase of doped polyaniline via its polymerization *in situ*. Additionally, the PANI-DBSA phase was protected from fragmentation caused by the elastic recovery of the elastomeric matrix, with the phase of polycaprolactone that reinforced the matrix, thereby preserving the obtained material conductivity even during its cycling tensile deformation within the range up to 2.1% strain.

5.6   ACKNOWLEDGEMENT

5.7   REFERENCES

[1]   P. S. Chum, K. W. Swogger, *Prog Polym Sci* **2008**, *33*, 797.

[2]   S. Bensason, J. Minick, A. Moet, S. Chum, A. Hiltner, E. Baer, *J Polym Sci B Polym Phys* **1996**, *34*, 1301.

[3]   A. B. Kornberg, M. R. Thompson, S. Zhu, *ACS Appl Polym Mater* **2021**.

[4]   A. B. Kornberg, M. R. Thompson, S. Zhu, *Ind Eng Chem Res* **2020**, acs. iecr.9b07010.

[5]   J. D. Eshelby, *Proc R Soc Lond A Math Phys Sci* **1959**.

[6]   J. D. Eshelby, *Proc R Soc Lond A Math Phys Sci* **1957**, *241*, 376.

[7]   J. D. Eshelby, *The Philosophical Magazine: A Journal of Theoretical Experimental and Applied Physics* **2010**, *6*, 953.

[8]   R. D. Thomson, J. W. Hancock, *International Journal of Fracture 1984 24:3* **1984**, *24*, 209.

[9]   B. Wilner, *J Mech Phys Solids* **1988**, *36*, 141.

[10]   S. Bensason, E. v. Stepanov, S. Chum, A. Hiltner, E. Baer, *Macromolecules* **1997**, *30*, 2436.

[11]   A. Pawlak, A. Galeski, A. Rozanski, *Prog Polym Sci* **2014**, *39*, 921.

[12]   R. F. Storey, J. W. Sherman, *Macromolecules* **2002**, *35*, 1504.

[13]   C. S. Hege, S. M. Schiller, *Green Chemistry* **2014**, *16*, 1410.

[14]   P. K. Roy, P. Surekha, C. Rajagopal, *J Appl Polym Sci* **2011**, *122*, 2765.

[15]   DOW, ENGAGE™ Polyolefin Elastomers **2019**, 4.

[16]   G. W. Gokel, J. A. Dean, *Dean's Handbook of Organic Chemistry*, McGraw-Hill handbooks, McGraw-Hill, **2004**.

[17]   D. M. Garcia Cruz, D. F. Coutinho, E. Costa Martinez, J. F. Mano, J. L. Gómez Ribelles, M. Salmerón Sánchez, *J Biomed Mater Res B Appl Biomater* **2008**, *87*, 544.

[18]   Federal Republic of Germany, "Surface Tension Values of Some Common Polymers/Test Liquids for Surface Energy Analysis," **2018**, www.surface-tension.de.

[19]   D. B. Malpass, *Introduction to Industrial Polyethylene: Properties, Catalysts, and Processes*, Vol. 45, John Wiley & Sons, **2010**.

[20]   P. Svoboda, D. Svobodova, P. Mokrejs, V. Vasek, K. Jantanasakulwong, T. Ougizawa, T. Inoue, *Polymer (Guildf)* **2015**, *81*, 119.

[21]   S.-G. R. Kim, A Study on the Foaming Behavior of Thermoplastic Polyolefm (TPO) Blends, University of Toronto, **2008**.

[22]   I. C. Sanchez, R. K. Eby, *Macromolecules* **1975**, *8*, 638.

[23]   J. Minick, A. Moet, A. Hiltner, E. Baer, S. P. Chum, *J Appl Polym Sci* **1995**, *58*, 1371.

[24]   W. Liu, W. J. Wang, H. Fan, L. Yu, B. G. Li, S. Zhu, *Eur Polym J* **2014**, *54*, 160.

[25]   C. B. Bucknall, *Polymer (Guildf)* **2007**, *48*, 1030.

[26]   I. C. Polpaya, C. L. Rao, S. Varughese, *Smart Materials, Adaptive Structures and Intelligent Systems (SMASIS)* **2016**.

[27]   L. Zhu, H. N. Fan, Z. Q. Yang, X. H. Xu, *Polym Plast Technol Eng* **2010**, *49*, 208.

5.8   GRAPHICAL ABSTRACT
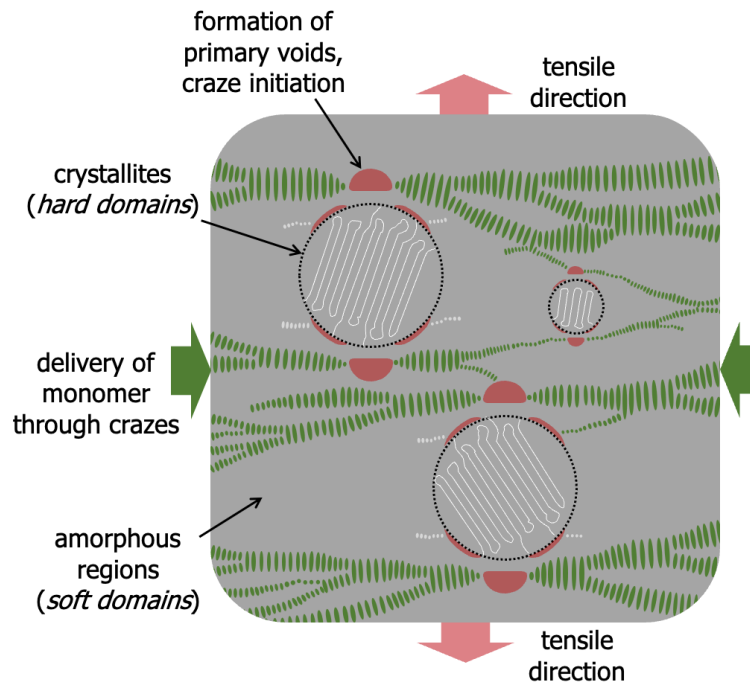
6   CONCLUSION AND FUTURE WORK

Contributing to the research and development of conductive co-continuous composite materials, we have presented a viable and affordable alternative for blending two components of different natures. Most importantly, we have demonstrated the possibility of obtaining electrically conductive composites by polymerizing the secondary fraction inside continuous pores formed in olefinic matrices by controlled cavitation under mechanical stress. We have shown that, under certain experimental conditions, such as the initial morphology of the matrix, thermodynamic compatibility between the reactive liquid medium and matrix, applied pressure, and degree of elongation of the matrix, the secondary fraction forms a network that can percolate throughout a matrix sample, thereby ensuring charge transport, which cannot be achieved by

melt or solution blending techniques without using such high concentrations of the secondary polymer that properties of the original matrix are significantly degraded.

As part of the progress of this experimental work, the novelty was achieved in the following aspects:

- It has been shown that the initial morphology of matrices ensured the desired frequency and distribution of primary matrix voids, which directly affected the cavitation behavior of these polymers under stress. Two approaches were investigated in the present dissertation: (1) development of the crystal-amorphous interface area via reducing the size of the crystallites to increase the primary voids created by cavitation, or (2) selecting the sequential length of copolymer segments for the modeled domain structures in which voids are generated by cavitation. In both cases, it was shown that there is a dependency in the level of percolation of the crazed network on the void characteristics of the matrix. However, it was also revealed that there are particular features of the studied systems, without considering which experimental procedures were used, that appeared to be ineffective or non-functional. Thus, there were positive and negative considerations for the ideal diameter of crazes; very wide crazes caused a drop in capillary pressure, while crazes that were too narrow inhibited or even restricted the passage of the secondary polymer precursor solution. Also, for example, an attempt to maintain the elasticity of the matrix sometimes resulted in the collapse of the secondary phase making it insulative. At the same time, excessive plastic deformation resulted in a loss of operational mechanical characteristics of the obtained materials. In the first case, the issue was solved

by conducting experiments in a high-pressure reactor to compensate for the decrease in the capillary pressure and by adjusting the thermodynamic compatibility between the components. In the second case, an additional reinforcing component was introduced into the matrix.

- A unique and elegant solution found within this research was using polyaniline fibers dispersed in an olefinic matrix. The fibers first acted as a nucleating agent and then increased the percolation of the conductive network by merging with the polyaniline fraction introduced into the matrix through synthesis.

- It has been established that the efficiency of penetration for a liquid into the matrix was a rate-determining factor in craze formation. Most of the procedural issues solved within this experimental work were related precisely to fulfilling this necessary condition. A number of engineering solutions have been found and applied to improve the efficiency of delivering liquid media to the otherwise stable void defects, thereby contributing to their opening. For example, an elastomer with multimodal sequence length of segments in its comonomer structure, resulted in the formation of the crystallites of different sizes, and consequently showed better penetration capacity.

- It is worth noting that the issue of initiating polymerization precursors at the required time, when the crazed network is already sufficiently developed and saturated with the reaction mixture, has also been solved. During the deformation of the samples and their simultaneous penetration by the reaction medium, the initiating agent was inhibited by cooling the cell down. Freezing of the medium was prevented by adding a lithium salt.

- The use of polyolefin elastomers as matrices has proven challenging and inefficient in most cases. However, the right choice of a multimodal elastomer, as well as its blending with rigid crystalline polycaprolactone, which was partially leached and replaced by a conductive polyaniline phase, appeared to be effective in obtaining a highly elastic and electron-conductive material, moderately resistant to cyclic mechanical loads.

Future research in this area may be related to a more complete and controlled recovery of elastic elastomeric matrices after stress relief when they are subjected to cyclic loading. This can be achieved by reducing the scale of the conductive channels, which would ensure the polymer chains' recombination. In the research by Galeski,[1] the author showed that the strain in stretching olefinic materials could be up to 80% reversible if they were pre-compressed by rolling. The author explained such a strong recovery by the highly oriented nodes formed in materials during compression. As mentioned in the previous chapter, there is usually a noticeable difference between the actual volume of the linear fraction and the crystallinity of olefins, such as elastomers with domain-like morphology, which indicates that a significant portion of the linear segments belongs to the amorphous phase. According to the research by Rozanski et al.,[2] and later by Kornberg et al.,[3–5] the crystallites to a certain point remain unaffected while polymer samples are deformed in a thermodynamically compatible environment. As a result, the additional crystal inclusions formed due to compression, undergoing only elastic deformation, trigger the formation of more narrow channels in the intermediate amorphous areas. With further deformation, even when the crystalline fraction begins to be consumed on drawn microfibrils, partial recovery is still possible after the load is removed according to the mechanism of

recrystallization described by Bensason.[4] As described by the author, small crystals experience chain rearrangements, therefore having a high potential for self-recovery. In light of the foregoing, it can be assumed that pre-compression of the materials by rolling can increase the efficiency of the resulting composites' design by promoting the emergence of narrower crazes. With the same level of percolation, this will decrease the content of the secondary conductive fraction and improve self-healing of the matrix polymers, accordingly promoting the preservation of the mechanical properties of the composites. This is especially relevant for ethylene-octene elastomers, which can potentially form additional crystallites due to the presence of the uncrystallized linear segments in the volume.

Other factors that can potentially improve the efficiency of craze formation are associated with an increase in the thermodynamic compatibility between the matrix and the liquid surrounding via searching for alternative penetrating liquids and fine-tuning the temperature regime of the experiment. In addition, raising the pressure in the reactor will also have a positive effect.

Another exciting and promising direction in this field is the effective grafting of conductive polymers onto a matrix via dopants, which would not only increase the reliability of the obtained materials but may also impart mechanical stimuli-responsiveness with a reversible change in electrical performance. Doping agents have to ensure efficient ionization of the conducting polymer backbones. For example, combining polyaniline or polypyrrole chains with benzenesulfonic acid groups provides the polymer's conductivity. However, the benzene ring of the acid may be further functionalized, for example, with units that contain click-chemistry groups, spiropyrans, or other reactive groups sensitive to those on the internal matrix surface.

The groups can also form an olefinic or rubber-like fraction, which imparts the resulting materials with additional flexibility.

The use of ionic liquids as a substitute for solid conductive polymers would enable the attainment of force sensitivity with a change in the materials' ionic conductivity. This approach essentially repeats the design of the materials with an acrylic hydrogel secondary phase. However, unlike hydrogels which require a liquid alkaline electrolyte and are relatively weak mechanically in a saturated state, ionic liquids are conductors intrinsically and cannot fail under stress. A change in the morphology of matrix crazes under load will also change the continuity and diameter of the liquid channels, ultimately affecting the overall level of percolation and, accordingly, the ion conductivity of the material.

REFERENCES

(1)   Galeski, A. Strength and Toughness of Crystalline Polymer Systems. *Prog Polym Sci* **2003**, *28* (12), 1643–1699. https://doi.org/10.1016/j.progpolymsci.2003.09.003.

(2)   Rozanski, A.; Galeski, A. Controlling Cavitation of Semicrystalline Polymers during Tensile Drawing. *ACS Macromolecules* **2011**, *44* (18), 7273–7287.

(3)   Kornberg, A. B.; Thompson, M. R.; Zhu, S. Developing Continuous Submicron-Scale Conductive Interpenetrating Hydrogel Network in Polyethylene Matrices through Controlled Crazing and Polymerization. *ACS Industrial Engineering Chemistry Research* **2020**. https://doi.org/10.1021/acs.iecr.9b07010.

(4)   Kornberg, A. B.; Thompson, M. R.; Zhu, S. Flexible Conductive Substrate Incorporating a Submicrometer Co-Continuous Polyaniline Phase within Polyethylene by Controlled Crazing. *ACS Appl Polymer Materials* **2021**. https://doi.org/10.1021/acsapm.0c01416.

(5)   Kornberg, A. B.; Thompson, M. R.; Zhu, S. Flexible Nanoscale Co-Continuous Structures Prepared by Controlled Crazing of Ethylene-Octene Elastomers and in Situ Polymerization of Conductive Networks. *Wiley The Canadian Journal of Chemical Engineering* **2022**. https://doi.org/10.1002/cjce.24796.

(6)   Bensason, S.; Stepanov, E. V.; Chum, S.; Hiltner, A.; Baer, E. Deformation of Elastomeric Ethylene-Octene Copolymers. *ACS Macromolecules* **1997**, *30* (8), 2436-2444. https://doi.org/10.1021/ma961685j.